1987

Progress Report No. 23

Biomedical Computer Laboratory

PROGRESS REPORT

No. 23

1 July 1986 - 30 June 1987

Biomedical Computer Laboratory

Institute for Biomedical Computing

Washington University

700 South Euclid Ave.

St. Louis, Missouri 63110

BIOMEDICAL COMPUTER LABORATORY

INSTITUTE FOR BIOMEDICAL COMPUTING

WASHINGTON UNIVERSITY

PROGRESS REPORT NO. 23

JULY 1, 1986 - JUNE 30, 1987

TABLE OF CONTENTS

I. INTRODUCTION

This progress report from the Biomedical Computer Laboratory (BCL) summarizes activities during the period from July 1, 1986 through June 30, 1987. The Biomedical Computer Laboratory collaborates with research investigators throughout the Washington University School of Medicine and its affiliated hospitals in the application of advanced computer techniques to problems in biology and medicine. This often requires work in areas stretching from basic biomedical sciences through mathematical models to equipment design. Our orientation is interdisciplinary with the recognition that effective communication for workers with differing backgrounds comes only through extended collaboration and mutual respect.

The vigorous development and evolution of specialized hardware and software systems for use in the solution of research and clinical problems has continued to be the central focus of BCL activities. Several systems now in clinical use have seen a progression from exploratory pilot studies, to major developmental project, to local clinical trial, to clinical trials in multiple locations, to public availability through commercial manufacture. Perseverance in this sometimes tedious chain of development has found reward in the effective fielding of specialized computer systems to the medical community.

One class of computer applications requires strong coupling of the computer to its environment for digital signal processing. These applications typically involve the use of commercially available minicomputers and microprocessors in conjunction with specialized hardware designed and built locally. We have pursued many such applications by bringing signals from hospital wards and research laboratories to BCL by means of either analog or digital tape recordings or telephone lines and, more frequently, by taking the computers to the investigator's laboratory or the patient's bedside. More recently, an emphasis at BCL has been on the development of a flexible digital communication capability for linking data sources and information destinations with research-oriented computational resources at BCL as well as at collaborators' sites.

Of particular importance to current and future BCL projects is the development, in a closely related sister lab (Computer Systems Laboratory, or CSL), of a capability for the design and fabrication of custom very-large-scale integrated (VLSI) circuits. The realization of such circuits through collaboration with CSL is already opening up new opportunities for solving problems intractable with conventional computing devices. The CSL has as its goal the development of innovative approaches to computing that will have important implications for medicine and biology in the future.

For those classes of applications dominated by information processing requirements, available arrangements have matured from telephone lines linking our minicomputers to the large IBM Systems at the Washington University Computing Facilities, through development and support of a minicomputer based MUMPS system, to the establishment of independent groups such as the Medical Computing Facility and the Medical Computing Service Group which serve the local medical complex. Diverse needs continue to be met by these various options as well as by an increasing number of independent computing facilities within medical school departments.

Still another class of applications requires extensive use of large-scale computational services. Many investigators are assisted in their research through the use of generalized numerical, non-numerical, and statistical routines. Such work is sometimes carried out by staff members of BCL, but primarily by members of the Division of Biostatistics under the direction of Dr. Dabeeru C. Rao, and the University Computing Facilities whose director is Robert J. Benson.

Over the years, the BCL has enjoyed collaborations with most departmental divisions within the medical school but has also found support and enrichment through close ties with other facilities throughout the University. These arrangements are of benefit both to the BCL and to graduate students who find projects and employment among the activities in the laboratory. The Department of Computer Science is under the direction of Dr. Jerome R. Cox, Jr., past Director of the BCL. Strong ties with the Department of Electrical Engineering are sustained through the Engineering School's Biomedical Engineering Program and common interests in digital signal processing techniques.

Three years ago, Washington University established an interschool Institute for Biomedical Computing. The new Institute encompasses the Biomedical Computer Laboratory and the Computer Systems Laboratory in an organizational setting designed to recognize and foster the joint interests in biomedical computing of the School of Medicine and the School of Engineering and Applied Science. The purpose of the reorganization is to recognize that the development and application of advanced computing and engineering technology to problems in biomedical science are essential components of the research and teaching activities of Washington University. Accordingly, attention has been given to the development of a stable organizational structure that will 1) provide a means by which the primary academic affiliations of its faculty can be in an organizational setting with an adequately broad commitment to research and teaching in biomedical computing; 2) establish a formal administrative connection to the School of Engineering and Applied Science that will facilitate the involvement of its students and faculty in research and instructional activities in biomedical computing; 3) establish mechanisms for administration, funding, and review of appointments, promotion, and tenure for the academic staff of this activity; 4) foster organizational and procedural coherence between the Biomedical Computer Laboratory and the Computer Systems Laboratory by placing them within a common administrative structure; 5) create a focal point for interdisciplinary teaching and student research, both in the School of Medicine and the School of Engineering and Applied Science, in areas that do not fit comfortably into existing departments; and 6) encourage a scholarly environment for the activities of the two computer laboratories that will promote and encourage teaching, research, and publication as vehicles for personal development and academic contribution.

In addition to current BCL and CSL space on the Medical School campus, space for part of the activities of the Institute has been provided on the Engineering School campus by completion of a fifth-floor addition to Lopata Hall in December of 1983. This new space (about 6000 square feet), called the Edward L. Bowles Laboratory, is immediately adjacent to the Departments of Computer Science and Electrical Engineering.

The Institute for Biomedical Computing (IBC) has replaced the former Washington University Computer Laboratories (WUCL) which was a less formal federation of BCL and CSL plus working groups within the Departments of Computer Science and Electrical Engineering. Dr. Charles E. Molnar, Director of the Computer Systems Laboratory, and Dr. Lewis J. Thomas, Jr., Director of the Biomedical Computer Laboratory, are respectively Director and Associate Director of the Institute. Both BCL and CSL continue to retain their identities and internal organizations. Accordingly, this Progress Report addresses activities centered primarily within BCL.

Planning and policy development of the Institute are overseen by a Governing Board, the membership of which is drawn from both Schools. The present composition of the Governing Board is:

J. R. Cox, Jr., Chairman, Department of Computer Science
N. Daw, Professor, Department of Cell Biology and Physiology and Department of Ophthalmology
R. G. Evens, Head, Department of Radiology
M. K. King, Dean, School of Medicine
D. M. Kipnis, Chairman, Department of Internal Medicine
E. L. MacCordy, Associate Vice-Chancellor for Research
J. M. McKelvey, Dean, School of Engineering and Applied Science
C. E. Molnar, Director, Institute for Biomedical Computing
P. Needleman, Head, Department of Pharmacology
D. L. Snyder, Chairman, Department of Electrical Engineering
L. J. Thomas, Jr., Associate Director, Institute for Biomedical Computing

To aid in long-range planning of the health-related activities of the Institute, a National Advisory Panel is convened periodically. Particular attention is given to the confluence of important needs in biology and medicine with the technical advances capable of meeting these needs. Successful development may suggest implementation on a larger, perhaps national scale. The present composition of the National Advisory Panel is:

Peter H. Abbrecht, M.D., Ph.D., Professor of Physiology and Medicine, Uniformed Services University of the Health Sciences, Bethesda, MD

Howard L. Bleich, M.D., Associate Professor, Beth Israel Hospital, Harvard Medical School

Wesley A. Clark, A.B., Clark, Rockoff & Associates, New York, NY

James N. Gray, Ph.D., Tandem Computer Company, Cupertino, CA

Frank E. Heart, M.S.E.E., Vice President and Director, Computer Systems Division, Bolt, Beranek & Newman, Cambridge, MA

David M. Kipnis, Professor and Chairman, Department of Internal Medicine, Washington University

Brian W. Matthews, Ph.D., Professor, Institute of Molecular Biology, University of Oregon

John M. Smith, Director, Sponsored Research Division, Computer Corporation of America, Cambridge, MA

Eugene A. Stead, Jr., M.D., Professor of Medicine, Department of Medicine, Duke University

Carlos Vallbona, M.D., Chairman, Department of Community Medicine, Baylor College of Medicine

II. SOURCES OF SUPPORT

During the period covered by this report the primary source of support for the Biomedical Computer Laboratory was from two grants from the National Institutes of Health, Division of Research Resources.

RR 01380	A Resource for Biomedical Computing.
RR 01362	Tissue Characterization via Ultrasonic Imaging.

Collaboration with other investigators often involved work already supported by other grants and contracts.

Public Health Services.

CA 41574	Accurate Photon Dose Calculations by Radiotherapy,
CA 42993	Plastic Scintillator as a Dosimeter in Radiotherapy,
CM 47696	Evaluation of High Energy Photon External Beam Treatment Planning,
CM 67915	Evaluation of High Energy Electron External Beam Treatment Planning,
EY 06582	Peripheral Tests of Color Vision in the Early Diagnosis,
GM 28232	Physical Mapping of Yeast Chromosomal DNA,
HL 07275	Cardiovascular System: Function, Regulation and Pharmacology
HL 13851	Cyclotron Produced Isotopes in Biology and Medicine,
HL 17646	Study of Ischemic Heart Disease,
HL 25944	Time-of-Flight Positron Tomography for Cardiac Imaging,
HL 28995	Adrenergic Factors and Arrhythmogenic Metabolites,
HL 28998	Tissue Characterization with Ultrasound,
HL 31531	Coronary Vascular Response to Injury: Role in Infarction,
HL 36773	Mechanisms of Arrhythmogenesis Following Infarction,
NS 06833	An Interdisciplinary Stroke Program,
NS 23007	Statistical Coding of Complex Stimuli in Auditory Nerve,
RR 01379	Research in VLSI Systems for Biomedical Applications.

National Science Foundation Grant.

ECS-82-15181 Study of Time-of-Flight Tomography.

Research support was also received from the following industrial collaborators.

AT&T Corporation, St. Louis, MO,
Biosensor Corporation, Brooklyn Center, MN,
Digital Equipment Corporation, Maynard, MA,
International Business Machines Corporation, St. Louis, MO,
Mead Johnson, Evansville, IN.

III. PERSONNEL

EMPLOYEES

Personnel employed by the Biomedical Computer Laboratory during the period covered by this report were:

Director

Lewis J. Thomas, Jr., M.D., and Associate Director of the Institute for Biomedical Computing, and Associate Professor of Biomedical Computing, Anesthesiology, Cell Biology and Physiology, Biomedical Engineering, and Electrical Engineering

Associate Director

G. James Blaine III, D.Sc., and Associate Professor of Biomedical Computing in the Institute for Biomedical Computing, Associate Professor of Computer Science in Radiology, and Affiliate Associate Professor of Electrical Engineering and Computer Science

Assistant Director

Russell E. Hermes, M.S., and Affiliate Assistant Professor of Electrical Engineering

Senior Research Associates

Jerome R. Cox, Jr., Sc.D., and Professor of Biomedical Computing in the Institute for Biomedical Computing, and Chairman and Professor of Computer Science, and Professor of Electrical Engineering

Harold W. Shipton, C.Eng., and Professor of Biomedical Engineering in the Institute for Biomedical Computing, and Acting Chairman and Professor of Electrical Engineering, and Chairman and Professor of Biomedical Engineering

Donald L. Snyder, Ph.D., and Professor of Biomedical Computing in the Institute for Biomedical Computing, and Professor of Electrical Engineering

Business Manager

Virginia M. Bixon, B.S.

Research Associates

R. Martin Arthur, Ph.D., and Professor of Biomedical Computing in the Institute for Biomedical Computing, and Professor of Electrical Engineering

Kenneth W. Clark, M.S.

Daniel R. Fuhrmann, Ph.D., and Assistant Professor of Electrical Engineering

Kenneth B. Larson, Ph.D., and Research Professor of Biomedical Computing in the Institute for Biomedical Computing, and Research Professor of Neurology (Biomedical Computing), and Research Professor of Biomedical Engineering

James G. Miller, Ph.D., and Professor of Physics, and Associate Director for Biomedical Physics, Laboratory for Ultrasonics, and Research Associate Professor of Medicine
Michael I. Miller, Ph.D., and Associate Professor of Biomedical Computing in the Institute for Biomedical Computing, and Associate Professor of Electrical Engineering
Gregory A. Mohr, Ph.D.
Frederick U. Rosenberger, D.Sc., and Associate Professor of Biomedical Computing in the Institute for Biomedical Computing, and Associate Professor of Electrical Engineering
Arthur W. Toga, Ph.D., and Research Assistant Professor of Neurology
Jonathon S. Turner, Ph.D., and Associate Professor of Computer Science
Raimond L. Winslow, Ph.D., and Assistant Professor of Biomedical Computing in the Institute for Biomedical Computing, and Research Assistant Professor of Ophthalmology

Research Assistants

David E. Beecher, M.S., and Lecturer in Computer Science
Michael A. Brown, M.S.
William P. Hellberg, B.S.
Joanne Markham, M.S., and Research Assistant Professor in Medicine
Stephen M. Moore, M.S.
John M. Ollinger, D.Sc.
Joseph J. Pais, M.A.
David G. Politte, M.S., and Research Assistant in Radiology
Kenneth B. Schechtman, Ph.D., and Assistant Professor of Biostatistics

Graduate Research Assistants

Steven R. Broadstone, M.S.
Mark R. Holland, M.A.
Neophytos Karamanos, B.S.
Mark E. Kaufmann, M.A.
Arun Kumar, M.S.
Stephen K. Liu, M.S.
David R. Maffitt, M.S.
Badrinath Roysam, M.S.
Evren Senol, B.S.
Kurt R. Smith, M.S.

Engineering Assistant

Stanley R. Phillips, A.A.S.

Electronic Technician

Deborah A. Schwab

Administrative Coordinator

Shirley A. Gonzalez-Rubio

Secretaries

Rebecca J. Bozesky
Polly E. Raith

The following members from other departments and divisions have joint appointments with the Biomedical Computer Laboratory to facilitate collaboration and enhance interdisciplinary research:

H. Dieter Ambos, Research Assistant Professor of Medicine (Cardiology)
William M. Hart, Jr., M.D., Ph.D., Professor of Ophthalmology
Rexford L. Hill III, M.S., Associate Professor of Computer Applications in Radiology
John W. Wong, Ph.D., Assistant Professor of Radiation Physics in Radiology

In addition, the following people worked at the laboratory for brief periods:

Gary E. Christensen
Gaurav K. Garg
Jason G. Gutenschwager
Yau-Man Kwan, M.S.
Joseph C. Lawrence, B.S.
Anders W. McCarthy
Tony Mazraani
Kevin E. Mark, B.S.
Frank W. Simcox, B.S.
Gregory M. Tormo
Brian D. Skinner, B.S.
Ellen E. Witte, B.S.
Qiang Wu

RESEARCH COLLABORATORS

During the period covered by this report the following investigators from other laboratories, departments, or institutions, collaborated with BCL staff members on problems of joint interest.

D. R. Abendschein, Ph.D., Medicine
D. I. Altman, M.D., Neurology
H. D. Ambos, Medicine
T. R. Baird, Medicine
D. G. Ballinger, B.S., Radiology
S. R. Bergmann, M.D., Ph.D., Medicine
J. J. Billadello, M.D., Medicine
W. R. Binns, Ph.D., Physics
M. A. Brown, M.B.B.S., Medicine
M. L. Cohen, M.D., Medicine
P. B. Corr, Ph.D., Medicine and Pharmacology
S. R. Devries, M.D., Medicine
R. E. Drzymala, Ph.D., Radiology
J. O. Eichling, Ph.D., Radiology
B. N. Emami, M.D., Radiology

J. W. Epstein, Physics
R. G. Evens, M.D., Radiology
D. C. Ficke, B.S., Radiology
H. L. Fontanet, M.D., Medicine
P. T. Fox, M.D., Neurology and Radiology
M. H. Gado, M.D. Radiology
W. S. Ge, B.S., Electrical Engineering
E. M. Geltman, M.D., Medicine
R. L. Grubb, Jr., M.D., Neurological Surgery
K. A. Hackman, B.S., Radiology
W. B. Harms, B.S., Radiology
W. M. Hart, Jr., M.D., Ph.D., Ophthalmology
P. Herrero, M.S., Medicine
P. Herscovitch, M.D., Neurology and Radiology
D. G. Hirsh, B.A., Office of the Network Coordinator
G. R. Hoffman, B.A., Radiology
J. Howe, Pathology
S. Igielnik, Ph.D., Medical Computing Facilities
M. H. Israel, Ph.D., Physics
A. S. Jaffe, M.D., Medicine
G. C. Johns, B.S., Computer Systems Laboratory
R. G. Jost, M.D., Radiology
M. R. Kilbourne, Ph.D., Radiology
J. Klarmann, Ph.D., Physics
H. A. Klotz, D.Sc., Electrical Engineering
K. E. Krippner, B.S., Radiology
M. P. Land, B.S., Pathology
E. T. Macke, M.S., Computer Systems Laboratory
J. W. Matthews, D.Sc., Computer Systems Laboratory
T. R. Miller, Radiology
M. A. Mintun, M.D., Radiology
C. E. Molnar, Sc.D., Computer Systems Laboratory
S. P. Monthofer, B.S., Radiology
D. W. Myears, M.D., Medicine
R. Nohara, M.D., Medicine
M. V. Olson, Ph.D., Genetics
R. E. Olson, Computer Systems Laboratory
C. A. Perez, M.D., Radiology
J. E. Perez, M.D., Medicine
J. S. Perlmutter, M.D., Neurology
S. M. Pogwizd, M.D., Medicine
W. J. Powers, M.D., Neurology and Radiology
J. A. Purdy, Ph.D., Radiology
M. E. Raichle, M.D., Neurology and Radiology
A. P. Rueter, B.S., Radiology
J. E. Saffitz, M.D., Ph.D., Pathology and Medicine
H. Serota, M.D., Medicine
B. A. Siegel, M.D., Radiology
J. R. Simpson, Ph.D., Radiology
B. E. Sobel, M.D., Medicine
A. W. Strauss, M.D., Pediatrics
S. P. Sutera, Ph.D., Mechanical Engineering
M. M. Ter-Pogossian, Ph.D., Radiology
R. G. Tilton, Ph.D., Pathology
T. O. Videen, Ph.D., Neurology

M. J. Welch, Ph.D., Radiology
D. E. Wexelblat, Pathology
J. R. Williamson, M.D., Pathology
J. W. Wong, Ph.D., Radiology
K. A. Yamada, Ph.D., Medicine
X. Ying, D.Sc., Radiology
J. B. Zimmerman, D.Sc., Radiology and Computer Science

Biosensor Corporation, Brooklyn Center, Minnesota

C. N. Mead, M.D.

Kilo Foundation, St. Louis, Missouri

C. M. Kilo, M.D.

Medical College of Ohio, Toledo, Ohio

S. S. Hancock, M.S.

IV. PHYSICAL RESOURCES

The Biomedical Computer Laboratory (BCL) was formed on April 15, 1964 and the original staff moved into 3,800 square feet (net) of laboratory space at 700 South Euclid Avenue in St. Louis. While remaining at this location, adjacent to the Washington University School of Medicine's main building complex, the floor space has been increased to the present 12,000 square feet (net). In 1984, the establishment of the interschool Institute for Biomedical Computing at Washington University (which encompasses both the BCL and the Computer Systems Laboratory (CSL)), added the 6000 square foot Edward L. Bowles Laboratory located in the fifth-floor addition to Lopata Hall immediately adjacent to the Departments of Computer Science and Electrical Engineering. In addition to the 700 South Euclid and Bowles Laboratory space, BCL staff members and systems frequently occupy other areas within the Washington University Medical Center at the sites of collaborative project activities.

While involved in addressing diverse biomedical problems for which digital computing techniques seemed promising and appropriate, the BCL has acquired the necessary instrumentation and computing resources. Starting with the early development of the Laboratory Instrument Computer (LINC) in the sixties and the Programmed Console in the early seventies, the BCL has applied computing systems and specialized instrumentation in collaborative research projects in biological modeling and algorithm development. Current computer resources include: Digital Equipment Corporation MicroVAX-II's, MASSCOMP Corporation SuperMicrocomputers, and personal-computer class microcomputers such as the Apple MacIntosh and IBM PC/AT. Biomedical imaging is supported by an MMS-X stroke graphics display system developed by the CSL, raster graphics display stations from Lexidata, MASSCOMP, and Digital Equipment Corporation, and a Datacopy reflectance camera for image acquisition.

Within the Resource, terminal access to computer systems is provided by TERRANET, a Resource developed local area network. Two thirty station TERRANET's support terminals and computers located throughout the laboratory space. Laboratory computer systems are connected by an Ethernet local area network. Internetwork communication between other departmental networks is provided via connections to the Mallinckrodt Institute of Radiology PACS network, and the Biomedical Research network (supported by a special instrumentation grant) currently being installed throughout both Washington University campuses. The networks provide resource personnel access to a broad spectrum of computing equipment, imaging modalities, and other services such as electronic mail.

A machine shop and reference room are located at the 700 South Euclid address and are shared with the CSL. Other physical resources include a well-stocked electronics shop, a large inventory of electronic and computer test equipment, microprocessor development systems, analog and digital recording instruments, and photographic supplies and equipment.

V. RESEARCH PROJECTS

Introduction

The research program of the Biomedical Computer Laboratory (BCL) is organized into six major project areas with the staff grouped into teams whose interests are focused correspondingly. Because of the emphasis of the Laboratory's activities in the area of information extraction from quantitative biomedical images, that category is divided into three sections, each dealing with a different imaging modality (positron-emission tomography, ultrasonic tissue characterization, and radiation-treatment planning). A total of 42 distinct project activities are grouped into the six project areas briefly summarized below. More specific summaries are given at the beginning of each of the project-report subsections.

For positron-emission tomography, work in support of applications and system improvements have continued on several fronts, but the main thrust of BCL activities has been in research on algorithms. Emphasis has been on application of the maximum-likelihood method for improving image quality and for achieving better estimates of physiological parameters through studies of dynamic distributions of tracers. Fundamental limitations in the use of the maximum-likelihood method for image reconstruction have been identified. Efforts to find sound ways to overcome those limitations are yielding results which show promise for reducing the artifacts that have plagued those applying the estimation-maximization algorithm to image reconstruction.

The work in ultrasonic tissue characterization emphasizes the interpretation of backscattered ultrasonic energy to achieve quantitative estimates of tissue properties, including anisotropy and the state of contraction of cardiac and skeletal muscle, while parallel efforts are directed toward design of a system to employ adaptive beamforming for backscatter measurements.

Work in radiation treatment planning continues to move ahead with enhancements and evaluations of our "delta volume" algorithm for three-dimensional absorbed-dose calculations, and display experiments employing high-performance stroke graphics for three-dimensional displays. New work now focuses on the physics of high-energy photon-dose deposition in heterogeneous media and on the development of a new method for quantitative treatment verification.

Ischemic heart disease and ECG analysis continues to be a major category of research activity, but the development of new algorithms for ECG processing has been discontinued, although some attention continues on exportation of the latest version of our "Argus" algorithm. Separate support is being sought for completing a clinical-event database for evaluating ambulatory ECG-monitoring systems. In the area of ischemic heart disease, more prominent are modeling, signal processing, and data analysis work in collaboration with the division of Cardiovascular Medicine as part of their broad program addressed to ischemic heart disease.

Systems for Specialized Biomedical Studies embraces a variety of projects that are less broad in scope either because they are in an earlier stage of development or because the nature of the work is necessarily more

specialized. The biomedical-imaging theme is well represented in this section, especially in the area of electron-microscopic autoradiography and automated image segmentation. Other work continues on DNA restriction mapping and new explorations have started in electron-microscopic stereopsis.

Projects under Resource Development Activities are directed toward improving the Laboratory's capabilities for addressing the needs of multiple research studies involving various facets of biomedical imaging. To that end, a now dominant and integrating activity is the development of a distributed facility for image presentation, analysis and quantification (IPAQ). Components of the IPAQ project include (1) the enhancement of our computational capabilities to support the development of computationally demanding algorithms for information extraction from multi-dimensional measurement data, (2) the establishment of a coherent software environment which incorporates a set of internally consistent software tools, image data formats and display methodologies, (3) the extension of our digital communication capabilities to include the sites of collaborators' data sources and information destinations, and (4) the exportation of specialized, tailored subsystems and/or satellite workstations which may incorporate custom-designed, very-large-scale integrated (VLSI) circuits in order to achieve practical realizations of especially demanding computations.

Individual Projects

A. Quantitative Imaging: Positron-Emission Tomography

Stimulated by the clinical impact of the EMI transmission tomographic scanner in 1973, experimental studies were initiated in collaboration with the Division of Radiation Sciences to evaluate positron concidence-detection as a method for emission reconstruction tomography. This collaborative activity resulted in a prototype scanner called PETT (Positron-Emission Transaxial Tomograph). Extensive studies in patients and animals were conducted with the PETT III scanner in collaboration with the divisions of Neurology and Cardiology. A subsequent scanner, PETT IV, utilized concepts developed with its predecessor but incorporated a novel technique for the simultaneous collection of four tomographic slices from a single set of detectors. Until its decommissioning three years ago, PETT IV was located in the Coronary Care Unit for use in the SCOR project for the quantification of regions of myocardial ischemia and infarction. Subsequent scanners have been developed that permit more rapid data collection and improved spatial resolution. One of these, PETT V, was used in experimental studies in dogs. PETT VI became operational during the summer of 1980 and employs fast detectors and an entirely circular motion. This tomograph was used in experimental studies in dogs (A-1) and in brain blood-flow studies (A-4). Developments in crystal technology and high-speed electronics now permit the propagation time of each of the two photons created in an annihilation to be measured. Theoretical and experimental studies of tomography systems that utilize this additional information continued, and the software and hardware needed to realize the predicted benefits have been developed. Super PETT I, the first operational system utilizing time-of-flight information, has been in routine use in the Coronary Care Unit for over two years now (A-1 to A-3). This tomograph was also used for the collection of experimental data used for the evaluation of reconstruction algorithms (A-5). A second generation time-of-flight tomograph, Super PETT II, for head and body scans has been developed and has now been moved to the Division of Radiation Sciences eventually to replace PETT VI. Studies to improve data acquisition and reconstruction algorithms for Super PETT I and Super PETT II continued during the year (A-6 to A-8). This work includes the identification of previously unrecognized fundamental limitations in the use of the maximum-likelihood technique for image reconstruction and in sound ways to overcome these limitations (A-6). The study of novel processing architectures for producing image reconstructions in clinically useful times continued (A-9, A-10). A new study was initiated of a positron-emission tomograph having a spherical geometry for imaging radionuclides in human infants (A-11).

A-1. PETT Experimental Studies

Personnel: S. R. Bergmann, M.D., Ph.D., Medicine
M. A. Brown, M.B.B.S., Medicine
P. Herrero, M.S., Medicine
J. Markham, BCL
D. W. Myears, M.D., Medicine
B. E. Sobel, M.D., Medicine
M. J. Welch, Ph.D., Radiology

Support: RR 01380
HL 13851
HL 17646

The overall aim of this project is to implement and evaluate procedures required to translate into intact animals the results obtained with selected positron-emitting tracers used to characterize myocardial metabolism and perfusion in isolated hearts and anesthetized, open-chest dog studies performed with the Isolated Probe Data Acquisition System (IPDAS) (E-2). Utilizing positron-emission tomography with PETT VI, the distribution of tracers and the time course of their uptake and clearance from myocardium can be quantified. Such studies are intimately related to the clinical studies using positron-emission tomography (A-2).

Although PET with ^{11}C-palmitate delineates infarct size and permits qualitative assessment of fatty acid utilization, quantification of oxidative metabolism in ischemia and reperfusion is limited by the complex alteration in the patterns of utilization of fatty acid and glucose. Because metabolism of acetate by myocardium is less complex than that of glucose or palmitate, we evaluated the kinetics of radiolabeled acetate in isolated rabbit hearts perfused with modified Krebs-Henseleit buffer. The steady-state extraction fraction of acetate averaged 61.5 ± 4% in control hearts, increased to 93.6 ± 0.9% in hearts rendered ischemic, and was 54.8 ± 4.0% in hearts reperfused after 60 minutes of ischemia. Oxidation of acetate, assessed from the rate of efflux of radiolabeled CO_2 in venous effluent and by clearance of ^{11}C-acetate measured externally with IPDAS correlated closely with the rate of oxygen consumption under diverse metabolic conditions (r=0.97).

After these initial studies in isolated perfused hearts were completed, we characterized with PET the response of myocardial oxidative and fatty acid metabolism in 5 dogs reperfused after one hour of LAD coronary artery occlusion. Serial images were acquired after ^{11}C-acetate and ^{11}C-palmitate administered in a random order. The rapid phase of clearance was calculated by multi-exponential curve fitting of partial volume and spillover corrected data. Clearance from normal myocardium was 4.4 ± 1.8 minutes after ^{11}C-acetate and 10.2 ± 7.3 minutes after ^{11}C-palmitate. In reperfused myocardium the $t_{1/2}$ were 10.8 ± 2.9 and 39.4 ± 23.9 minutes, respectively, despite flow that was 138 ± 47% of normal. Thus, during reperfusion, overall oxidative capacity is impaired by approximately 60% and fatty acid metabolism is effected to an even greater degree. Externally detectable clearance of ^{11}C-acetate provides a quantitative index of myocardial oxidative metabolism despite variation in the patterns of intermediary metabolism that confound interpretation of

results with conventionally used tracers such as ^{11}C-glucose, ^{18}F-deoxyglucose or ^{11}C-palmitate.

In the past year, we have made considerable progress in quantitation of myocardial blood flow (MBF) with $H_2{}^{15}O$. Measurement of MBF in absolute terms with PET has been limited by motion, partial volume, and spillover effects. Using a cardiac phantom we validated corrections for these with an analytical technique based on convolution of the tomographic point spread function with the measured dimensions of the phantom. Correction for these errors can be derived based on the assumptions that the point spread function in one dimension is Gaussian and that the activity in blood pool and tissue are uniformly distributed. Analytical profiles were obtained by convolving a cylinder (for blood pool) and an annulus (for tissue) of uniform activity with the point spread function. These profiles were compared with PET reconstructions of a heart phantom. Correlation was excellent. Integrations of the profiles were used to yield recovery coefficients and spillover fractions. For a blood pool radius of 17 mm and a myocardial wall thickness of 10 mm, 59% of the tissue counts were recovered while 27% of the counts spilled into the blood pool. Conversely 87% of blood pool counts were recovered while 13% of the counts spilled into myocardium. Subsequently, MBF was quantitated in 6 dogs with myocardial ischemia and in 6 healthy, normal human volunteers. After an intravenous bolus of $H_2{}^{15}O$, data was acquired for 90 seconds and time-activity curves in the left ventricular and myocardial regions of interest were fitted to a one-compartment model. In dogs, absolute MBF measured with PET correlated closely with microsphere-determined MBF ($r=0.96$) with flows ranging from 0.18 - 2.02 ml/gm/min. In humans, MBF at rest averaged 1.01 ± 0.34 ml/gm/min and increased more than threefold with dipyridamole. Thus, absolute MBF can be obtained with $H_2{}^{15}O$ and PET if appropriate corrections are made for motion, partial volume, and spillover effects. Use of this technique should aid in assessment of cardiac disease and their response to therapeutic interventions.

Our major goal in the coming year is to evaluate whether recovery of function after reperfusion correlates with recovery of oxidative metabolism detectable noninvasively with ^{11}C-acetate. We will continue to refine our technique for partial volume and spillover corrections, and hope to evaluate the influence of cardiac motion on quantitative recovery of PET data.

Results for the past year provide a foundation for the use of ^{11}C-acetate as a marker of myocardial oxidation. Development and refinement of these techniques for assessment of myocardial perfusion and metabolism with positron-emitting tracers provides the foundation for interpretation of the clinical tomographic studies.

A-2. Super PETT I Cardiac Studies

Personnel: E. M. Geltman, M.D., Medicine
H. D. Ambos, Medicine
T. R. Baird, Medicine
D. E. Beecher, BCL
A. S. Jaffe, M.D., Medicine
J. Markham, BCL
B. E. Sobel, M.D., Medicine
M. M. Ter-Pogossian, Ph.D., Radiology
M. J. Welch, Ph.D., Radiology

Support: RR 01380
HL 13851
HL 17646

This project is designed to characterize regional myocardial metabolism and perfusion quantitatively with positron-emission tomography (PET) in normal subjects and patients with coronary artery disease at rest and in response to stress induced with vasodilators or dynamic exercise. It is designed also to assess the efficacy of reperfusion induced by thrombolysis, balloon angioplasty, surgical revascularization, and combinations of the three reflected by myocardial perfusion and metabolic activity.

The development of a method for the accurate noninvasive assessment of myocardial perfusion with $H_2{}^{15}O$ and PET has been a major focus of this project. Since the initiation of this project, extensive studies have been carried out to determine the optimum protocol for patient positioning and restraint, administration of tracer, data acquisition, and data processing. During this interval 64 subjects (47 males and 17 females) aged 26 to 83 years (mean 53.7) were studied. Coronary artery disease was documented in 46 of these 64 patients. Studies were performed in the resting state exclusively in 24 subjects and before and after dipyridamole infusion in 40. The administered dose of $H_2{}^{15}O$ ranged from 20 to 170 mCi (mean 77.8 mCi) and 0.29 to 1.98 mCi/kg. $H_2{}^{15}O$ was administered as a bolus, a constant infusion, or a bolus followed by an infusion. Data collection and processing intervals varied from 40 seconds to 5 minutes. The protocol ultimately utilized in the final test-set of patients and controls was predicated on the optimum balance between instrument performance (avoidance of saturation of detectors and data transfer rates), dosimetry, counting statistics, image quality, and brevity of data collection to minimize problems related to recirculation of tracer. Twenty-three subjects (9 normal volunteers and 14 patients with coronary artery disease) were studied to determine the sensitivity and specificity with which this noninvasive technique can identify patients with angiographically documented coronary artery disease. All subjects were studied at baseline and after intravenous infusion of dipyridamole. At rest, the myocardial region demonstrating the lowest relative $H_2{}^{15}O$ activity exhibited 71 ± 2.7% of counts in the region with peak activity in the control group and 60 ± 4.6% of peak counts in the patient group ($p < .05$). After dipyridamole stress, differences distinguishing the two groups became particularly clear. In the control group, activity in the region demonstrating the lowest relative radioactivity averaged 77 ± 1.5% of that in the region with

peak activity whereas in the patient group counts in the region demonstrating the lowest relative activity averaged 51 ± 5.9% of that in the region with peak activity ($p < .01$). There was a clear separation between the two groups with little overlap. With a retrospectively determined lower limit of normal, the two groups could be separated with a sensitivity of 86% and a specificity of 100%. In addition, in 13 of the 14 studies from individuals with coronary artery disease, the region of lowest relative perfusion corresponded anatomically to the area of myocardium distal to a stenosed vessel. Thus, the technique developed with ^{15}O labeled water and PET can noninvasively identify patients with coronary artery disease with high sensitivity and specificity. With the implementation of a method for absolute quantification of myocardial perfusion which we have recently developed, critical evaluation of interventions designed to improve coronary blood flow should be possible.

Previous studies outlined in earlier progress reports have demonstrated the feasibility of employing dynamic high-resolution positron-emission tomography for the delineation of regional myocardial metabolism and perfusion. We have previously evaluated the effects of pharmacologic interventions with thrombolytic agents and calcium channel blockers on myocardial viability detected tomographically with ^{11}C-palmitate. In addition, we have been studying the effects of long-term endurance exercise training on regional myocardial metabolism and perfusion. Normal myocardium preferentially utilizes exogenous free fatty acids during oxidative metabolism at rest and during pacing stress. However, myocardial utilization of unaltered fatty acids has not been characterized after dynamic exercise in humans. Accordingly, 5 normal subjects and 8 patients with coronary artery disease were studied with dynamic positron-emission tomography and ^{11}C-palmitate before and after upright bicycle exercise. In normal subjects, clearance of ^{11}C-palmitate was homogeneous at rest and after maximal exercise. In contrast, in each subject, the half-time of ^{11}C-palmitate clearance increased substantially from 22.5 ± 2.6 (SEM) minutes to 75.6 ± 31.1. Among patients, the half-time also increased in each after exercise from 21.6 ± 2.1 to 65.4 ± 21.3. Plasma glucose, glycerol, and free fatty acid concentrations did not change with exercise, but lactate increased from 1.1 ± 0.1 to 9.9 ± 2.9 μM/ml. Thus, clearance of ^{11}C-palmitate is markedly delayed after dynamic exercise in both normal subjects and patients with coronary artery disease, probably reflecting mobilization of endogenous myocardial lipids or utilization of alternative substrates. Studies are continuing in this area to determine the effects of submaximal compared to maximal exercise and to assess the dynamics of regional myocardial metabolism in trained versus untrained subjects.

Studies in progress are designed to characterize the dynamics of accumulation of $H_2{}^{15}O$ in normal subjects and in patients with coronary artery disease. Initial experiments were designed to characterize regional dynamic time activity curves with respect to one and two compartment Kety-Schmidt models in experimental animals and in patients. Data are being compared with results of quantitative coronary angiography with instrumentation signature-analysis techniques. Clinical studies are designed to characterize the dynamics of labeled fatty acid and labeled acetate deposition and clearance from myocardium of normal subjects, patients with chronic stable ischemic heart disease, and patients with acute myocardial infarction with and without reperfusion induced by coronary thrombolysis with t-PA or percutaneous transluminal coronary

angioplasty. Initial results indicate that myocardial accumulation and clearance of ^{11}C-palmitate are homogeneous in normal subjects and that clearance is delayed in zones of recent ischemia. Zones of remote infarction exhibit depressed accumulation of tracer. Uptake and clearance of ^{11}C-acetate appear to parallel myocardial oxygen utilization closely.

The approach under development should permit noninvasive delineation of altered regional myocardial metabolism and perfusion in patients with functionally significant coronary artery disease. During the past year we have established the utility of positron-emission tomography for objective assessment of interventions designed to salvage ischemic myocardium. In addition, we have validated a method for assessment of myocardial perfusion at rest and with vasodilator stress employing the freely diffusible tracer, $H_2{}^{15}O$, that permits noninvasive assessment of myocardial perfusion without distortion resulting from changes in myocardial metabolism.

A-3. Corrections for PET Cardiac Studies

Personnel: J. Markham, BCL
S. R. Bergmann, M.D., Ph.D., Medicine
P. Herrero, M.S., Medicine

Support: RR 01380
HL 17646

Previous studies have demonstrated that myocardial blood flow measured with the positron-emitting tracer $H_2{}^{15}O$ correlates well with estimates of blood flow obtained with radiolabeled microspheres when the arterial input function is known and tissue radioactivity is sampled directly. The one-compartment Kety-Schmidt model can be extended for noninvasive measurement of myocardial blood flow with positron-emission tomography (PET) if radioactivity in the blood and myocardium are known. However, measurement of tracer concentration in the left ventricular blood pool and myocardial tissue with PET are subject to errors due to partial volume effects, apparent loss of activity when imaging an object small with respect to the resolution of the tomograph, and activity spillover, apparent smearing of activity into adjacent regions, as well as cardiac and respiratory motion. Regional corrections for partial volume and spillover errors can be derived based on the assumptions that the reconstructed point-spread function in one dimension is Gaussian and that activity in the blood pool and tissue are uniformly distributed. Analytical profiles were obtained by convolving a disk, representing the blood pool, and an annulus, representing the left ventricle, of uniform activity with the point-spread function measured experimentally. Correlation of these profiles with PET reconstructions of a heart phantom were excellent. Integrations of the profiles were used to yield regional recovery coefficients and spillover fractions. For a blood pool radius of 15 mm and a myocardial thickness of 10 mm, 59 percent of the tissue activity was recovered while 27 percent of the activity spilled into the blood pool. Approximately 87 percent of the

blood pool activity was recovered while 13 percent of this activity spilled into the tissue region.

Myocardial blood flow was estimated from PET images, corrected for partial volume and spillover errors, for fourteen different regions in seven different dogs. Correlations between PET estimates of flow and estimates obtained from microspheres and tissue samples were good in eleven of the regions. Estimates of flow could not be obtained for three ischemic regions where activity curves had large errors due to spillover of activity from surrounding normal tissue and decreased activity levels associated with low flows. Future work will seek to determine if this limitation can be overcome by additional corrections or by improving estimates of regional tissue activity.

A-4. In Vivo Measurements of Regional Blood Flow and Metabolism in the Brain

Personnel: M. E. Raichle, M.D., Neurology and Radiology
D. I. Altman, M.D., Neurology
D. C. Ficke, B.S., Radiology
P. T. Fox, M.D., Neurology and Radiology
R. L. Grubb, Jr., M.D., Neurological Surgery
P. Herscovitch, M.D., Neurology and Radiology
M. R. Kilbourn, Ph.D., Radiology
K. B. Larson, BCL
J. Markham, BCL
M. A. Mintun, M.D., Radiology
J. S. Perlmutter, M.D., Neurology
W. J. Powers, M.D., Neurology and Radiology
M. M. Ter-Pogossian, Ph.D., Radiology
M. J. Welch, Ph.D., Radiology

Support: RR 01380
HL 13851
HL 25944
NS 06833
ECS 8215181
Washington University

Because of the previously noted (PR 21, D-3; PR 22, D-4) deficiencies of compartmental models for estimating cerebral blood flow with PET using radioactive water as a tracer, we have been led to the formulation and testing of distributed-parameter models for this purpose. The distributed-parameter models we have investigated take into account longitudinal gradients of tracer concentration along the capillaries but assume that transverse gradients are zero. The resulting conservation conditions take the form of sets of partial differential equations in the concentrations, with axial distance and time as independent variables and with capillary and cellular permeabilities, surface areas, volumes, and thermodynamic-activity coefficients as parameters. We have obtained

analytical solutions for the conservation equations in the form of unit-impulse and unit-step responses suitable for simulations of dynamic residue-detection data.

Encouraged by close agreement between our model predictions and external counting-rate data obtained in animal experiments [1] (PR 21, D-3; PR 22, D-4), we have continued with our investigations of the possibility of applying our distributed-parameter model for measurement of cerebral-blood flow (CBF) in patients using positron-emission tomography (PET). Measurements of brain- and arterial-radioactivity histories required to implement our model were obtained following the rapid intravenous injection of $H_2{}^{15}O$. The PET VI tomograph was used to collect cerebral count data in sequential time frames of 10 or 20 sec over a 4-min period. Blood samples drawn every 4 to 5 sec were used to construct the arterial time-activity curves. These were convolved numerically with the step response for a capillary-tissue unit of our model, and the resulting scan simulations were fit to the sequential PET-scan data using weighted nonlinear least-squares approximation. Best-fit regional parameter estimates were obtained for CBF, permeability-surface-area product (PS) of the blood-brain barrier, diffusive conductance in tissue, and extravascular volume. The local arrival time, t_0, of the arterial input in relation to the time of radiotracer injection was also included as a parameter. Computed data for representative gray- and white-matter regions are tabulated below:

	CBF, ml/(min hg)	PS, ml/(min hg)	t_0, sec
Parietal gray matter	71	71	10.12
Insular gray matter	66	131	8.02
White matter	41	54	9.43

The estimates of regional PS for water are similar to those obtained with $H_2{}^{15}O$ and ^{11}C-butanol as a freely diffusible reference tracer [2]. Our approach provides a more realistic model for CBF measurements and also permits the calculation of other parameters of physiologic interest. An additional advantage provided by our model is that it remains valid for tomographic data collected later than the 40-sec limit [3] imposed by the Kety model, and can thus lead to statistically improved parameter estimates even for tomographs unable to operate at the high counting rates achievable with advanced PET devices.

1. Larson, K. B., Markham, J., and Raichle, M. E., "Tracer-Kinetic Models for Measuring Cerebral Blood Flow Using Externally Detected Radiotracers," Journal of Cerebral Blood Flow and Metabolism (in press).

2. Herscovitch, P., Raichle, M. E., Kilborne, M. R., and Welch, M. J., "Measurement of Cerebral Blood Flow and Water Permeability with Positron-Emission Tomography Using O-15 Water and C-11 Butanol," Journal of Cerebral Blood Flow and Metabolism, 5:S567-S568, 1985.

3. Raichle, M. E., Martin, W. R. W., Herscovitch, P., Mintun, M. A., and Markham, J., "Brain Blood Flow Measured with Intravenous $H_2{}^{15}O$. II. Implementation and Validation," Journal of Nuclear Medicine, 24:790-798, 1983.

A-5. Study of the Use of Maximum-Likelihood Image Reconstruction for Super PETT I Phantom Data

Personnel: D. G. Politte, BCL
S. K. Liu, BCL
J. Markham, BCL
D. L. Snyder, BCL
L. J. Thomas, Jr., BCL

Support: RR 01380

In this study we have tested simultaneously several of the recent developments in image reconstruction of time-of-flight positron-emission tomography data with the expectation-maximization (EM) algorithm. These developments include speeding the computations by performing the calculations in a rotated coordinate system (A-7) and incorporating constraints which the estimates must satisfy, to suppress the noise and edge artifacts which appear when unconstrained maximum-likelihood estimation is used (A-6).

The circular voids of the Lucite phantom shown in Figure 1 were filled with oxygen-15 water. The phantom was assembled, inserted into the patient opening of Super PETT I and scanned for 15 minutes.

Software which was developed previously (PR 22, D-3) was used to retain data with 96 quantized angles instead of the usual 16 used in the reduced-angle reconstruction algorithm (PR 22, D-7). The data were precorrected for photon attenuation and random coincidences in the usual manner using data from the transmission and blank scans.

Images were reconstructed in a rotated coordinate system using the confidence-weighting (CW) and EM algorithms. Artifact-suppression constraints were incorporated into the EM algorithm; this involved the use of a resolution kernel, which suppresses the edge overshoots, and a sieve kernel, which suppresses the noise artifact. The widths of these circularly symmetric kernels were systematically varied to assess qualitatively their effect on the two artifacts. We found that a proper combination of the two kernels can eliminate both artifacts simultaneously while preserving resolution identical to or slightly better than that of the CW images.

In the future we plan to include the attenuation and randoms corrections internal to the EM algorithm instead of precorrecting the data. This should result in a more accurate estimate of the radioactivity distribution.

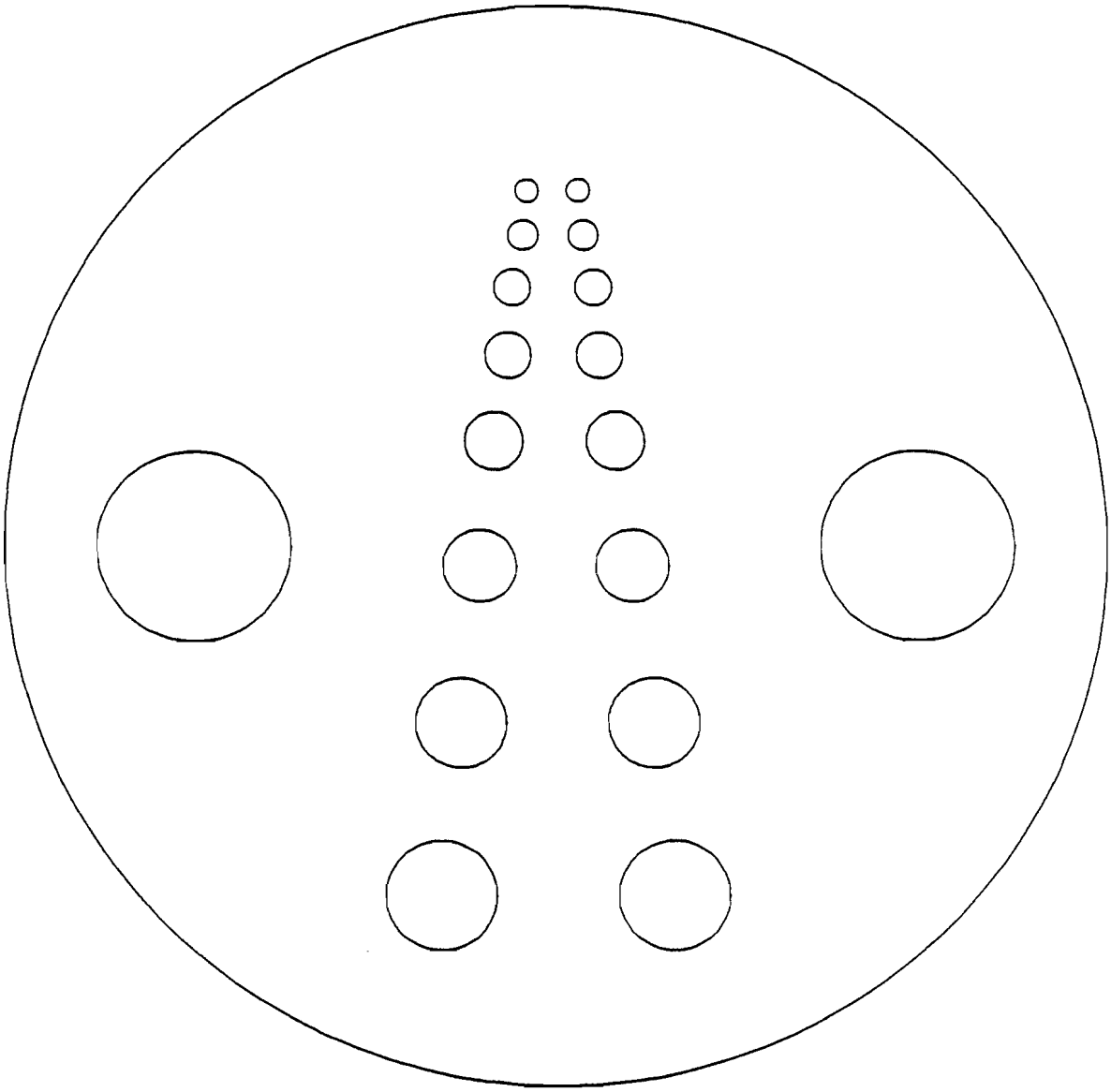

Figure 1. Lucite phantom used in project A-5. The circles (with the exception of the outer circle) represent voids which were filled with 0-15 water. The outer diameter of the phantom is 21.6 centimeters. The diameter of the smallest void is 4.7 millimeters; the two largest voids on either side have diameters of 38 millimeters. The large voids are useful for testing the edge- and noise-artifact suppression techniques. The smallest voids are useful for estimating the resolution of the reconstructed images.

A-6. Noise and Edge Artifacts in Maximum-Likelihood Reconstructions for Emission Tomography

Personnel: D. L. Snyder, BCL
G. J. Blaine, BCL
S. K. Liu, BCL
M. I. Miller, BCL
D. G. Politte, BCL
K. R. Smith, BCL
L. J. Thomas, Jr., BCL

Support: RR 01380

Images produced in emission tomography with the expectation-maximization algorithm have been observed to become more noisy and to have large distortions near edges as iterations proceed and the images converge toward the maximum-likelihood estimate. It is our conclusion that these artifacts are fundamental to reconstructions based on maximum-likelihood estimation as it has been applied usually; they are not due to the use of the expectation-maximization algorithm, which is but one numerical approach for finding the maximum-likelihood estimate. We have developed a mathematical approach for suppressing both the noise and edge artifacts by modifying the maximum-likelihood approach to include constraints which the estimate must satisfy [1].

1. Snyder, D. L., Miller, M. I., Thomas, Jr., L. J., and Politte, D. G., "Noise and Edge Artifacts in Maximum-Likelihood Reconstructions for Emission Tomography," IEEE Transactions on Medical Imaging (in press).

A-7. Investigation of Methods for Speeding Maximum-Likelihood Image Reconstruction with the EM Algorithm

Personnel: S. K. Liu, BCL
G. J. Blaine, BCL
S. M. Moore, BCL
D. G. Politte, BCL
D. L. Snyder, BCL
L. J. Thomas, Jr., BCL

Support: RR 01380

Several methods for speeding maximum-likelihood image reconstruction with the expectation-maximization (EM) algorithm have been incorporated into our software and tested extensively during the past year. These techniques are listed below:

Rotated coordinates - Performing the computations in a rectilinear coordinate system which is rotated such that one of the axes is

parallel to the photon flight-lines at each angle confers two advantages. First, the two-dimensional convolutions required in the algorithm are simplified because one of the functions being convolved, an asymmetric Gaussian, is separable in the rotated system; the two-dimensional convolutions can be equivalently implemented as two cascaded one-dimensional convolutions. Second, it is possible to decrease the sampling density on the axis parallel to the photon flight-lines and still maintain adequate sampling because the measurement error of the scanner is much broader along this axis than transverse to it. This allows the one-dimensional kernel along this axis to be represented by fewer samples.

Linear line search - This technique computes a new estimate of the radioactivity distribution by forming a linear combination of two estimates computed previously by the usual algorithm. The combination is selected to maximize the likelihood at this step.

All of these techniques were tried on simulated data with parameters consistent with the Super PETT I device. Image quality was evaluated using metrics such as signal-to-noise ratio in selected regions of the image, resolution, likelihood, and the Kullback-Leibler information-divergence. The new approaches achieve image quality that is at least as good as the previous implementations but with a factor of twenty reduction in the computation time [1].

1. Liu, S. K., "Efficient Computation of the EM Algorithm in Time-of-Flight Positron-Emission Tomography," Master of Science Thesis, Washington University, BCL Monograph No. 485, 1987.

A-8. Implementation of the Weighting Algorithm for Dynamic Tracer Studies

Personnel: J. M. Ollinger, BCL
K. A. Hackman, B.S., Radiology
J. Markham, BCL
M. A. Mintun, M.D., Radiology
D. L. Snyder, BCL

Support: RR 01380
NS 06833

The development of methods for maximum-likelihood estimation of parameters in dynamic tracer studies using either positron-emission tomography (PET) list-mode or projection data has been completed (PR 22, D-11; PR 23, A-1, A-2). The basic method utilizes the expectation-maximization (EM) algorithm of Dempster, Laird, and Rubin [1] and consists of two algorithms, a weighting algorithm which estimates a histogram of activity levels and a parameter-estimation algorithm which computes parameter estimates from the histograms [2,3]. Extensive testing has

demonstrated that, for simulated data, the weighting algorithm generates histograms with much less noise than the standard approach and the parameter-estimation algorithm yields parameter estimates which are significantly more accurate.

Efforts in the past year have been directed toward implementation of the algorithms for real PET data. The weighting algorithm has been implemented for use with PETT VI projection data and is being tested with phantom data. Preliminary results suggest that the histograms generated from phantom data are less noisy than those generated by the standard approach and that the method does not degrade resolution. Application of the weighting algorithm to list-mode PET data has begun and will require substantial effort in the next year.

1. Dempster, A. P., Laird, N. M., and Rubin, D. B., "Maximum Likelihood from Incomplete Data via the EM Algorithm," Journal of the Royal Statistical Society, 39(1):1-38, 1977.

2. Ollinger, J. M., "Algorithms for Parameter Estimation in Dynamic Tracer Studies Using Positron-Emission Tomography," Doctoral Dissertation, Washington University, BCL Monograph No. 476, August 1986.

3. Ollinger, J. M., "Estimation Algorithms for Dynamic Tracer Studies Using Positron-Emission Tomography," IEEE Transactions on Medical Imaging, MI-6(2):115-125, June 1987.

A-9. Investigation of the Use of Residue-Number Arithmetic for a High Speed Implementation of the EM Algorithm for PET

Personnel: H. A. Klotz, D.Sc., Electrical Engineering
D. L. Snyder, BCL

Support: Washington University

A special-purpose hardware-architecture is proposed to implement the expectation-maximization algorithm to compute, in clinically useful times, the maximum-likelihood estimate of a radionuclide distribution for a positron-emission tomograph having time-of-flight measurements [1]. Two-dimensional convolutions required for forming the estimate are converted into a series of one-dimensional convolutions which can be evaluated in parallel. Each one-dimensional convolution is evaluated using a number-theoretic transform. All numerical calculations are performed using finite-field arithmetic. In order to avoid the use of large finite fields and to increase parallelism, each convolution is performed by a series of convolutions with small digits in a Galois field. The hardware architecture allows a two-dimensional convolution of dimension N by N to be formed with O(N) operations, permitting one iteration of the expectation-maximization algorithm to be formed in approximately 100 milliseconds when N=128 and the number of view angles is 32.

1. Klotz, Jr., H. A., and Snyder, D. L., "A Hardware Architecture Using Finite-Field Arithmetic for Computing Maximum-Likelihood Estimates in Emission Tomography," Electronic Systems and Signals Research Laboratory Report, Washington University, 1987.

A-10. Mapping the EM Algorithm onto Parallel Architectures

Personnel: K. R. Smith, BCL

Support: RR 01380

Methods for accelerating the computation of the expectation-maximization (EM) algorithm have been under intense investigation in recent years. This interest motivated a study which consists of mapping the EM algorithm onto parallel architectures [1]. Participation at a parallel computation workshop at the University of Colorado allowed us to experiment with several machines.

The initial thrust of the study was to identify three parallel architecture classes: network-centered, bus-centered, and processor-centered, and to subsequently discover the type of computing algorithms which best map onto these different types of architectures. Scrutiny of the EM algorithm shows the following possible partition points: 1) partition by angle, and 2) partition by pixel. Using these two parallel algorithms, the EM algorithm has been mapped onto a number of different parallel architectures which sufficiently represent the three architectural classes identified earlier. The calculations were all performed in the (x,y) coordinate system (in contrast with A-7) on deterministic data. Timing estimates for these mappings are tabulated below:

Processor	Class-ification	Computation Time (Iteration)	Communication Time (Iteration)	Total Time (Iteration)	Convergence Time*
MASSCOMP MC55020	Fast, Sequential Processor	-	-	14 min	23.3 hr
Mercury ZIP 3232	Pipeline Array Processor	-	-	11 min	18.3 hr
NCR GAPP**	Systolic Array Processor	2.4 sec	20 msec	2.4 sec	4 min
NCUBE** (512 k RAM)	Hypercube MIMD Parallel Processor	12.5 sec	4.5 sec	17 sec	28 min
InMOS Transputer T800**	Mesh MIMD Parallel Processor	6.25 sec	2.8 sec	9 sec	15 min
Multiple TMS320C30 DSPs**	Custom MIMD Parallel Processor	14.4 sec	1.7 sec	16.1 sec	26 min

* Note 1 - Convergence time is based on 100 iterations of the EM algorithm.
** Note 2 - The iteration times on the GAPP, NCUBE, Transputer, and Multiple DSPs are estimates based on simulations.

Future plans for this research are quite varied. We plan to map the newest version of the EM algorithm onto a shared memory parallel computer called the Alliant in August of 1987. On a more imaginative note, the possibility of designing a 16 node TMS320C30 multiprocessor for the backplane of the MicroVAX is appealing and realistic. Work continues with the GAPP architecture and the possibilities therein. Also, designing a parallel-pipelined VLSI chip based on [2] is a realistic long-term goal.

1. Smith, K. R., "Mapping the EM Algorithm for Time-of-Flight Positron Emission Tomography onto Parallel Architectures," BCL Monograph No. 484, Washington University, May 1987.

2. Klotz, Jr., H. A., and Snyder, D. L., "A Hardware Architecture Using Finite-Field Arithmetic For Computing Maximum-Likelihood Estimates in Emission Tomography," Electronic Systems and Signals Research Laboratory Report, Washington University, 1987.

A-11. Preliminary Studies for a Spherical PET Instrument

Personnel: K. R. Smith, BCL
G. J. Blaine, BCL
D. G. Politte, BCL
D. L. Snyder, BCL
L. J. Thomas, Jr., BCL

Support: RR 01380

Interest in a spherical positron-emission tomography (SPET) instrument was initiated in August of 1986. The subject of interest for SPET evolved from neonates to small primates to the current interest in full-sized subjects (i.e. 20 cm). Motivation for SPET is the possibility of full three-dimensional viewing, smaller resolution, and improved signal-to-noise ratio. Several important research topics have been identified as feasibility studies. Following are the current topics of research:

1) detector geometry,
2) sampling density,
3) a three-dimensional EM reconstruction algorithm, and
4) scatter-correction studies.

Each of these topics has been researched in the last year with encouraging results. The detector geometry poses a difficult but very interesting problem. Methods for positioning detectors on the sphere have been studied using mathematical techniques from geodesic-dome design, hereafter referred to as "geodesic math", and also using a physical phenomena known as spherical harmonics. We have found that the method using spherical harmonics does not lend itself to this problem. We have also discovered a "geodesic math" method which seems to be the most efficient approach for detector positioning on a sphere. Research continues on the angular sampling density, but generalization from two-dimensional angular sampling theory suggests using 2500 different sampling angles over the hemisphere. A three-dimensional expectation-maximization (EM) reconstruction algorithm has been derived which elegantly handles the presence of missing view angles inherent in SPET [2]. Finally, scatter is currently being studied using Monte Carlo simulations with the desire that a scatter-correction technique may be discovered.

The future research in SPET involves studying the collected photon energy spectra using Monte Carlo simulations and also suggesting and testing scatter-correction algorithms. This could be accomplished by reconstructing with and without simulated scatter and also with and without scatter correction in order to examine the effectiveness of different scatter-correction techniques. The three-dimensional EM reconstruction algorithm will be tested for robustness and for sufficiency of the angular sampling density. Phantoms will be generated with the appropriate Poisson distribution and subsequently reconstructed in order to test the SPET EM reconstruction algorithm. Results to date are encouraging and the possibility of an effective scatter-correction algorithm mark SPET as a viable and timely research effort.

1. Smith, K. R., "Preliminary Study of Three-Dimensional Image Reconstruction for Spherical BabyPET," BCL Working Note No. 77, March 1987.

2. Smith, K. R., "Derivation of the 3-D EM Reconstruction Algorithm Incorporating Missing View Angles," BCL Working Note No. 78, April 1987.

3. Smith, K. R., "Compton Scatter - A Closer Look," BCL Working Note No. 79, June 1987.

A-12. Development Activities in Radiation Sciences

Personnel: D. E. Beecher, BCL
D. G. Ballinger, B.S., Radiology
D. C. Ficke, B.S., Radiology
P. T. Fox, M.D., Neurology and Radiology
G. R. Hoffman, B.A., Radiology
M. A. Mintun, M.D., Radiology
M. E. Raichle, M.D., Neurology and Radiology
T. O. Videen, Ph.D., Neurology

Support: RR 01380
HL 17646
NS 06833

During the past year there have been some major changes in the computing environment to support the routine use of Super PETT II H (head) and Super PETT II B (body) scanners in Radiation Sciences. These scanners are still directly supported by the slice processor scheme as outlined in (PR 22, D-12). However, a new super minicomputer (Concurrent 3280 MPS with 1 APU) has just been purchased and will serve as a common host for both the body and the head unit. This new host has a 12 MIP capacity and will help to remove some of the burden of image reconstruction from the slice processors. The 3280 is still in the debugging phase and should be ready for routine use by September of this year.

Various networking issues have been addressed with the installation of PENnet, which allows all the computer systems in Radiation Sciences to communicate. Users currently have access to a virtual terminal facility as well as a file transfer facility between Concurrent hosts. Networking media currently consists of high-speed synchronous lines but plans are underway to use a high-speed Ethernet link between the larger machines.

As mentioned in (PR 22, D-13), we have successfully completed the installation of a new satellite system at the University of Arizona. The principle investigator, Dr. Lauter, has already begun processing data from our facility at the remote location.

Our work in new visual-stimulus software (PR 22, E-7) has been successfully completed and is now being used routinely in a variety of ongoing research projects.

B. Quantitative Imaging: Ultrasonic Tissue Characterization

Although ultrasound has proven to be a useful source of diagnostic information, results of examinations based on current ultrasonic methods are primarily qualitative and pictorial. Presently, ultrasound is employed widely for delineation of cardiac physiology and anatomy with M-mode and two-dimensional echocardiography, as well as for analysis of intracardiac flow velocities by Doppler techniques. In a collaborative effort with Cardiology and the Department of Physics work has continued on methods of tissue characterization via ultrasound. Our overall goal is to use ultrasound for the non-invasive identification of tissue pathologies within two-dimensional images of tissue properties that relate to structural components of cardiac muscle.

Specific objectives of this effort are 1) to investigate the magnitude and character of anisotropy in tissue, 2) to systematize the representation of the ultrasonic field and to reduce the data needed to describe that field by determining the moments of the spatial distribution of energy over the receiver aperture, 3) to seek improvement in measurement capability of imaging systems via interactive, adaptive beamforming for both linear and variable-aperture transducer arrays, 4) to test the hypothesis that quantitative images based on intrinsic tissue properties can be produced with reflected ultrasound, and 5) to construct a digital multiprocessor system to perform post-echo ultrasonic estimation of attenuation, phase velocity and backscatter in two dimensions.

A significant obstacle to the application of myocardial tissue characterization based on quantitative backscatter to studies of patients results from the fact that clinical applications require measurements to be made with the propagation of sound at varying angles relative to the average fiber orientation of the heart. Consequently we continue to focus on the extent of angular variation of the ultrasonic properties of the heart resulting from these fiber orientations. In particular we quantified anisotropy in open chest dogs via measurements of integrated backscatter (B-1). We also estimated the effects of myocardial fiber orientation on long-axis, short-axis, and four-chamber views of the heart (B-2). In a related fundamental study we generalized the scattering amplitudes and cross-sections for embedded scatterers which satisfy the first Born approximation (B-3).

Quantitative images based on ultrasonic tissue properties have been made at the BCL for several years using transmitted ultrasound with a multiple-frequency tomographic reconstruction system. We are now able to reconstruct tomograms with reflected ultrasound using the complete dataset and have developed and implemented algorithms to generate complete-dataset reconstructions at a 30-Hz frame rate (B-4). To study the diffraction effects of transducer arrays we used our system which produces images from reflected data to make images of point scatterers viewed by simulated transducer elements (B-5).

B-1. Anisotropy in the Beating Hearts of Open-Chest Dogs

Personnel: M. R. Holland, BCL and Physics
J. G. Miller, BCL and Physics
G. A. Mohr, BCL and Physics

Support: RR 01362
HL 17646

To characterize the anisotropy of backscatter from myocardium in open-chest dogs studied in vivo and to relate the anisotropic behavior to the previously demonstrated cyclic variation of backscatter, we made use of the technique referred to as polar backscatter [1-5]. For this approach the interrogating transducer is maintained as a fixed angle (in these experiments 30°) from the surface normal and the azimuthal angle is then varied systematically. A water-filled cylinder serves as an acoustic delay line so that the interrogated tissue volume is at the transducer's focus. The end of the cylinder is coupled directly to the epicardial surface of canine hearts during open chest measurements of dogs. Time-gating circuitry permits characterization of the backscatter from the middle segment of the myocardial thickness where the fibers are predominantly oriented circumferentially. Backscatter was measured over a range of angles by rotating the transducer about the perpendicular axis. This allowed interrogation of the mid-myocardial fibers at angles ranging between 60° and 90° relative to the fiber axes.

Integrated backscatter is measured throughout the cardiac cycle. As a control, each region of myocardium from which the backscatter is measured as a function of angle is characterized also with a second transducer held perpendicular to the surface of the tissue. For both the angle-dependent measurement and the normal-incidence control measurement the depth of the electronic gate was varied synchronously with wall thickening in order to keep the measurement volume within the tissue layer of interest. In addition, each measurement of backscatter was corrected for attenuation based on the appropriate depth and on an average attenuation coefficient derived from previous measurements performed in vitro.

Two transducers were employed simultaneously (Figure 1) in a specially fabricated holder. One was perpendicular to the base of the holder and the other at a fixed polar angle of thirty degrees from perpendicular. The perpendicular transducer was operated in standard M-Mode imaging format. Monitoring of the M-Mode display enabled the operator to maintain the perpendicular transducer orientation. The criteria for determining perpendicularity were that the transducer appeared by visual inspection to be perpendicular to the surface of the heart, that the M-Mode image showed sharp delineation of the epicardial surface, and that wall thickening during systole and thinning during diastole were appropriately synchronized with respect to the electrocardiogram.

Both transducers were broadband (5 MHz nominal center frequency), 1.2 cm in diameter and were focused at 5 cm. The base of the holder was

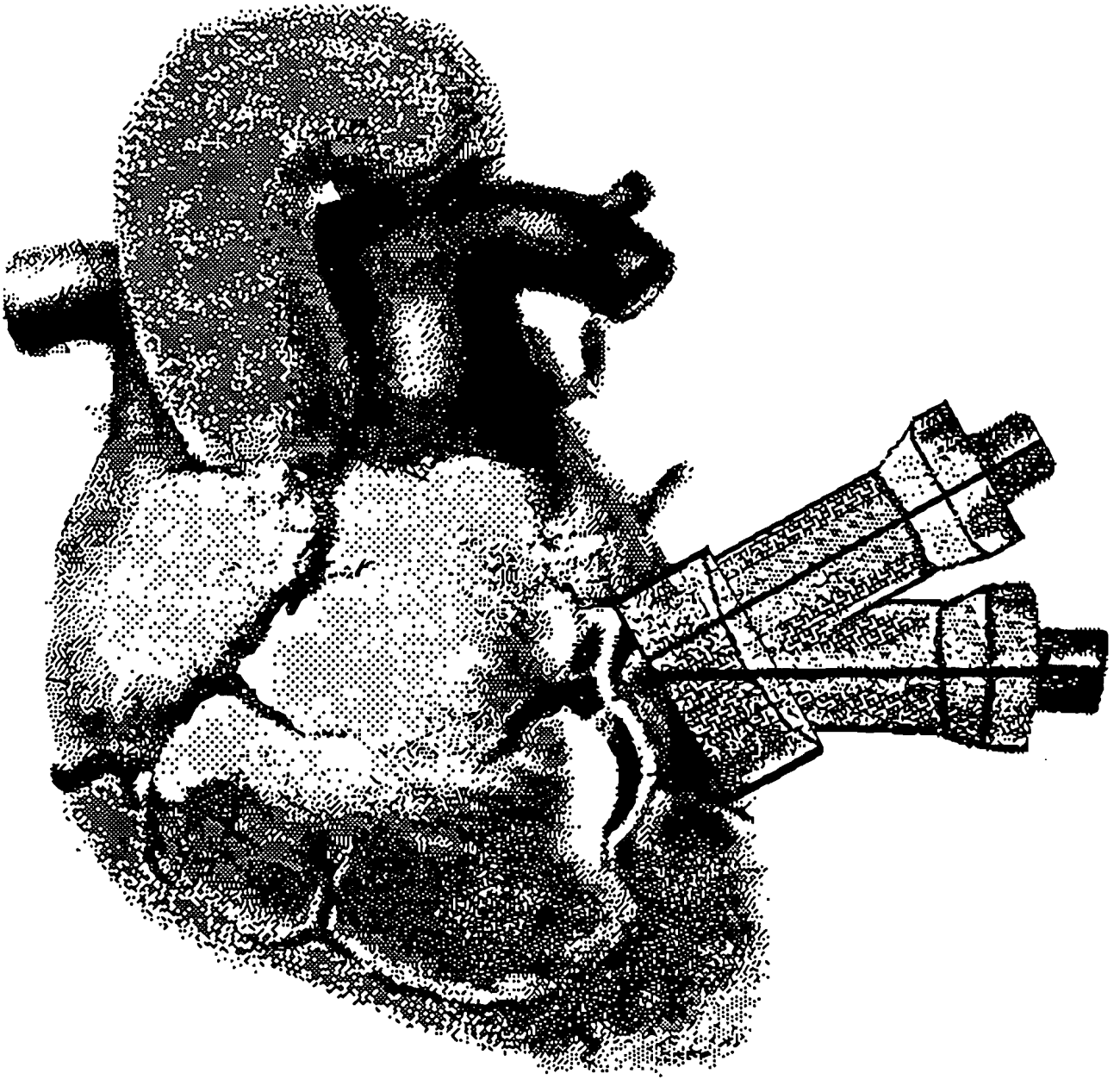

Figure 1. Drawing of the holder used in the experiments. The water-filled holder served as an acoustic delay line and held the two transducers, one at normal incidence and the second at a fixed polar angle (θ) of 30° from the first.

sealed with a flexible latex layer and its body was filled with water, which provided an acoustic delay line. When applied to the epicardial surface of the heart, the holder positioned the transducers so that the focal zones of the transducers overlapped with the mid-myocardial region in diastole. In systole the epicardial surface of the heart pushed upward, compressing the latex tip toward the transducers, shortening the ultrasonic water path by a few millimeters. Accordingly, the focal zones were cyclically deeper in the myocardium in systole and shallower in diastole. However, they remained within the middle segment of the myocardial wall throughout the heart cycle. The two transducers were excited alternately to avoid interference between the resulting ultrasonic signals. Thus, backscatter measurements could be obtained from the transducer angled at 30° while the perpendicular transducer was used to ensure the desired orientation of the pair relative to the epicardial surface. We employed a real-time integrated-backscatter system in which a cadmium sulfide acoustoelectric receiver is used to measure the energy in a short segment of backscattered rf signal. The output of the real-time integrated-backscatter system is recorded (HP 5180 Transient Waveform Recorder) at a sampling rate of 200 Hz. At this sampling rate the recorder can record data from about five full cardiac cycles in each 1024-point trace.

As the heart contracts and relaxes, the thickness of the myocardial wall varies. In order to restrict our investigation to the middle segment of the myocardial wall which contains predominantly circumferentially-oriented fibers [6], circuitry was constructed to produce a gating signal that would track the motion of the mid-myocardium. Synchronization with the cardiac cycle was accomplished with the signal from the left ventricular pressure monitor. This signal was low-pass filtered and amplified, with gain and offset adjusted until the resulting electrical signal was observed to follow accurately the ventricular wall motion depicted on the M-Mode display. The resulting voltage controlled a timer which triggered the gate so that the gate remained within the middle segment of the ventricular wall at all times. The gate-control voltage was recorded along with the integrated backscatter signal on a second channel of the waveform recorder. The time delay (and therefore the depth within the tissue) that corresponds to a particular voltage was calibrated by applying DC voltages at levels that shift the gate in small increments, measuring both the gate shift and voltages, and fitting a straight line to the resultant points. The recorded voltages for the gate's position were interpolated to units of time from this fit. The gate's time delay was transformed to a depth in the myocardium, based on the assumption that the speed of sound in myocardium is approximately constant throughout the cardiac cycle.

Wall thickness was determined directly from the perpendicular transducer's M-mode display. For the angled (30°) transducer, wall thickness can be reliably measured only at end-diastole. Wall thicknesses at other intervals during the cardiac cycle are estimated from the thickness measured directly at end-diastole and fractional wall thickening measured with the perpendicular transducer. Wall thickening in our measurement was typically of the order of thirty to fifty percent, consistent with published measurements for open chest dogs [7].

For these studies we define a coordinate system based on anatomical features of the heart shown in Figure 2. The axis of alignment is defined

by a line from the apex of the heart to the region of the bifurcation of the left coronary artery into the anterior descending and circumflex vessels, a readily detectable visual marker. This axis is approximately perpendicular to the predominant fiber orientation in the middle segment of the myocardium, according to Streeter et al. [6]. To be consistent with the definition of fiber axes in our previous work [8,9], we denote this as the 90° and 270° axis of the azimuthal angle ϕ. Thus fibers are oriented along the 0° (or 180°) axis. The angle Γ between the incident ultrasonic wave and the muscle fiber axes is given by [9]

$$\Gamma = \cos^{-1}\left[|\cos(\phi)|\ \sin(\theta)\right] . \qquad (1.1)$$

A set of backscatter measurements from the region of interest was obtained with the plane of incidence oriented initially along the ϕ=90° axis. Measurements were then obtained at increments of 30° in azimuthal angle through a full 360°. The series was completed with repeat 90° measurements to verify consistency. In addition, backscatter measured with the fixed, perpendicular transducer and calibration measurements were obtained at the beginning and at the end of the azimuthal series.

A set of measurements consisted of ten sites over the left ventricular wall for each animal. The region of the left ventricle characterized encompassed a zone from near the apex to near the base and from the locus of the left descending coronary artery to that of the left posterior descending. Each trace included data from approximately five cardiac cycles.

Cyclic variation of integrated backscatter throughout the cardiac cycle was evident in each animal and at each azimuthal orientation. The cyclic variation of backscatter exhibited a consistent phase, reaching a maximum at end-diastole and a minimum at end-systole in agreement with previous reports [9-15]. Integrated backscatter measurements throughout the cardiac cycle, averaged for all dogs at each of four azimuthal angles (ϕ=0°, 90°, 180°, 270°), are presented in Figure 3, with measurements from individual dogs aligned at end-diastole. Thus the point at which end-systole occurs is blurred because of animal-to-animal variation in the fraction of the cardiac cycle comprising systole. It is evident in Figure 3 that the ϕ=0° and ϕ=180° azimuthal angles, where the angle to the fiber axes Γ is 60°, exhibit a lower magnitude of backscatter than the ϕ=90° and ϕ=270° azimuthal angles of insonification, where Γ is 90°.

Figure 4, panel a), depicts the average fiber direction in a typical region of interest and three insonification directions. Panel b) depicts integrated backscatter measured at end-diastole and at end-systole for each of the three orientations. The results obtained at perpendicular incidence (i.e., at θ=0° and at θ=30°, ϕ=90°) are essentially identical.

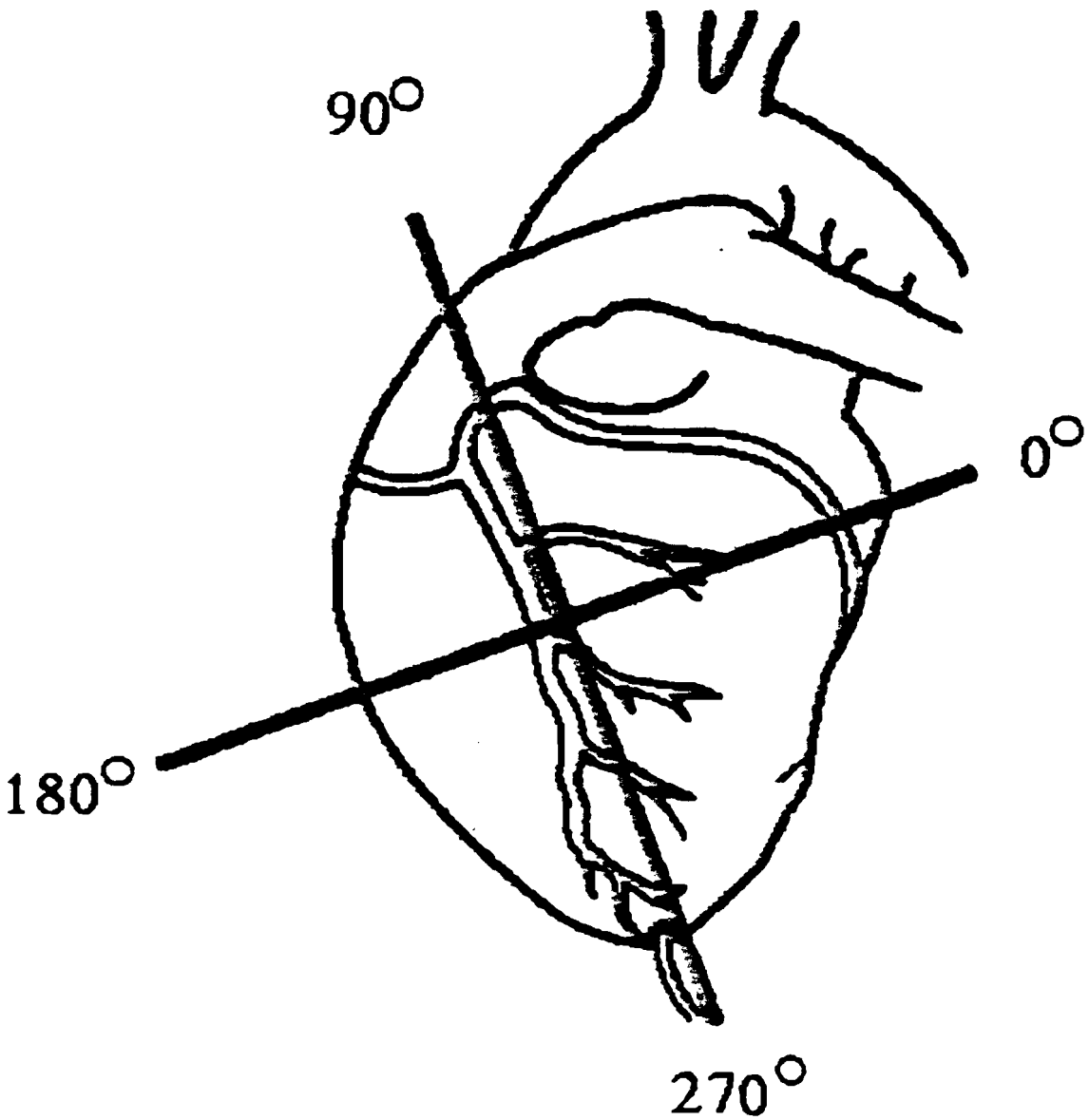

Figure 2. Sketch of canine heart, showing major landmarks, with the coordinate axes used in defining azimuthal angle (ϕ) superimposed.

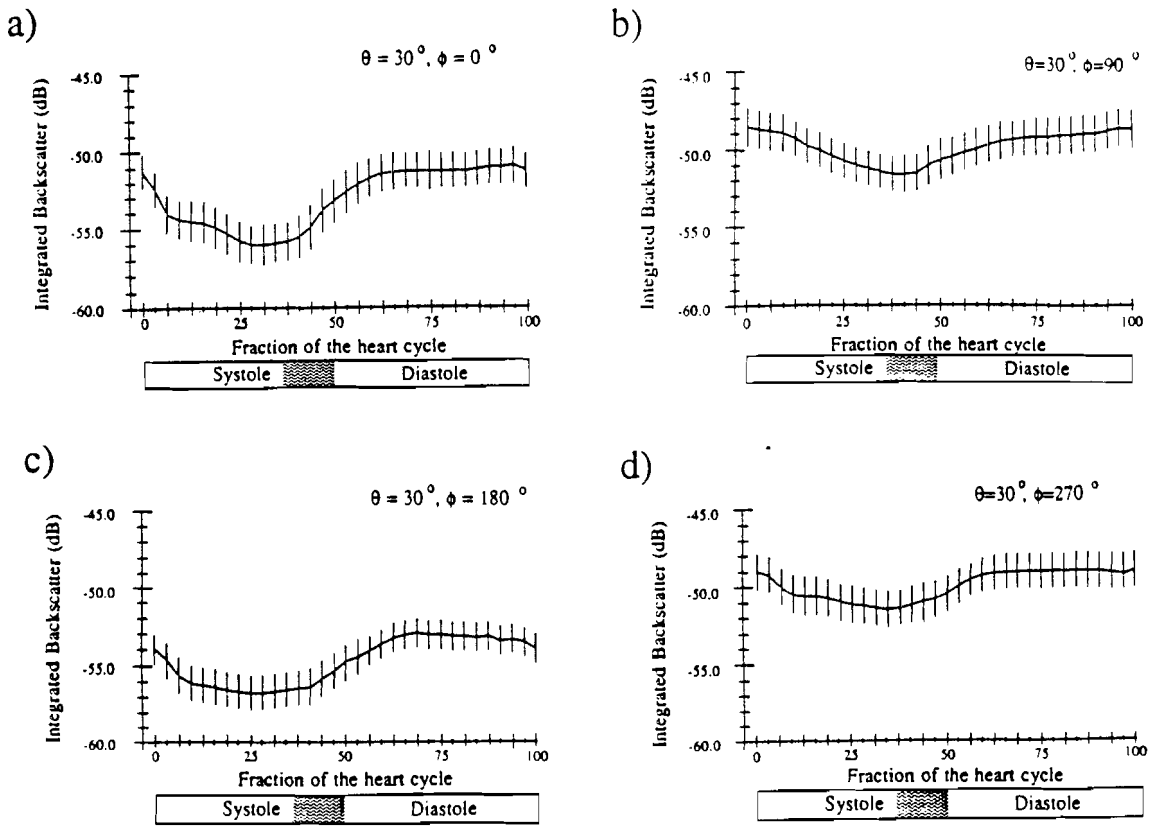

Figure 3. Integrated backscatter, averaged for all animals, measured throughout the cardiac cycle with polar angle θ=30° in four cardinal azimuthal directions, ϕ=0°, 90°, 180°, and 270°.

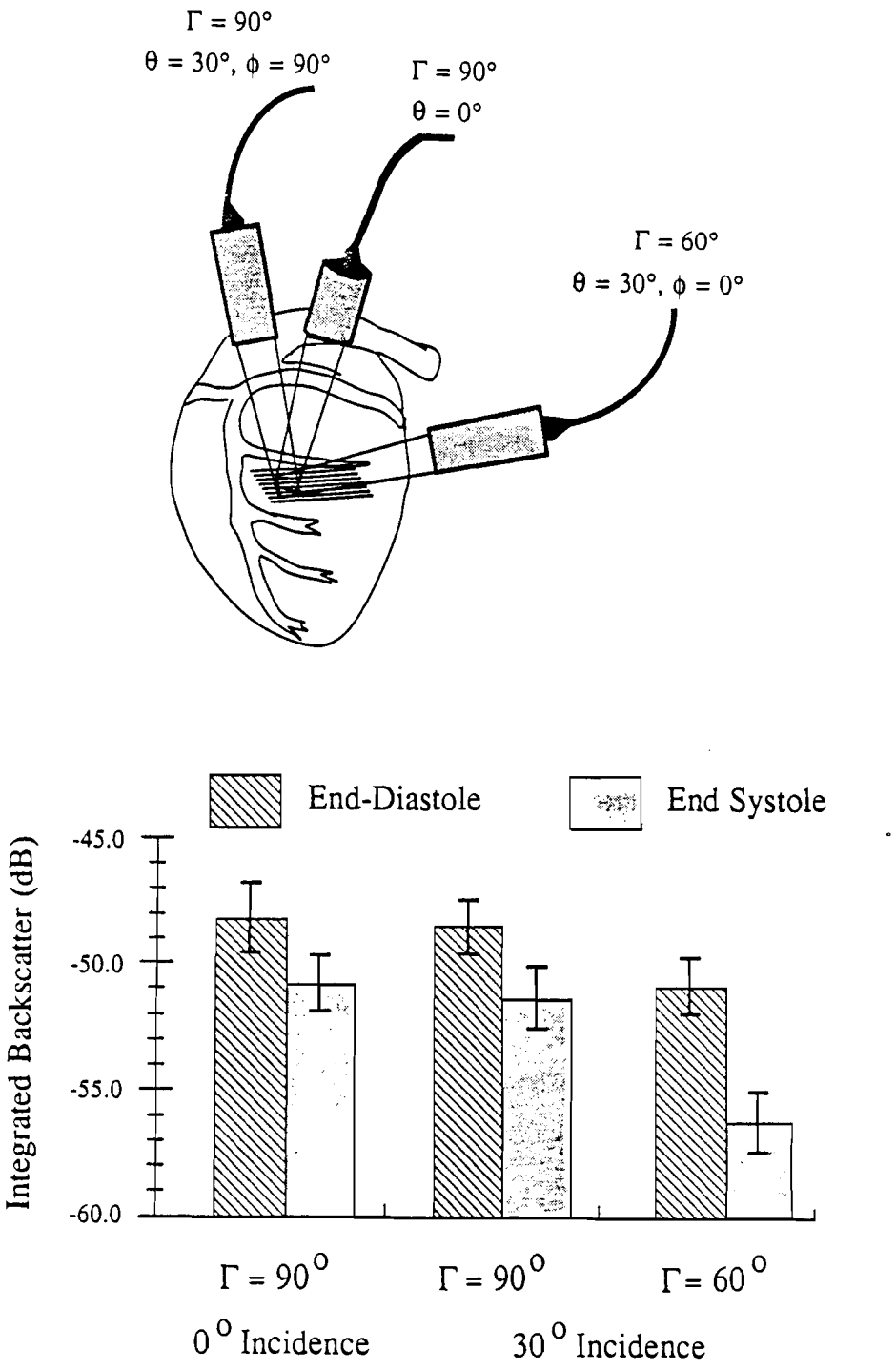

Figure 4. Panel a) illustrates three special directions of insonification at which measurements were carried out. In Panel b) the integrated backscatter at end-diastole and end-systole is presented at these three directions: perpendicular to fiber axes (Γ=90°) both at normal incidence (θ=0°) and non-normal incidence (the average of measurements at θ=30°, ϕ=0°, 180°, and 360°).

In Figure 3 and 4b, animal-to-animal variations in absolute values of integrated backscatter result in relatively large standard errors. Consequently, angular variations can be delineated more directly by expressing the backscatter at any angle relative to that measured at perpendicular incidence (Γ=90°) at end-diastole. Subtracting this baseline backscatter (expressed in dB) from each value yields the results presented in Figure 5. At end-diastole the backscatter shows anisotropy with an excursion of 3.2 dB. Insonification perpendicular to the fibers (ϕ=90° or 270°, so that Γ=90°) at end-diastole. Subtracting this baseline backscatter (expressed in dB) from each value yields the results presented in Figure 5. At end-diastole the backscatter shows anisotropy with an excursion of 3.2 dB. Insonification perpendicular to the fibers (ϕ=90° or 270°, so that Γ=90°) yields maximum backscatter, and insonification at a 0° azimuthal angle (ϕ=0° or 180°, hence Γ=60°) a minimum value. Values at end-systole exhibit qualitatively similar differences, with lower average value, but greater variation as a function of azimuthal angle.

These data were fit arbitrarily to curves of the form $A+B\cos(2\phi+\delta)$, where A is the average value of integrated backscatter, B is the relative amplitude of variation, ϕ is the azimuthal angle, and δ is a phase shift. A least-squares fitting procedure yields B = 1.6 ± 0.2 dB (mean ± SEM) for end diastole and B = 1.6 ± 0.2 dB (mean ± SEM) for end systole, corresponding to peak-to-peak variations of 3.2 dB at end-diastole and 5.0 dB at end-systole. These results are significantly different from B=0, as would be expected for an isotropic medium ($p<0.001$ for both end-diastole and end-systole, using the Student t-test modified by Bonferroni's procedure [16] for multiple comparisons). The predicted angle of maximum backscatter is 90° [9]. Based on the fits to the data, the angular maxima occur at 105.4° ± 9.1° (mean ± SEM) for end diastole and 81.1° ± 5.8° (mean ± SEM) for end systole, values which are not significantly different from 90° at the 0.05 confidence level (using the Student t-test modified by Bonferroni's procedure for multiple comparisons).

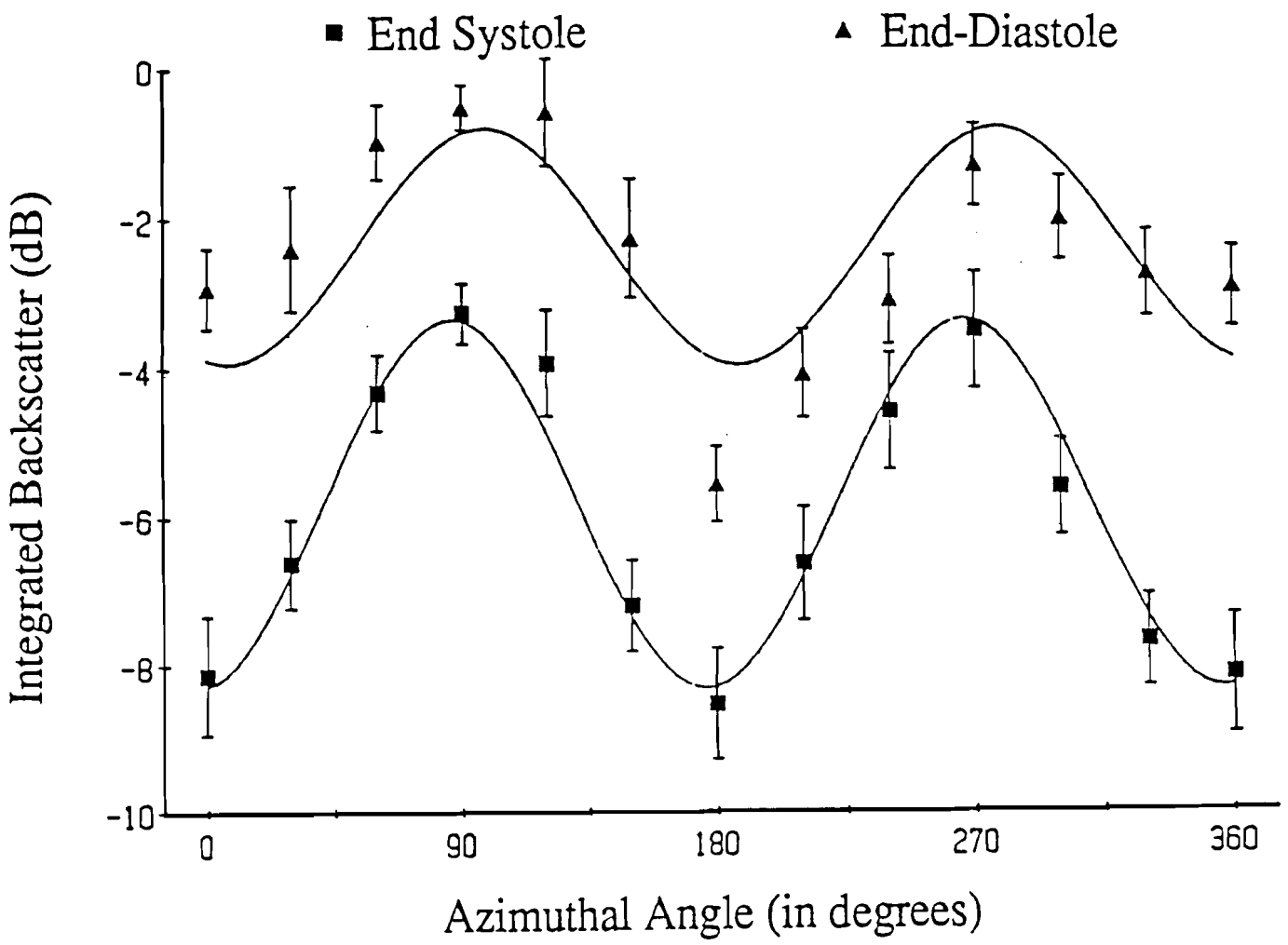

Figure 5. Average integrated backscatter at end-diastole and end-systole as a function of azimuthal angle (ϕ) normalized to the values obtained at end-diastole with the reference (i.e., perpendicular) transducer. The symbols show measured averages and their standard errors whereas the continuous lines show fits to a phenomenological cosinusoidal form.

1. Brown, A. F., "Materials Testing by Ultrasonic Spectroscopy," Ultrasonics, 11:202-210, 1973.

2. Bar-Cohen, Y. and Crane, R. L., "Acoustic-Backscattering Imaging of Subcritical Flaws in Composites," Materials Evaluation, 40:970-975, 1982.

3. Thomas, III, L. J., Madaras, E. I., and Miller, G. J., "Two-Dimensional Imaging of Selected Ply Orientations in Quasi-Isotropic Composite Laminates Using Polar Backscattering," Proceedings of the 1982 IEEE Ultrasonics Symposium, IEEE Catalog No. 82CH1823-4, pp. 965-970, 1982.

4. Blodgett, E. D., Thomas, III, L. J., and Miller, J. G., "Effects of Porosity on Polar Backscatter From Fiber Reinforced Composites," Review of Progress in Quantitative Nondestructive Evaluation, 5B:1267-1274, 1986.

5. Blodgett, E. D., Freeman, S. M., and Miller, J. G., "Correlation of Ultrasonic Polar Backscatter With the Deply Technique for Assessment of Impact Damage in Composite Laminates," Review of Progress in Quantitative Nondestructive Evaluation, 5B:1227-1238, 1986.

6. Streeter, Jr., D. D., Spotnitz, H. M., Patel, D. P., Ross, Jr., J., and Sonnenblick, E. H., "Fiber Orientation in the Canine Left Ventricle During Diastole and Systole," Circulation Research, 24:339-347, 1969.

7. Myers, J. H., Stirling, M. C., Choy, M., Buda, A. J., and Gallagher, K. P., "Direct Measurement of Inner and Outer Wall Thickening Dynamics With Epicardial Echocardiography," Circulation, 74:164-172, 1986.

8. Mottley, J. G. and Miller, J. G., "Anisotropy of Ultrasonic Attenuation in Canine Heart and Liver," Ultrasonic Imaging, 4:180, 1982 (abstract).

9. Mottley, J. G., "Physical Principles of the Ultrasonic Attenuation and Backscatter of Soft Tissues: Dependence on the Angle of Propagation and the Physiologic State," Department of Physics, Washington University, St. Louis, MO, 1985 (Ph.D. Dissertation).

10. Madaras, E. I., Barzilai, B., Perez, J. E., Sobel, B. E., and Miller, J. G., "Changes in Myocardial Backscatter Throughout the Cardiac Cycle," Ultrasonic Imaging, 5:229-239, 1983.

11. Barzilai, B., Madaras, E. I., Sobel, B. E., Miller, J. G., and Perez, J. E., "Effects of Myocardial Contraction on Ultrasonic Backscatter Before and After Ischemia," American Journal of Physiology, 247:H478-H483, 1984.

12. Mottley, J. G., Glueck, R. M., Perez, J. E., Sobel, B. E., and Miller, J. G., "Regional Differences in the Cyclic Variation of Myocardial Backscatter That Parallel Regional Differences in Contractile Performance," Journal of the Acoustical Society of America, 76:1617-1623, 1984.

13. Olshansky, B., Collins, S. M., Skorton, D. J., and Prasad, N. V., "Variation of Left Ventricular Myocardial Gray Level on Two-Dimensional Echocardiograms as a Result of Cardiac Contraction," Circulation, 70:972-977, 1984.

14. Wickline, S. A., Thomas, III, L. J., Miller, J. G., Sobel, B. E., and Perez, J. E., "A Relationship Between Ultrasonic Integrated Backscatter and Myocardial Contractile Function," Journal of Clinical Investigation, 76:2151-2160, 1985.

15. Wickline, S. A., Thomas, III, L. J., Miller, J. G., Sobel, B. E., and Perez, J. E., "The Dependence of Myocardial Ultrasonic Integrated Backscatter on Contractile Performance," Circulation, 72:183-192, 1985.

16. Wallenstein, S., Zucker, C. L., and Fleiss, J. L., "Some Statistical Methods Useful in Circulation Research," Circulation Research, 47:1-9, 1980.

B-2. Anticipated Effects of Anisotropy for Images Obtained Through Standard Echocardiographic Windows

Personnel: G. A. Mohr, BCL and Physics
M. R. Holland, BCL and Physics
J. G. Miller, BCL and Physics

Support: RR 01362
HL 17646

We investigated the anticipated consequences of oriented myocardial fibers for the long axis plane, short axis plane, and four chamber plane, as illustrated in Figure 1. In the long-axis plane, insonification is approximately perpendicular to the predominant fiber orientation throughout most of the middle and basal portions of the left ventricular posterior wall, and in the majority of the mid- and basal portions of the anterior interventricular septum, as illustrated in Figure 2. Consequently, compensation for attenuation and interpretation of the magnitude of integrated backscatter is relatively straightforward for images obtained in this plane. Even the papillary-muscle region exhibits a fiber orientation that is encountered primarily in a perpendicular fashion in the parasternal long-axis view. Because we anticipate that the effects of anisotropy will be relatively minor in this view, initial attempts at tissue characterization in normal volunteers and patients experiencing acute

ischemic injury were carried out in this view. Preliminary results [1] of these investigations are encouraging.

In contrast, for images obtained in short-axis views, both parasternal and subcostal, angles between the insonifying beam and fibers with specific orientations encompass a large range. Initial efforts to apply quantitative backscatter analysis without accounting for the consequences of anisotropy in studies of normal volunteers were unsuccessful, presumably because of the following effects. As illustrated in Figure 3 for parasternal short-axis images, at both the level of the mitral valve (basal region) and of the mid-ventricular region, the mid-myocardial portion of the anterior septum and the most posterior region of the left ventricular free wall contains fibers which are primarily perpendicular to the insonifying beam. In contrast, the anterior left ventricular free wall and inferior septum exhibit fiber directions that are practically parallel to the ultrasonic beam. As a consequence, the magnitude of backscatter is expected to vary markedly in quantitative images. For regions in which the fibers are approximately parallel to the beam, backscatter is least and attenuation is highest. Thus, the apparent backscatter should be substantially lower in the lateral segments of short axis images. We have observed this phenomenon in initial studies of normal volunteers in the parasternal short-axis view.

In four-chamber views, the geometry is somewhat more complicated. Near the apex, the fibers spiral substantially, so that the beam encounters fibers at an angle of approximately 45 degrees. The average angle of incidence changes gradually toward perpendicularity as the ultrasound propagates toward more basal regions and the direction of the fibers becomes more nearly circumferential. Further, the fiber distribution is not as uniform in the apical mid-myocardium as it is in the more basal regions [2]. Thus, the expected effects include decreased backscatter in the apical regions, which gradually increases as more basal regions are imaged. Initial investigations of normal volunteers qualitatively show this behavior, lending support to this model.

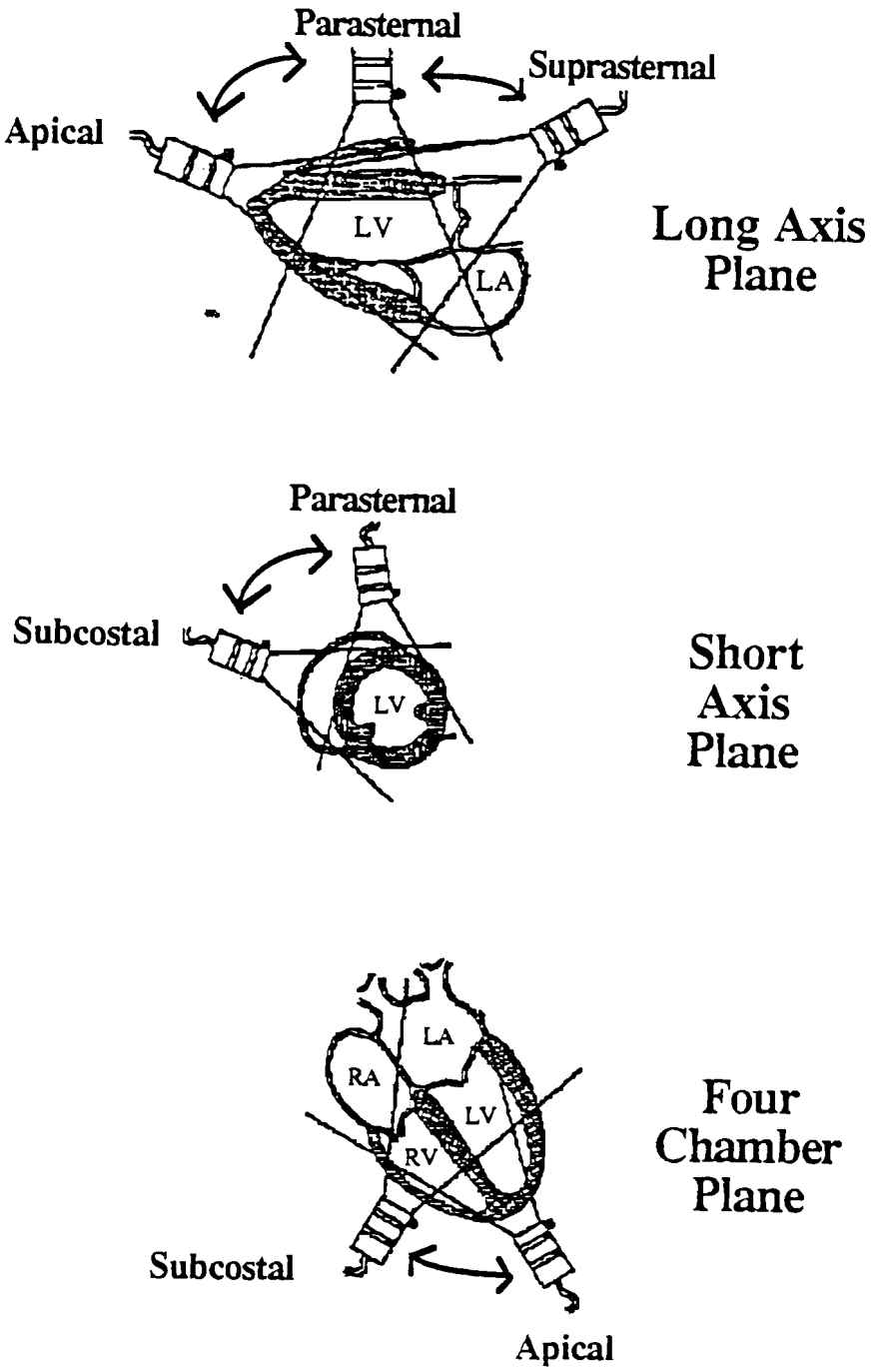

Figure 1. Diagrams indicating the locations of the transducer for the standard views in each of three orthogonal planes: a) long-axis, b) short-axis, and c) four-chamber.

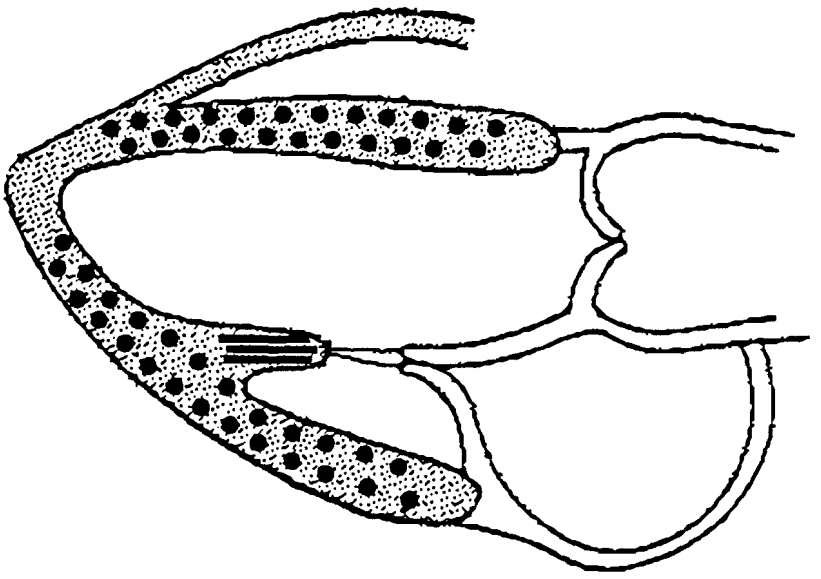

Fibers Perpendicular to the Imaging Plane

Fibers Parallel to the Imaging Plane

Figure 2. Sketch of the approximate orientation of fibers encountered in long-axis views.

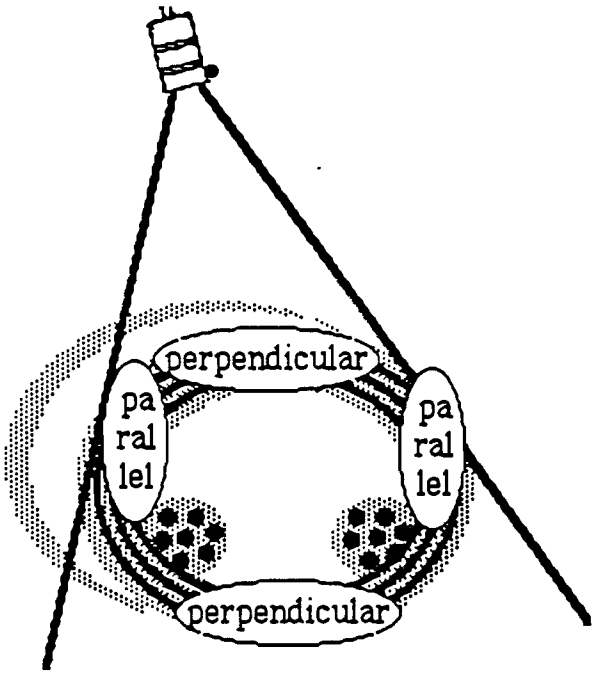

Fibers Perpendicular to the Imaging Plane

Fibers Parallel to the Imaging Plane

Figure 3. Sketch of the approximate orientation of fibers encountered in the parasternal short-axis view.

1. Vered, Z., Barzilai, B., Mohr, G. A., Thomas, III, L. J., Sobel, B. E., Miller, J. G., and Perez, J. E., "Ultrasonic Tissue Characterization in Man With Real-Time Quantitative Integrated Backscatter Imaging and Delineation of Integrated Backscatter Dependence on the Cardiac Cycle," Journal of the American College of Cardiology, 9:212A, 1987 (abstract).

2. Streeter, Jr., D. D., Spotnitz, H. M., Patel, D. P., Ross, Jr., J., and Sonnenblick, E. H., "Fiber Orientation in the Canine Left Ventricle During Diastole and Systole," Circulation Research, 24:339-347, 1969.

B-3. Generalization of Scattering Amplitudes in Perfectly Elastic Scattering to an Arbitrary Direction and Polarization of the Incident Field in the First Born Approximation

Personnel: M. R. Kaufmann, BCL and Physics
J. G. Miller, BCL and Physics

Support: RR 01362

Gubernatis et al. [1] derived the scattering amplitudes and differential cross-sections for a scatterer embedded in a host medium in the first Born approximation. The purpose of our work was to generalize the work of Gubernatis et al. to permit the choice of an arbitrary direction and polarization for the incident ultrasonic field. This generalization is useful in our investigation of the role of the anisotropy of scattering in myocardial tissue characterization.

Both the scatterer and the surrounding host medium are assumed to be homogeneous, isotropic, perfectly elastic media. We denote the density of the host medium by ρ, its elastic constants by λ and μ, and the differences in these parameters between host and scatterer by $\delta\rho$, $\delta\lambda$, and $\delta\mu$. Denoting the longitudinal and transverse sound speeds of the host medium by c_L and c_T, we write the longitudinal and transverse wave vectors as $\alpha = k_L = \frac{\omega}{c_L}$ and $\beta = k_T = \frac{\omega}{c_T}$. The particle displacement field incident on the scatterer is taken to be a monochromatic plane wave and can be written in its most general form as

$$u^0(r,t) = ae^{i\alpha\hat{e}^0\cdot r - i\omega t} + be^{i\beta\hat{e}_0\cdot r - i\omega t}, \qquad (3.1)$$

where $\hat{e}^0$ is the direction of propagation of the incident field and a and b are the respective polarization vectors for the longitudinal and transverse components of the incident field. Presumably, a is parallel to e^0 and b is perpendicular to $\hat{e}^0$, since a is a longitudinal polarization and b is a transverse polarization.

A scattered field $u^s(r,t)$ can then be calculated. However, the calculation of Gubernatis et al. was carried out in the special case of propagation of the incident field in the +z direction ($\hat{e}^0=\hat{k}$) with the following three special cases of polarization: (1) $a=a\hat{k}$ and $b=0$ (longitudinal polarization), (2) $a=0$ and $b=b\hat{i}$ (transverse polarization along the x-axis), and (3) $a=0$ and $b = \frac{u}{\sqrt{2}}\{\hat{i} + i\hat{j}\}$ (right-hand circular transverse polarization).

Their results for each of these three special cases are as follows. (The superscript "(1)" indicates the first iteration of the Born series, i.e., the first Born approximation.) For special case (1), the scattered displacement field is

$$u^{s(1)}(r) = a\hat{r}\,\frac{\alpha^2 e^{i\alpha r}}{4\pi r}\left[\frac{\delta\rho}{\rho}\cos\theta - \frac{\delta\lambda+2\delta\mu\cos^2\theta}{\lambda+2\mu}\right] S(\alpha,\alpha;\theta,\phi) +$$

$$+ a\hat{\theta}\,\frac{\beta^2 e^{i\beta r}}{4\pi r}\left[\frac{2\alpha\delta\mu\cos\theta\sin\theta}{\beta\mu} - \frac{\delta\rho\sin\theta}{\rho}\right] S(\alpha,\beta;\theta,\phi)\ . \qquad (3.2)$$

For case (2),

$$u^{s(1)}(r) = b\,\frac{\beta^2 e^{i\beta r}}{4\pi r}\left\{\left[-\frac{\delta\rho\sin\phi}{\rho} + \frac{\delta\mu\sin\phi\cos\theta}{\mu}\right]\hat{\phi} +\right.$$

$$\left. + \left[\frac{\delta\rho\cos\theta\cos\phi}{\rho} - \frac{\delta\mu\cos2\theta\cos\phi}{\mu}\right]\hat{\theta}\right\} S(\beta,\beta;\theta,\phi) +$$

$$+ b\hat{r}\,\frac{\alpha^2 e^{i\alpha r}}{4\pi r}\left[\frac{\delta\rho\sin\theta\cos\phi}{\rho} - \frac{\beta}{\alpha}\,\frac{\delta\mu\sin\theta\cos\phi}{\lambda+2\mu}\right] S(\beta,\alpha;\theta,\phi). \qquad (3.3)$$

Finally for case (3),

$$u^{s(1)}(r) = u\,\frac{\beta^2 e^{i\beta r}}{4\pi r}\,e^{i\phi}\left\{\left[\frac{\delta p}{p}\,\frac{1+\cos\theta}{2} - \frac{\delta\mu}{\mu}\,\frac{\cos\theta+\cos2\theta}{2}\right]\hat{x}^+ +\right.$$

$$\left. + \left[\frac{\delta\rho}{\rho}\,\frac{\cos\theta-1}{2} + \frac{\delta\mu}{\mu}\,\frac{\cos\theta-\cos2\theta}{2}\right]\hat{x}^-\right\} S(\beta,\beta;\theta,\phi) +$$

$$+ u\hat{r}\,\frac{\alpha^2 e^{i\alpha r}}{4\pi r}\,e^{i\phi}\left[\frac{\delta\rho}{\rho}\sin\theta - \frac{\beta}{\alpha}\,\frac{\delta\mu}{\lambda+2\mu}\sin2\theta\right] S(\beta,\alpha;\theta,\phi), \qquad (3.4)$$

where

$$\hat{x}^{\pm} = \frac{1}{\sqrt{2}}\left[\hat{\theta} \pm i\hat{\phi}\right]\ . \qquad (3.5)$$

The shape factors S, in Gubernatis' notation, are defined by

$$S(\gamma,\gamma';\theta,\phi) = \int_{V_s} d^3r' \; e^{i(\gamma\hat{k}-\gamma'\hat{r})\cdot r'} \tag{3.6}$$

where γ and γ' each can be either α or β, θ and ϕ are the outgoing angles (in a spherical polar coordinate system), $\hat{k}$ is the incident direction, $\hat{r}$ is the outgoing direction (determined by θ and ϕ), and V_s denotes the region of space occupied by the scatterer. Note that in all of these formulas there is an implicit harmonic time dependence, so that the total displacement field is

$$u^{(1)}(r,t) = u^0(r,t) + u^{s(1)}(r)e^{-i\omega t} \; . \tag{3.7}$$

In our studies of the anisotropy of scattering from myocardial tissue fibers, the calculations can be carried out more straightforwardly if the direction of insonification is not fixed in some particular direction, but rather can be taken to be any incoming direction. Then, for example, backscattering from a cylindrical fiber can be calculated for any direction of insonification, not just $\hat{k}$. Consequently, we have generalized the calculations of Gubernatis et al. by deriving the scattering amplitudes for an arbitrary direction of propagation $\hat{e}^0$ and any arbitrary directions a and b of polarization. The incident displacement field is taken to be exactly Eq. (3.1), with no special cases assumed.

Beginning with Eq. (3.1) of Ref. 1 and taking their calculation [1] as a guide, we assume that the scatterer is isotropic and calculate the far-field ($r\to\infty$) scattered displacement field. Appropriately substituting the incident field u^0 for the total field u (in order to obtain the first Born approximation), after rather extensive algebraic manipulation and simplification we obtain the result

$$\begin{aligned}
u^{s(1)}(r) = u^0(r) &+ \hat{r}\,\frac{\alpha^2 e^{i\alpha r}}{4\pi r}\, S_{LL}(\theta,\phi,\theta^0,\phi^0)\left[\frac{\delta\rho}{\rho}(a\cdot\hat{r}) - \frac{\delta\lambda(a\cdot\hat{e}^0)+2\delta\mu(\hat{e}^0\cdot r)(a\cdot r)}{\lambda+2\mu}\right] + \\
&+ \frac{\beta^2 e^{i\beta r}}{4\pi r} S_{LT}(\theta,\phi,\theta^0,\phi^0)\left[\frac{\delta\rho}{\rho}\left(a-\hat{r}(a\cdot\hat{r})\right)+\frac{\beta}{\alpha}\,\frac{\delta\mu}{\lambda+2\mu}\left(2\hat{r}(\hat{e}^0\cdot\hat{r})(a\cdot\hat{r})-a(\hat{e}^0\cdot\hat{r})-\hat{e}^0(a\cdot\hat{r})\right)\right] + \\
&+ \hat{r}\,\frac{\alpha^2 e^{i\alpha r}}{4\pi r}\, S_{TL}(\theta,\phi,\theta^0,\phi^0)\left[\frac{\delta\rho}{\rho}\,(b\cdot\hat{r}) - \frac{\beta}{\alpha}\,\frac{\delta\lambda(\cdot\hat{e}^0)+2\gamma\mu(\hat{e}^0\cdot\hat{r})(b\cdot\hat{r})}{\lambda+2\mu}\right] + \\
&+ \frac{\beta^2 e^{i\beta r}}{4\pi r}\, S_{TT}(\theta,\phi,\theta^0,\phi^0)\left[\frac{\delta\rho}{\rho}\left(b-\hat{r}(b\cdot\hat{r})\right) + \frac{\delta\mu}{\mu}\left(2\hat{r}(\hat{e}^0\cdot r)(b\cdot\hat{r})-b(\hat{e}^0\cdot\hat{r})-\hat{e}^0(b\cdot\hat{r})\right)\right].
\end{aligned} \tag{3.8}$$

Here, we have introduced a slightly different notation for the shape factors,

$$S_{XY}(\theta,\phi,\theta^0,\phi^0) = \int_{V_s} d^3r' e^{i(k_x\hat{e}^0 - k_Y\hat{r})\cdot r'} \tag{3.9}$$

where X and Y each can be either L (longitudinal) or T (transverse). Note that the incident direction $\hat{e}^0$ is determined by the incoming angles θ^0 and ϕ^0 and that the outgoing direction $\hat{r}$ is determined by the outgoing angles θ and ϕ.

If we write α and β in terms of c_L and c_T, i.e., $\alpha = k_L = \frac{\omega}{c_L}$ and $\beta = k_T = \frac{\omega}{c_T}$, take $a = \hat{a}^0$ and $b = \hat{e}^0$ (causing certain dot products to vanish), and use the vector identity

$$b(a\cdot c) - a(b\cdot c) = (a\times b)\times c, \tag{3.10}$$

we can rewrite the equations and obtain

$$u^{s(1)}(r) = u^0(r) + \hat{r}a\frac{\omega^2 e^{i\omega r/c_L}}{4\pi r c_L^2} S_{LL}(\theta,\phi,\theta^0,\phi^0)(\hat{e}^0\cdot\hat{r})\left[\frac{\delta\rho}{\rho} - \frac{\delta\lambda + 2\delta\mu(\hat{e}^0\cdot\hat{r})}{\lambda + 2\mu}\right] +$$

$$+ \left[(\hat{e}^0\times\hat{r})\times\hat{r}\right]a\frac{\omega^2 e^{i\omega r/c_L}}{r\pi r c_T^2} S_{LT}(\theta,\phi,\theta^0,\phi^0)\left[-\frac{\delta\rho}{\rho} + \frac{c_L}{c_T}\frac{2\delta\mu}{\lambda+2\mu}(\hat{e}^0\cdot\hat{r})\right] +$$

$$+ \hat{r}\frac{\omega^2 e^{i\omega r/c_L}}{r\pi r c_L^2} S_{TL}(\theta,\phi,\theta^0,\phi^0)(b\cdot\hat{r})\left[\frac{\delta\rho}{\rho} - \frac{c_L}{c_T}\frac{2\delta\mu}{\lambda+2\mu}(\hat{e}^0\cdot r)\right] +$$

$$+ \frac{\omega^2 e^{i\omega r/c_T}}{4\pi r c_T^2} S_{TT}(\theta,\phi,\theta^0,\phi^0)\left[\left[(\hat{r}\times b)\times\hat{r}\right]\left[\frac{\delta\rho}{\rho} - \frac{2\delta\mu}{\mu}(\hat{e}^0\cdot\hat{r})\right] + \left[\hat{e}^0\times b)\times\hat{r}\right]\left[\frac{\delta\mu}{\mu}\right]\right]. \tag{3.11}$$

This generalized formulation of the scattered field allows straightforward substitution into the equation of any incoming direction $\hat{e}^0$ and any outgoing direction $\hat{r}$. Our extension removes the necessity for a three-dimensional rotation of the scatterer volume V_s for each incident direction (which would be necessary if the incident direction were fixed to a particular direction as was the case in the original formulation).

A similar generalization is also useful in calculating scattered fields in the time domain, in which the incident wave is a short pulse rather than a monochromatic plane wave as above. For example, the generalization is easily made to formulas published by Rose and Richardson

[2] which have proven useful in our studies of scattering from oriented fibers.

1. Gubernatis, J. E., Domany, E., Krumhansl, J. A., and Huberman, M., "The Fundamental Theory of Elastic Wave Scattering by Defects in Elastic Materials: Integral Equation Methods for Application to Ultrasonic Flaw Detection," Materials Science Center, Cornell University, Ithaca, NY, 1976, unpublished.

2. Rose, J. H. and Richardson, J. M., "Time Domain Born Approximation," Journal of Nondestructive Evaluation, 3:45-53, 1982.

B-4. Ultrasonic Reflection Tomography

Personnel: S. R. Broadstone, BCL
R. M. Arthur, BCL

Support: RR 01362

Although state-of-the-art phased-array sector scanners produce images with good axial and azimuthal resolution, their performance is often compromised by constraints applied for real-time operation. If in-phase detection of backscattered signals is not performed at each image point in the field of view, accurate estimation of tissue properties is compromised. Consequently, an off-line imaging system was designed and built to investigate improvements for on-line or real-time imaging systems (PR 22, B-4).

The purpose of a quantitative imaging system is to extract physical properties of a medium of interest using scattered energy. Three approaches to solving problems of this type exist. Solutions can be found iteratively (generalized inversion), by exact direct inversion, or by approximate direct inversion [1]. We analyzed two methods for finding approximate direct solutions to two-dimensional inverse scattering problems as they apply to medical imaging using ultrasound. Specifically we compared the well-known paraxial approximation [2,3] to a new approximation based on the method of moments for accuracy and speed.

Speed of digital image generation based on solution of the linearized wave equation is proportional to the number and type of arithmetic operations required to backproject received ultrasonic energy. Ideally, a pixel value should be modified by backscattered signals in the time of a single arithmetic operation. We compared both paraxial and moment approximations in forward-difference formulations which can be computed in a single-addition time.

Approximate Direct Solution Methods

Inversion of the approximate direct solution of the acoustic wave equation [4] in the time domain results in the mapping of backscattered

signals to spatial locations which are consistent with measured times of flight [5,6]. Application of this geometrical or ray-tracing interpretation requires computing the time of flight T from the ultrasonic transmitter to a field point of interest and back to the receiver.

$$T = \frac{1}{c_o} (r_1 + r_2) , \tag{4.1}$$

where c_o is the background velocity [7],

$$r_1 = \left[(x-x_t)^2 + (z-z_t)^2\right]^{1/2} \tag{4.2}$$

$$r_2 = \left[(x-x_r)^2 + (z-z_r)^2\right]^{1/2} \tag{4.3}$$

(x_t,z_t) is the location of the transmitting transducer and (x_r,z_r) the location of the receiving transducer.

If ultrasonic energy is transmitted from and detected by the same transducer, arcs of constant time of flight in two dimensions are circles centered at the transducer [5]. When the transmitting and receiving transducers are not the same, arcs of constant time of flight are ellipses whose foci are the locations of the transmitting and receiving transducers.

Unfortunately, because of the number of arithmetic operations which includes computation of squares and square roots, calculation of the time of flight is a time-consuming task. To obtain faster reconstructions, the time-of-flight computation has often been approximated to reduce the number and complexity of arithmetic operations. The cost of using simpler expressions for the time of flight is, of course, inaccuracy in the time-of-flight calculation.

The exact form of the time of flight can be rewritten as a binomial expansion. Truncation of the expansion after the constant and linear terms yields the paraxial approximation [2,3] to the time of flight,

$$\hat{T}_p = \frac{1}{c_o} (z + \frac{x^2}{2z}) . \tag{4.4}$$

Although possessing fewer arithmetic operations than the exact expression for the time of flight, the computation of T using equation (4) still involves division, multiplication, and addition. Furthermore, as its name implies, it is accurate only near the propagation axis of the transducer. Accuracy of the approximation can be improved by keeping higher-degree terms in the expansion at the expense of more arithmetic operations.

An alternate time-of-flight approximation possessing arbitrary accuracy can be found by expanding the time-of-flight profile in terms of

its spatial moments. Using this approach, time-of-flight profiles can be approximated by a two-dimensional polynomial in azimuth and range

$$\hat{T}_m = \frac{1}{c_0} \sum_{k=0}^{K} \sum_{l=0}^{L} a_{k,l} x^k z^l , \tag{4.5}$$

where x is the azimuth and z the range. Coefficients are found by minimizing the mean-square error between the polynomial and the exact time-of-flight profile,

$$a_{k,l} = \int_{Z_1}^{Z_2} \int_{X_1}^{X_2} x^k x^l \left[x^2 + z^2\right]^{1/2} dx\, dz . \tag{4.6}$$

For most regions of interest the time-of-flight profiles are relatively smooth. Consequently, a second-degree polynomial containing 9 coefficients was chosen for the method-of-moments approximation in this study,

$$\hat{T}_{m_{deg2}} = \frac{1}{c_0} \left[a_{2,2}x^2z^2+a_{2,1}x^2z+a_{2,0}x^2+ \right. \tag{4.7}$$

$$\left. a_{1,2}xz^2+a_{1,1}xz+a_{1,0}x+a_{0,2}x^2+a_{0,1}z+a_{0,0}\right].$$

Because the method-of-moments polynomial possesses positive integer powers in x and z, it can be formulated as a stable forward-difference equation in the discrete case with a finite number of terms. Given an nth degree polynomial, $(n+1)^2$ forward differences describe the time-of-flight profile. We previously described an application-specific integrated circuit which could implement a 9-coefficient, forward-difference equation in a single-addition time [8]. The circuit must be seeded with forward differences (9 for a second-degree polynomial). It then calculates approximate values for round-trip times as sample addresses within memory containing backscattered signals. Because only 9 coefficients are required to map a 512 × 512 field of view, this structure requires loading 262,135 fewer terms than a look-up table to map the same region.

This circuit can also implement the paraxial approximation in a single-addition time if the paraxial approximation is modified to contain a finite number of integer powers of x and z. A simple way to modify the paraxial approximation for single-addition operation is to eliminate the division by the range variable,

$$\hat{T}_p \approx \frac{1}{c_0} \left(z + \frac{x^2}{2\, z_0}\right) . \tag{4.8}$$

With the denominator of the second term in the paraxial approximation fixed, the paraxial approximation can be formulated as stable forward-difference equation containing 4 terms. These terms are a constant, first differences in x and in z, and a second difference in x.

Including the next higher-degree term from the binomial expansion in the time-of-flight approximation requires expanding the parallel structure required to implement the forward-difference equation in a single-addition time [8]. The structure must be increased from 9 to 25 coefficients because the resultant approximation is fourth degree in x.

Approximation Errors

For comparison, each approximation was implemented for regions of interest centered about the range axis and for regions 15 degrees off the range axis. Fifteen degrees is often assumed to be the off-axis limit of the paraxial approximation.

A typical center frequency for medical ultrasonic transducers is 3.5 MHz. A 512 × 512 image reconstructed from backscattered signals sampled at 12.5 MHz, which is a suitable periodic sampling rate for a 3.5 MHz transducer, is about 3 × 3 cm. The maximum error in the spatial location of a backprojected sample, was determined over 3 × 3 cm regions of interest for distances from 0 to 30 cms.

Figure 1 shows the maximum approximation error over 3 × 3 cm regions of interest on axis and at 15 degrees for the paraxial approximation and for the method of moments using a second-degree, two-dimensional polynomial. Although the method of moments is a consistently better approximation, we note that the error for both approximations is largest for regions near the transducer. An aperiodic sample rate of 1/3 the center frequency wavelength provides a measure of the useful range of the approximations. Note that the 1/3 wavelength line in all figures is its backprojected value which is half that in the medium. This criterion leads to a fully useful range where the error is below the 1/3 wavelength value. The range is fully useful in that the criterion is met for every pixel in the 3 × 3 cm region of interest.

In Figure 2 we compare the forward-difference forms of the paraxial and method-of-moments approximations, i.e., forms that can be implemented in single-addition times. The forward-difference form of the moments approximation with a minimum fully useful range of 3 cm on axis and 6 cm at 15 degrees is the same as that shown in Figure 1. In the forward-difference form the paraxial useful range increased to 22 cm on axis and was > 30 cm at 15 degrees. These results for the forward-difference forms of the approximations are summarized and extended to 30 degrees in Table 1.

Enlarging the extent of the time-of-flight profile increased the error for both approximations. The error in the moment approximation with a second-degree polynomial was, however, more than 12 dB better than the paraxial approximation for a 12 × 12 cm region of interest on axis.

The mean value of the moment-approximation errors for both 3 × 3 and 12 × 12 cm regions of interest was zero. If the 1/3 wavelength criterion

is applied to the RMS error, the minimum useful range for a 3 × 3 cm region is about 1 cm. It is about 3 cm for a 12 × 12 cm region of interest.

Table 1.
Minimum Fully-Useful[1] Range: Transducer to 3 × 3 cm View Region

	On axis	15 degrees	30 degrees
Method of moments: Second-degree polynomial[2]	3.0	6.0	6.0 cm
Paraxial approximation[2]	22.0	> 30	----

[1]Maximum error less than 1/3 wavelength at 3.5 MHz
[2]Forward-difference form (single-addition time)

The paraxial and moments approximations are comparable for small regions of interest on axis. For off-axis regions of interest, however, the method-of-moments error is not much worse than the on-axis case, whereas the paraxial approximation degrades rapidly with off-axis angle. The method-of-moments approximation with a second-degree polynomial therefore in general provides a much more accurate representation of the exact time of flight than the paraxial approximation, which is also a second-degree polynomial.

New time-of-flight values can be found in a single-addition time using the forward-difference forms of both the paraxial and method-of-moments approximations. The cost of reducing the paraxial computation to a single-addition time is a substantial increase in error. Method-of-moments approximations of a given degree can be found in single-addition times with no increase in error compared to a least-squares-error fit of the time-of-flight profile.

1. Calogero, F. and Degasperis, A., Spectral Transform and Solitons: Tools to Solve and Investigate Nonlinear Evolution Equations, vol. I, North-Holland Publishing Company, New York, 1982.

2. Claerbout, J. F., Imaging to Earth's Interior, Blackwell Scientific Publishing Company, London, 1985.

3. Corl, P. D., Kino, G. S., DeSilets, C. S., and Grant, P. M., "A Digital Synthetic Focus Acoustic Imaging System," in Acoustic Imaging, A. F. Metherell, ed., Plenum Press, New York, 8:39-53, 1980.

4. Morse, P. M. and Ingard, K. U., Theoretical Acoustics, McGraw-Hill, St. Louis, 1968.

5. Fawcett, J. A., "Inversion of N-Dimensional Spherical Averages," SIAM Journal of Applied Mathematics, 45:336-341, 1985.

6. Ozbek, A. and Levy, B. C., "Inversion of Parabolic and Paraboloidal Projections," IEEE Transactions on Acoustics, Speech and Signal Processing, in press.

7. de Vries, D. and Berkhout, A. J., "A Note on the Effect of Velocity Errors in Computerized Acoustic Focusing Techniques," Journal of the Acoustical Society of America, 74:353-356, 1983.

8. Broadstone, S. R. and Arthur, R. M., "An Approach to Real-Time Reflection Tomography Using the Complete Dataset," IEEE 1986 Ultrasonics Symposium Proceedings, IEEE Catalog No. 86CH2375-4, B. R. McAvoy, ed., New York, 2:829-831, 1986.

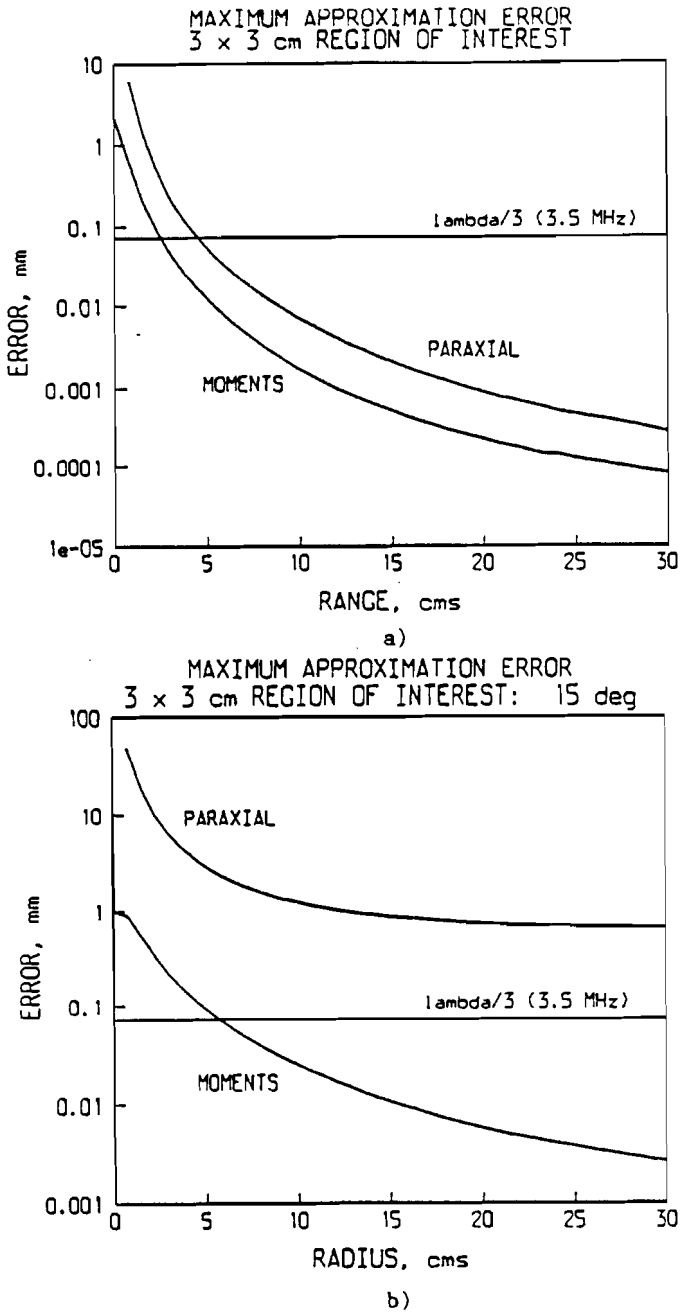

Figure 1. Maximum approximation errors (a) on axis and (b) at 15 degrees for the paraxial and moments approximations over a 3 × 3 cm region of interest. The paraxial approximation error was calculated using the constant and linear terms in the binomial expansion of the time-of-flight profile. A second-degree polynomial in azimuth and range was used to fit the time-of-flight profile on a least-squares-error basis for the method-of-moments approximation.

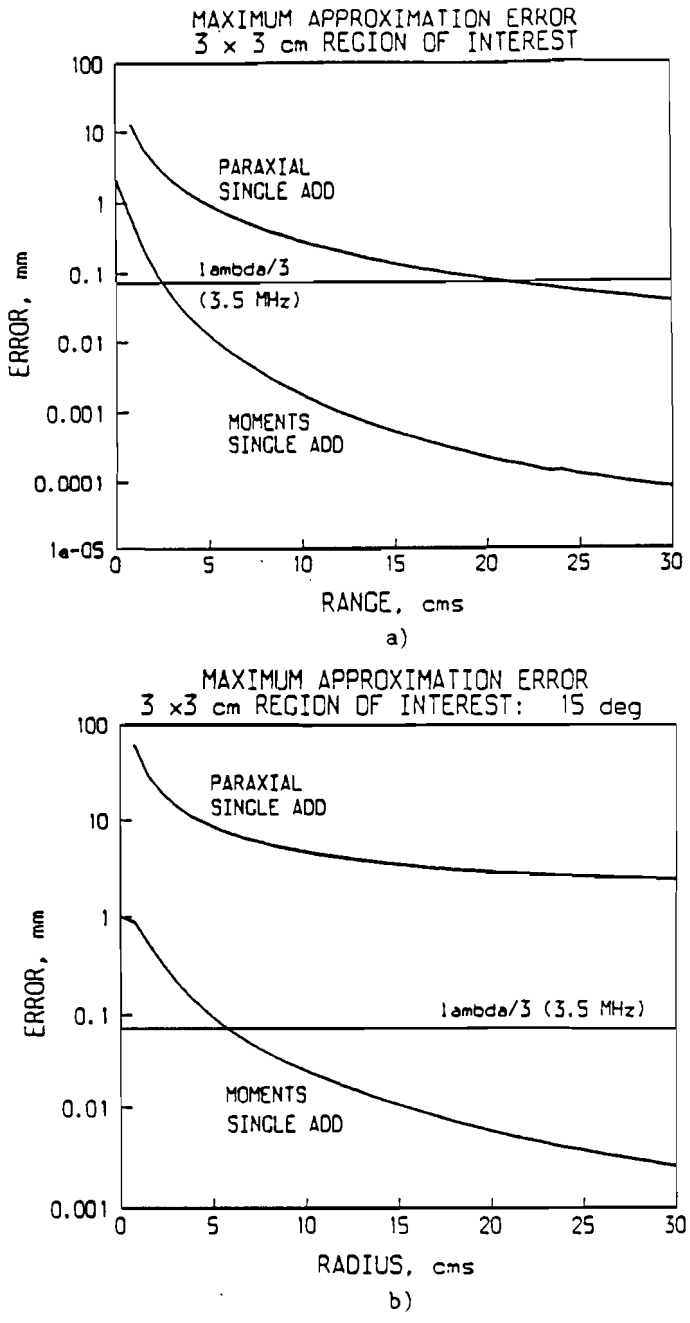

Figure 2. Maximum approximation errors (a) on axis and (b) at 15 degrees for the forward-difference forms of the paraxial and moments approximations over a 3 × 3 cm region of interest. The paraxial approximation error was calculated with the division by range in the linear term of the binomial expansion of the time of flight replaced by a scale factor. A second-degree polynomial in azimuth and range was used to fit the time-of-flight profile on a least-squares-error basis for the moments approximation.

B-5. The Transfer Function of Transducer Elements

Personnel: R. M. Arthur, BCL
S. R. Broadstone, BCL

Support: RR 01362

Transducer behavior must be taken into account in order to make quantitative ultrasonic measurements. Clearly, the content of the beam of a phased array is dependent on the beam profiles of the individual elements in that array. The energy transmitted or received by a transducer element is dependent on signal frequency and on the angle of propagation or incidence (PR 22, B-5). In addition, imaging with at a focused transducer array is clearly affected by the choice of background velocity used during that reconstruction.

To investigate this effect, we calculated the transmitted and received signals produced by an array of rectangular elements assuming they underwent uniform longitudinal motion. Diffraction patterns of rectangular pistons were calculated using the method of Lockwood and Willette [1]. These methods treat an element as a collection of point sources and yield the impulse response of the element as a function of time at any field point. The calculated backscattered signals were then used to reconstruct the image of point scatterers in a homogeneous medium.

In addition to an impulse we described transducer motion with simple functions, including a three-cycle, center-frequency sinusoid with a half-sine envelope. To represent the actual element motion we measured the pressure on the propagation axis of 1.1 × 13.0 mm elements (separation, 1.4 mm) of the 3.5 MHz array. We deconvolved this signal with the impulse response of the element to get an equivalent uniform motion. We calculated signals backscattered from a point at a range of 5 cm on the axis of a 32-element array composed of elements like those measured. Signals were found by convolving the motion functions with the impulse response of each element into a medium with a 1500 m/s phase velocity.

A point image was reconstructed for each drive function via synthetic focus with the complete-dataset over a 512 × 512 view region, which was 3.8 mm on a side (see Figure 1). The full-width half maximum (FWHM) for the lateral spread of the impulse-motion image was 1.9 mm. It was 0.8 mm for both measured and sine-envelope motion. When the velocity on reconstruction was varied by 40 m/s compared to the known 1500 m/s, the FWHM of the images resulting from sine-envelope motion did not change significantly. Pixel values, however, did change. At 1460 m/s the peak and standard deviation went down 3.1 and 1.6 dB, respectively, compared to the 1500 m/s image. At 1540 m/s, peak and standard deviation were down 3.7 and 1.6 dB, respectively. As expected, entropy had a minimum at 1500 m/s where it was 3.14. Entropy increased to 3.43 at 1460 m/s and to 3.47 at 1540 m/s.

1. Lockwood, J. C. and Willette, J. G., "High-Speed Method for Computing the Exact Solution for the Pressure Variations in the Nearfield of a Baffled Piston," Journal of the Acoustical Society of America, 53:735-741, 1973.

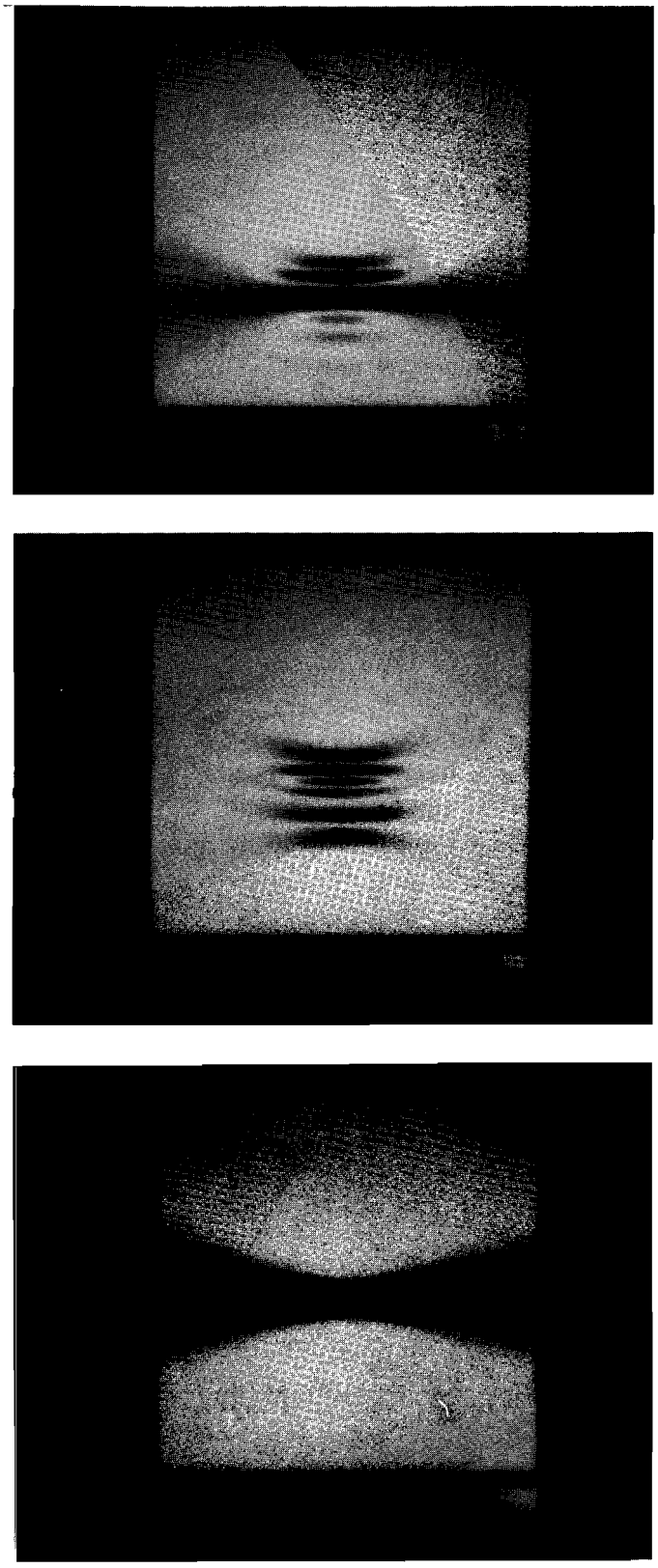

Figure 1. Image of a point scatterer as viewed at a range of 5 cm by a 32-element array of 1.1 × 13.0 mm rectangular pistons driven by a) an impulse, b) a three-cycle sine with a half-sine envelope, and c) an equivalent, uniform drive inferred from measured element response.

C. Quantitative Imaging: Radiation Treatment Planning

This work is centered in Mallinckrodt Institute of Radiology, and represents a set of activities targeted to providing more effective radiation therapy treatment of cancer by improving the dose calculation accuracy, the evaluation of treatment plans, and verification of dose delivery. Important insight into the importance of interactive 3-D display to insure effective evaluation of treatment plans is described in Section C-1. Sections C-2 and C-3 report on research aimed at improving the accuracy of dose calculation and Section C-4 describes work aimed at improving verification of dose delivery.

C-1. Evaluation of Three-Dimensional Treatment Planning

Personnel: J. A. Purdy, Ph.D., Radiology
R. E. Drzymala, Ph.D., Radiology
B. N. Emami, M.D., Radiology
W. B. Harms, B.S., Radiology
K. E. Krippner, B.S., Radiology
J. W. Matthews, D.Sc., Computer Systems Laboratory
J. R. Simpson, Ph.D., Radiology
J. W. Wong, Ph.D., Radiology

Support: RR 01380
CM 47696
CM 67915
RR 01379

In September 1984, the National Cancer Institute (NCI) funded a three year multi-institutional effort to develop criteria, guidelines and methodology for the performance and evaluation of state-of-the-art high-energy-photon external-beam treatment planning [1,2]. In August, 1986, the NCI funded a similar effort for electron-beam treatment planning. These tasks were to be accomplished by extensive treatment planning for actual patients using state-of-the-art computerized treatment planning and imaging systems.

The collaborating institutions participating in the photon treatment planning project are: Washington University School of Medicine in St. Louis, Massachusetts General Hospital, Memorial Sloan-Kettering Cancer Center and the University of Pennsylvania. The collaborating institutions participating in the electron treatment planning project are Washington University School of Medicine in St. Louis, University of Michigan, and the University of Texas M.D. Anderson Hospital and Tumor Institute in Houston, Texas. Each project established a Working Group, which consists of medical physicists, radiation oncologists and computer scientists from each collaborating institution, and which mets three times a year to develop strategies to accomplish the project's research goals and to review the progress of the participating institutions.

In last year's report, we presented the results of our efforts in implementing a prototype 3-dimensional radiation therapy planning (RTP) system having both real-time display and advanced dose algorithm capabilities for calculating and displaying the dose distribution and patient anatomy for non-coplanar fields and arbitrary planes in the patient [3]. The system consists of a CMS Modulex computer interfaced to a MMS-X display system and a DEC MicroVAX II/Numerix array processor system.

The majority of the effort during this reporting period went into actual 3-D treatment planning and plan evaluations for specific categories (accruals). To date, we have completed the 75 accruals for the photon project and will begin planning for the electron contract during the next reporting period. The photon accruals include 4 conventional plans, 16 plans based on standard beam arrangements, 16 uncertainty (CT-electron conversion change) plans, 16 plans studying the effects of heterogeneities, 16 best plans and 7 other plans investigating the use of different photon-beam energies and the Delta Volume algorithm.

The use of the system in developing the treatment planning accruals has revealed numerous problems in the computer code. Considerable time and effort has been required to isolate and correct the problems. Unfortunately, there is no way to avoid this time-consuming "debugging" approach as this 3-D system is a "one-of-a-kind" system.

During the past year, we have also enhanced the 3-D RTP system's features, having now completed software which provides for dose calculations with and without compensating filters, dose-volume histogram generation, arbitrary-plane display and dose-surface computation and display on the MMS-X.

The display of an image of arbitrary orientation calculated from axial CT data is necessary for true three-dimensional (3-D) treatment planning. In our system, the plane of interest is selected by designating three non-colinear points via cursor on the display screen showing six pre-selected CT axial slices. Two scales are provided on the display screen for reference purposes - a linear (cm) scale on the horizontal axis and an axial slice number scale on the vertical axis. In addition, we can display the plane as an object on the MMS-X. This allows the treatment planner to observe the intersection of the plane with critical structure and target-volume contours as viewed from any arbitrary direction and aids the plan evaluator in interpreting the gray-scale display on the Modulex.

Dose-volume histograms (DVH's) are another planning evaluation aid that has proven to be extremely valuable in 3-D treatment planning. DVH's are a way of condensing the three-dimensional dose-distribution data into graphical form. Using DVH's, one can very quickly determine if critical structures receive doses exceeding tolerance and/or if the target volume is adequately covered. However, we have found that DVH's can be misleading if either the dose-matrix elements or the patient-structure volume elements (voxels) are too coarse.

Examples of DVH's generated by our algorithm for a critical organ site, the spinal cord, are shown in Figure 1. The histograms were computed using different voxel sizes but using the same 3-D dose matrix calculated for an anterior-posterior parallel opposed-beam arrangement, used to treat

a patient with Hodgkin's Disease. The calculated total volume is more than three times greater for the higher resolution and the histograms differ significantly in shape. The latter could lead to different evaluations for the appropriateness of a particular beam arrangement if based on DVH's.

While DVH's provide information on the existence and magnitude of "hot" and "cold" spots within the irradiated volume, they do not indicate their location. The sheer volume of dose data in 3-D planning makes it difficult to interpret or assimilate in a 2-D format such as isodoses displayed on 2-D axial, sagittal or coronal gray-scale images of the patient's anatomy. We now have the capability of generating isodose surfaces from the calculated 3-D dose matrix and displaying them as wire frame surfaces on the MMS-X. This feature has proven to be a valuable aid in evaluating these hot/cold spots.

A major effort during this reporting period was the testing and debugging of the Delta Volume (DV) computations for the array processor and the communication software between the Modulex and the MicroVAX. Recall that we first implemented the DV algorithm in a research environment on our VAX 11/780. That implementation was used to verify the algorithm's ability to deal with complex geometrical heterogeneities. However, it only computed a correction factor and was limited as to the kinds of beam set-ups which could be accommodated. In short, that implementation was a point-dose calculator but not a treatment planning system.

From our experience with the research implementation and estimates we made for the treatment planning we were considering, it was clear that the algorithm could not remain on the VAX. As a project in VLSI design, a chip was designed to do the ray-trace part of the computation. However, due to uncertainties about functionality and schedule, it was decided to implement the algorithm on a very fast array processor (AP) as part of our 3-D RTP system [4].

Execution time was the major motivation for considering an array processor but cost was also a concern. We considered those with the highest speed available but under $100,000. This eliminated a large number of AP's which shared memory with the host computer and several in the 5 to 10 million instructions per second (mips) range. We realized floating point would be very convenient but it was considered to be of lesser importance than absolute speed.

Also, because of our participation in the photon planning research contract for which we wished to use the DV algorithm, only a limited time period was available for the development of the RTP system. It was thus decided that only an AP with an available FORTRAN compiler would be considered. A symbolic debugger was also felt to be desirable.

Based on these constraints, we selected the model 432 array processor from Numerix, Inc. (Newton, Massachusetts). It has an advertised speed of 30 million floating point operations per second and they offered a FORTRAN 77 compiler. An Array processor Video Interactive Debugger, AVID, was also available as the company offered host support on either the DEC RSX or VMS operating systems.

One of the concerns we had about the model 432 AP was the memory size. It came as a 64 kword machine, expandable to 128 kword. Although this seemed marginal, again, to contain costs, we chose the 64 kword configuration. Because of this memory limitation, the calculation method was dictated on several occasions by available memory rather than other programmer expediencies. Machines now available from Numerix and other vendors boast of memories of many megabytes and the price for these units are now quite reasonable as well.

We have now completed the delta volume implementation in our 3-D RTP system and a careful comparison with the results from dose verifications measurements is ongoing. The findings will be discussed in the next reporting period. A comparison of time requirements for dose calculation using the DV algorithm for the AP implementation and the VAX 780 implementation is shown in Figure 2.

In summary, these initial studies in 3-D treatment planning have provided important information as to what planning aids are needed. In addition, the analysis of the treatment-planning accrual data will be incorporated into a report which will provide insight into the role of this advanced technology in radiation treatment planning.

1. Purdy, J. A., Wong, J., and Harms, W., "New Developments in Three Dimensional Radiotherapy Treatment Planning," Radiotherapy Systems Research, 3:1-25, 1986.

2. Purdy, J. A., Wong, J. W., Harms, W. B., Emami, B., and Matthews, J. W., "State of the Art of High Energy Photon Treatment Planning," in Treatment Planning in the Radiation Therapy of Cancer, Frontiers of Radiation Therapy Oncology, J. M. Vaeth and J. Meyer, eds., Vol. 21, pp. 4-24, 1987.

3. Purdy, J. A., Wong, J. W., Harms, W. B., Drzymala, R. E., Emami, B., Matthews, J. W., Krippner, K., and Ramchandar, P. K., "Three Dimensional Radiation Treatment Planning System," in The Use of Computers in Radiation Therapy, I.A.D., Bruinvis, P. H. Van der Giessen, H. J. Van Kleffens, and F. W. Wittkamper, eds., Elsevier Science Publishers, North Holland, pp. 277-279, 1987.

4. Krippner, K., Wong, J. W., Harms, W. B., and Purdy, J. A., "The Use of an Array Processor for the Delta Volume Dose Computation Algorithm," in The Use of Computers in Radiation Therapy, I. A. D. Bruinvis, P. H. Van der Giessen, H. J. Van Kleffens, and F. W. Wittkamper, eds., Elsevier Science Publishers, North Holland, pp. 533-536, 1987.

5. Krippner, K., Wong, J. W., Harms, W. B., and Purdy, J. A., "Implementation of a Scatter Ray-Trace Dose Calculational Algorithm on an Array Processor," Medical Physics, 14:452, 1987 (abstract).

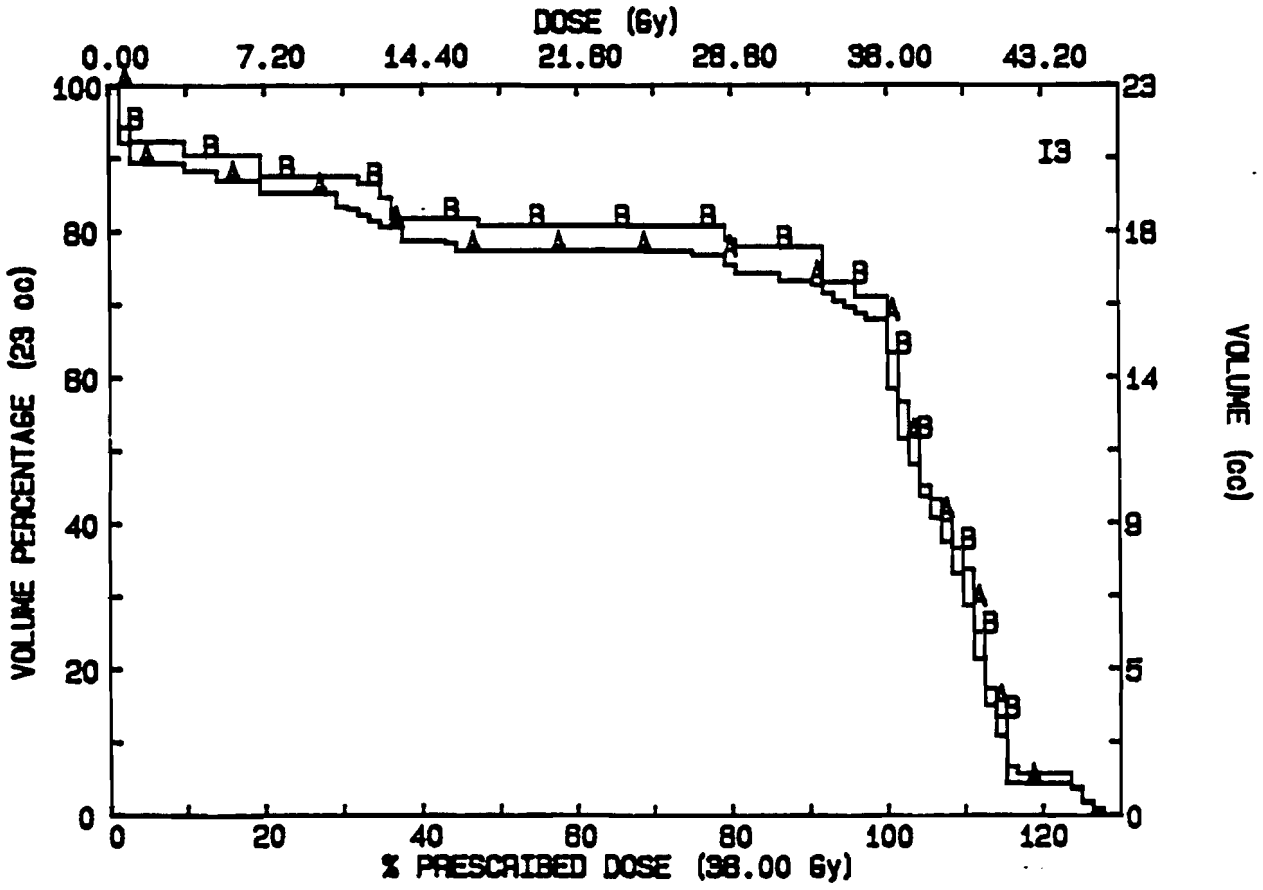

Figure 1. The effect of voxel resolution. The DVH's shown are of the spinal cord for an external photon beam treatment of a patient with Hodgkins disease. (A) Resolution of 0.25 cm. (B) Resolution of 0.5 cm.

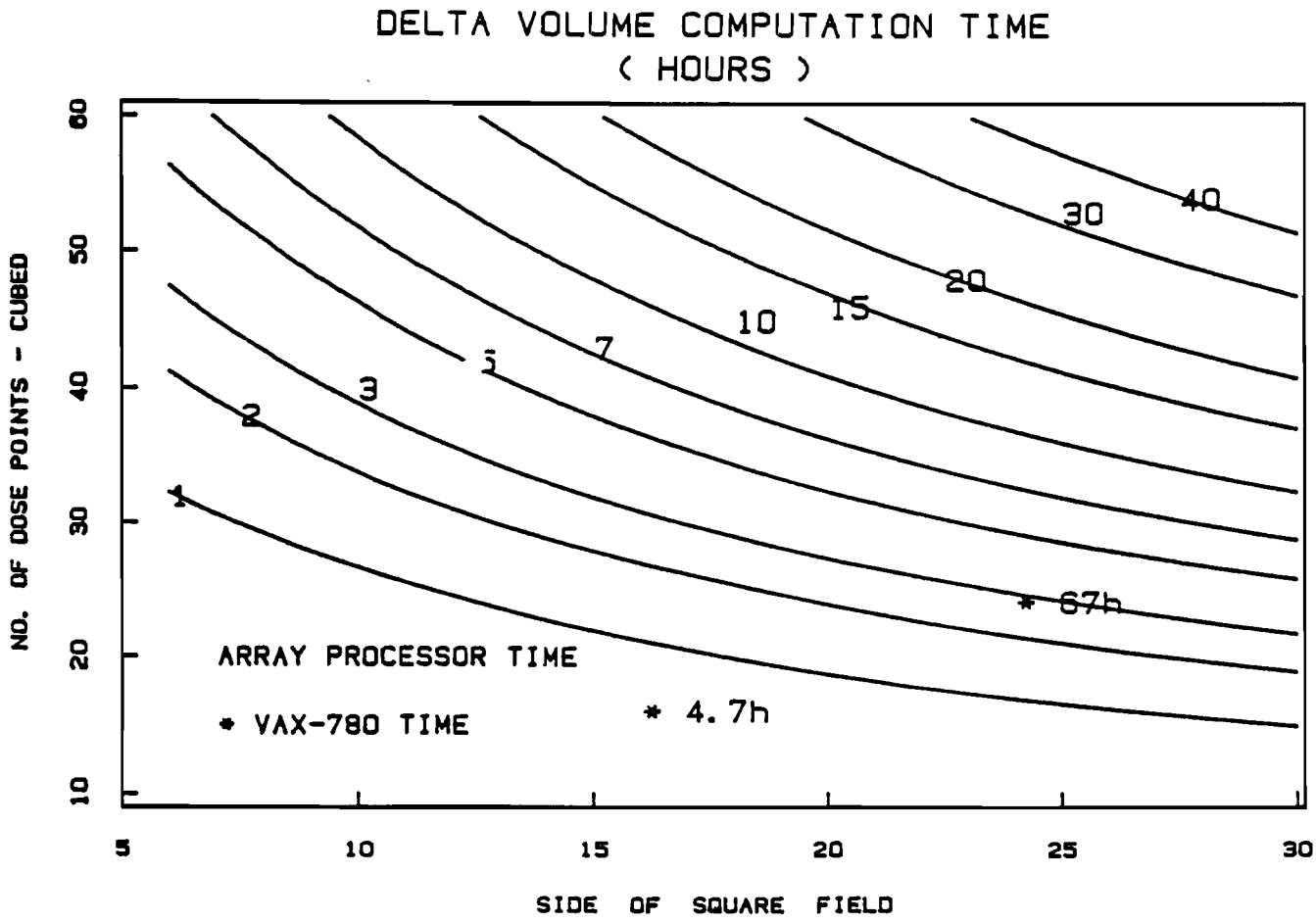

Figure 2. Contour lines showing the Delta Volume computation times (in hours) on the array processor for different combinations of beam areas and number of dose points. In addition, the times for 16^3 and 24^3 calculations on the VAX/780 are shown.

C-2. The Effects of Atomic Constituents and Dimensions of the Target on the Charged Particles Emitted from Photon Interaction

Personnel: J. W. Wong, Ph.D., Radiology
W. S. Ge, B.S., Electrical Engineering
S. S. Hancock, M.S., Medical College of Ohio
S. P. Monthofer, B.S., Radiology

Support: RR 01380
CA 41574
RR 01379

In order to extend our Delta-Volume photon dose calculation algorithm to higher photon energies than Cobalt-60, electron transport must be incorporated into our existing photon transport model. An important study is to characterize the energy and spatial distribution of the charged particles set in motion in the medium due to photon interactions [1,2].

In our current photon transport model, local electron energy deposition is assumed and it is adequate to employ the theoretical Klein-Nishina cross-section for a single electron to describe the distribution of the scattered photon component. However, due to multiple coulomb scatterings, the theoretical distribution of the emitted electrons from a single interaction is not acceptable at higher photon energies. Multiple electron scatterings are affected by the atomic number and the size of the interaction site. Atomic number of the target also affects the amount of pair productions which we noted in PR 22. During the past year, we performed studies to characterize the relation of photon interaction and electron emission with respect to the target's composition and dimension. The finding is of particular importance to our Delta-Volume algorithm where a dose calculation volume is partitioned into discrete subunits.

Besides the experimental studies that were reported last year and are still on-going, we performed Monte Carlo simulation using the Stanford EGS4 photon and electron transport code. Figure 1 shows our irradiation geometry where a pencil photon beam of 3 or 5 Mev impinges on a water or aluminum target with diameter of 1, 2.5, or 5 mm. The rest of the medium is vacuum. Because of the finite target size which represents an extended source, the energy and the fluence of the emitted charged particles crossing a spherical boundary at a radii of 2, 5 and 10 cm away are scored. The charged particles set in motion due to Compton and pair-production interactions are also separated as the former is affected by electron density and the latter by atomic number and density.

Figure 2 shows, for the charged particles emitted by pair production in the 3-Mev case, the probability of particle detection normalized to the number of photon interactions in the target plotted vs angle at a detection radius of 2 cm. Not surprising, the aluminum target has a stronger multiple scattering effect. As the target size increases, a substantial number of charged particles do not exit the target. Figure 3 shows charged particle distributions due to 3-Mev pair production in a 2.5-mm water target as detected at different radii. The distributions are very similar and do not vary significantly for larger target radii, suggesting an equilibrium condition. Figure 4 shows the distributions for the 2.5-mm

aluminum target in the 5-Mev case with the detection at 2 cm away. The results point to the substantial amount of pair production and to the backward scattering of Compton electrons. There is no backscatter Compton component in an ideal point target.

For the next year, we plan to:

a. extend the above simulations for a broad photon beam that covers the entire target,

b. incorporate the information into a photon-transport model to predict dose buildup in the surface and beam-edge regions, and in inhomogeneous geometries,

c. apply this knowledge in the estimation of accuracy in photon dose calculations.

1. Wong, J. W., Ge, W. S., Monthofer, S., and Hancock, S. S., "Spatial Distributions of Charged Particles Emitted by Pair Productions," Medical Physics, 14:474, 1987.

2. Yu, C. X., Wong, J. W., and Purdy, J. A., "Photon Dose Perturbations Due to Small Inhomogeneities," Medical Physics, 14(1):78-83, 1987.

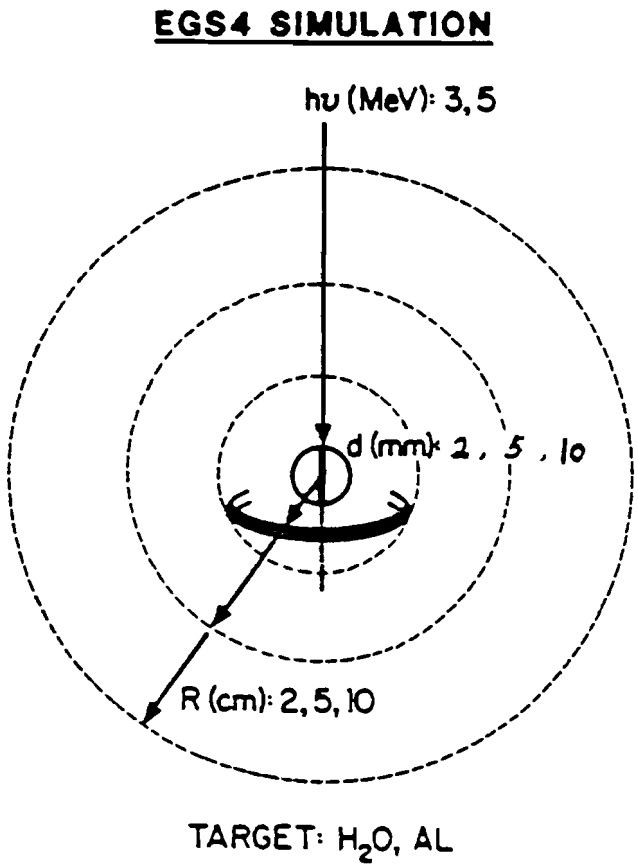

Figure 1. Target Geometry Used for Simulation.

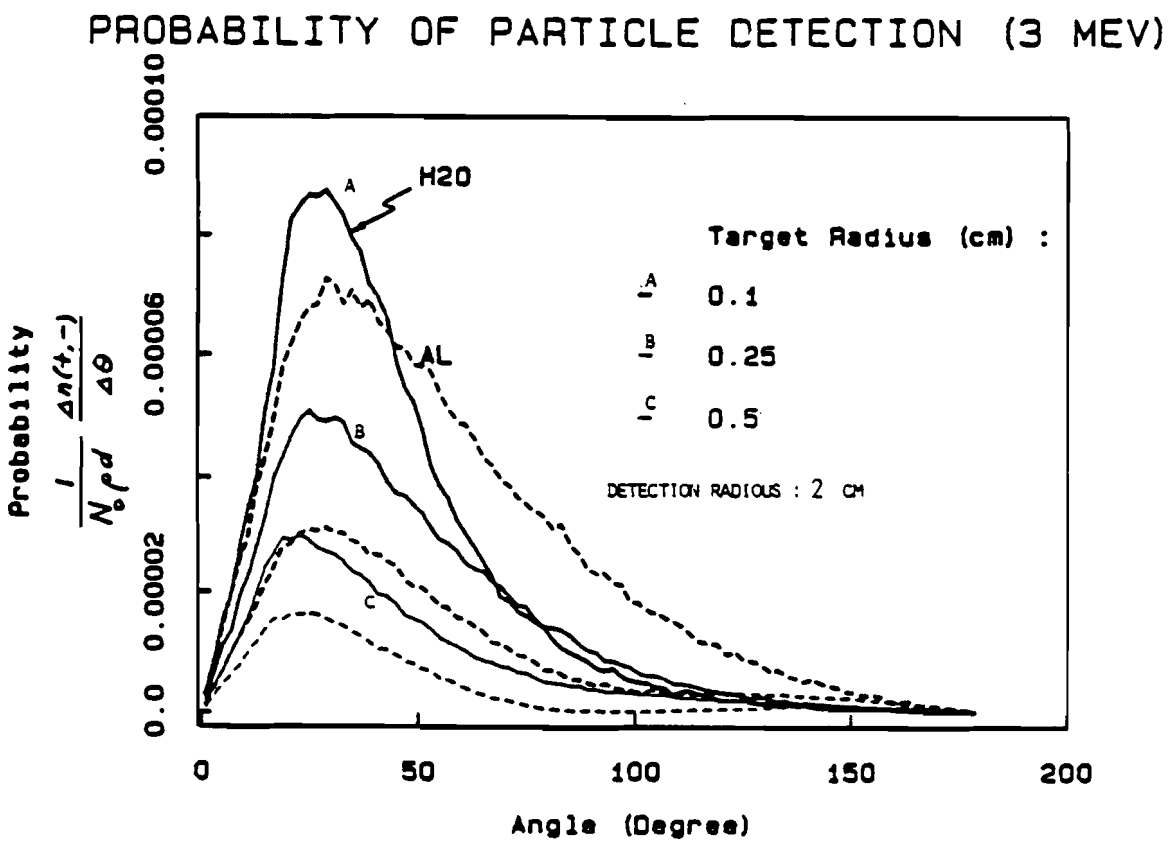

Figure 2. Probability of Particle Detection vs Angle for 3 Mev Beam.

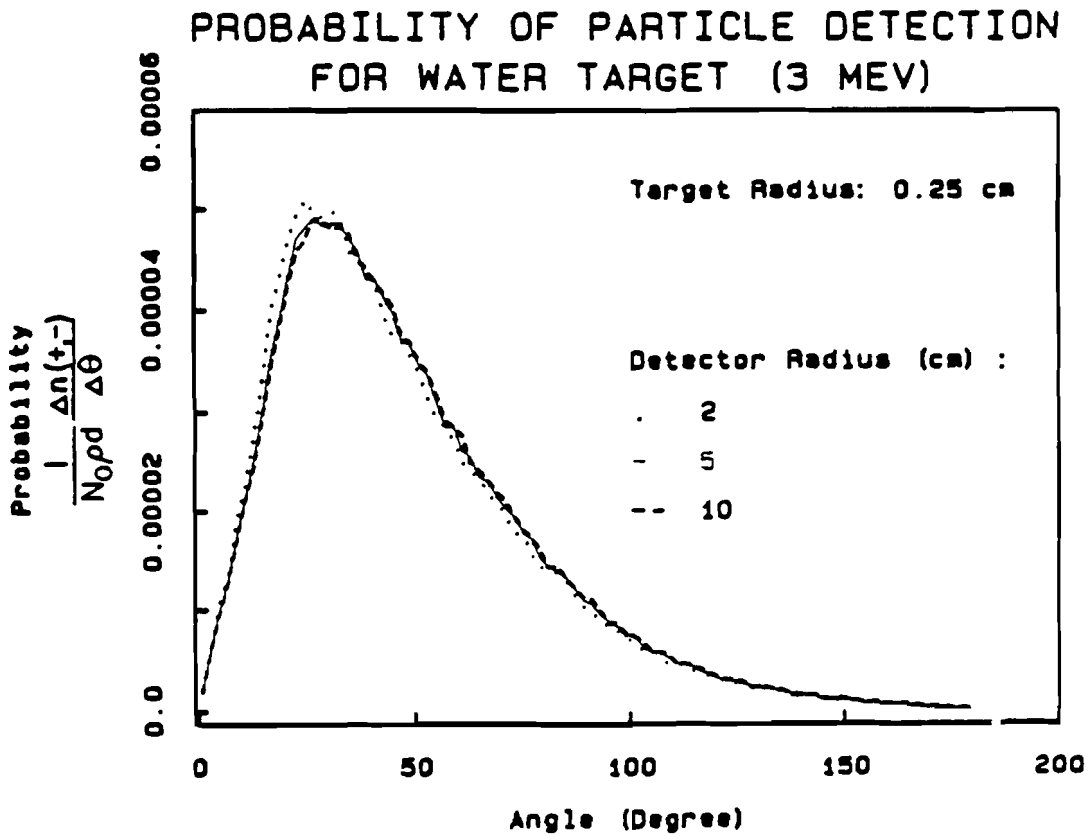

Figure 3. Probability of Particle Detection vs Angle for Water Target.

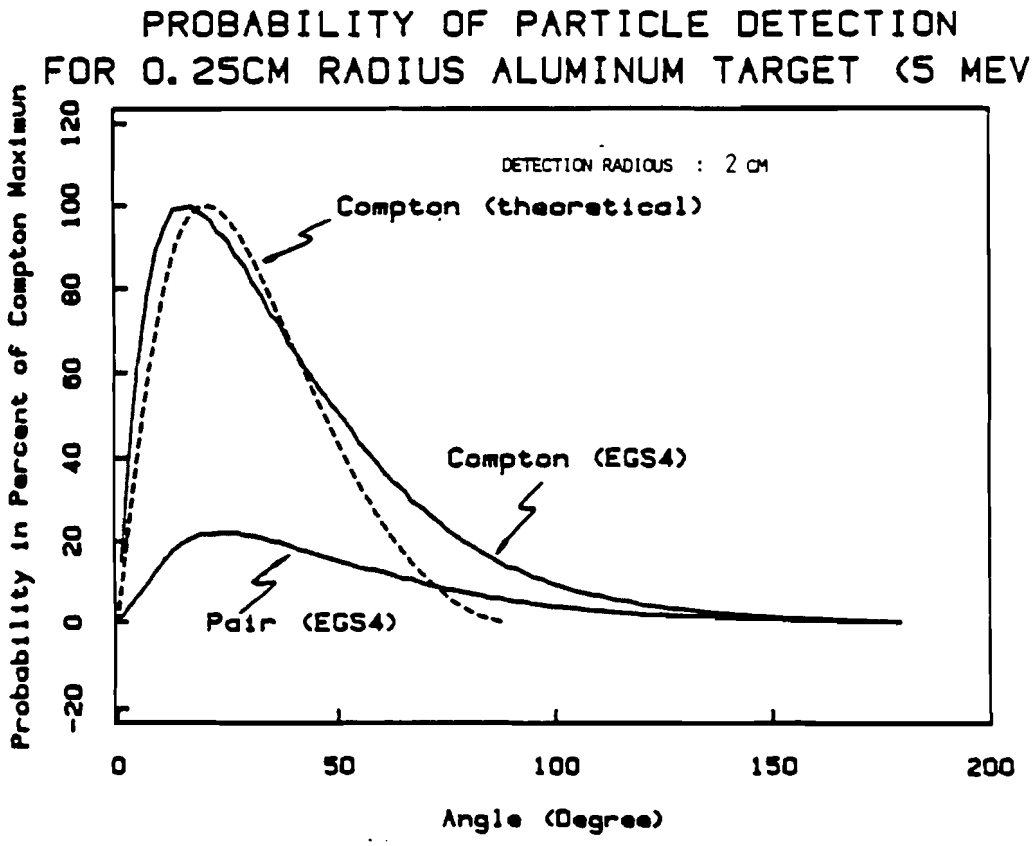

Figure 4. Probability of Particle Detection vs Angle for Aluminum Target and 5 Mev Beam.

C-3. Dose Calculation Accuracy and Time Tradeoffs

Personnel: F. U. Rosenberger, BCL and Computer Systems Laboratory
J. W. Matthews, D.Sc., Computer Systems Laboratory
J. W. Wong, Ph.D., Radiology
X. Ying, D.Sc., Radiology

Support: RR 01380
RR 01379
Mallinckrodt Institute of Radiology

We have identified several computation alternatives with the potential to dramatically improve accuracy and reduce computation time of the delta-volume algorithm. The dramatic decrease in the cost of random access memory and magnetic disk storage along with the emergence of optical disk technology makes the use of pre-computed tables increasingly attractive. Preliminary calculations indicate that use of pre-computed tables for the first-scatter path-attenuation calculations [1,2] can reduce the computation time requirements significantly. Table 1 shows a comparison of the relative time required for numerical integration, analytic, and table-look-up methods. For 1% accuracy in the attenuation calculations, the table look-up method is clearly superior and it maintains a slight superiority over numerical integration when 8% error is allowed. Table 2 shows the storage requirements as a function of the treatment-volume dimensions for a brute-force implementation; they are clearly substantial for the larger volumes. These storage requirements can be greatly reduced by taking advantage of symmetry at some increase in computation time, or by use of a variable grid size with small voxels for scatter near the dose point, and increasing voxel size for scatter further away from the dose point. A variable grid would also substantially reduce the number of calculations required. Efforts are presently underway to evaluate the effects on calculation accuracy of varying the computation grid size.

A proposal has been submitted requesting support for evaluation of algorithm accuracy and computation time for dose calculation in radiation treatment planning. There are many tradeoffs that can be made between accuracy and computation time including the choice of specific algorithm, options in algorithm implementation, and the coarseness of the grid or step size used for numerical calculations. We plan to quantify the magnitude of computation errors in the presently used delta volume algorithm [1] for dose calculation due to voxel size, beam spectrum, source size, angle approximations, and coordinate transformations, and to develop a modified implementation of this algorithm that will provide superior accuracy and reduced computation time compared to present implementations, along with the ability to trade accuracy for computation time over a significant range. The specific aims from this proposal are:

1) to quantify the effect of voxel size on accuracy for dose calculation;

2) to quantify the effect of beam spectrum on accuracy for dose calculation;

3) to quantify the effect of finite source size on accuracy;

4) to investigate and quantify the effects of coordinate transformations in calculations for arbitrary beam orientation and for generating tables used in calculations;

5) to study the interaction of error sources to determine the validity of estimating their combined effects by superposition;

6) using the results from specific aims 1 through 5, determine implementation parameters for delta-volume dose calculation that realize optimum tradeoffs between accuracy, computation time, and storage requirements;

7) using the results from specific aim 6, implement a prototype variable-voxel-size algorithm to provide more accurate and faster dose calculation than existing delta volume implementations along with the capability to tradeoff accuracy for computation time;

8) incorporate explicit calculation of electron transport, and if necessary, pair-production into the delta volume algorithm to provide improved accuracy for high energy treatment beams.

1. Rosenberger, F. U., Krippner, K., Stein, Jr., D., and Wong, J. W., "Implementation of Delta-Volume Dose Calculation Algorithm," Proceedings of the Eighth International Conference on the Use of Computers in Radiation Therapy, Toronto, Canada, pp. 78-82, July 9-12, 1984.

2. Wong, J., "A New Approach to Photon Dose Calculations in Radiotherapy Treatment Planning," Department of Medical Biophysics, University of Toronto, Toronto, Canada, July 1982 (Ph.D. Dissertation).

Table 1
Relative First-Scatter Path-Length Computation Times

N	Numerical Integration Maximum Error Per Path			Analytic	Table Look-Up
	8%	4%	1%		
10	0.24	0.453	1.7	0.76	0.045
15	2.78	5.16	19.5	12.7	0.73
20	15.6	29	109	93	5.30
25	60	111	417	441	24.8
30	178	330	1245	1569	87.4
40	1001	1855	6997	11662	645

Table 2
Storage Requirements for First-Scatter Pre-Stored Path Lengths

Length of Volume Side in Voxels	Pointer Table	Path-Length Table	Electron Density Table	Total Storage Required in Bytes
N	$2(2N-1)^3$ $N<8$ $4(2N-1)^3$ $N\geq 8$	$(2N-1)^3\cdot(6N+8)$ $N<40$ $(2N-1)^3\cdot(9N+8)$ $N\geq 40$	$2N^3$	
5	1,458	27,702	250	29,410
10	27,436	466,412	2000	495,848
15	97,556	2,390,122	6,750	2,494,428
20	237,276	7,592,832	16,000	7,846,108
30	821,516	38,611,252	54,000	39,486,768
40	1,972,156	122,273,372	128,000	124,373,828
50	3,881,196	444,396,942	250,000	448,528,138

C-4. Development of a Plastic Scintillator Sheet as a Large-Area Dosimeter

Personnel: W. S. Ge, B.S., Radiology
W. R. Binns, Ph.D., Physics
J. W. Epstein, Physics
M. H. Israel, Ph.D., Physics
J. Klarmann, Ph.D., Physics
J. W. Wong, Ph.D., Radiology

Support: RR 01380
CA 42993
RR 01379
Physics Department

We are continuing our development of a plastic scintillator sheet as a rapid large-area dosimeter [1-3]. The dosimetry system consists of a piece of plastic scintillator standing vertically along the beam axis in a water tank. The scintillation output is captured by a digital camera which is interfaced to an IBM PC.

In our previous study, water scintillation was found to contribute about 20% of the signal. During the past year, we have modified our setup to reduce the effect of water scintillation. A piece of black plastic is placed behind the scintillator to reduce the effect of water scintillation by half. The water tank now has two viewing windows. While the plastic scintillation signals are captured on one side, turning the tank around allows background measurements on the other side.

Since water scintillation has a wide spectrum, a combination of a yellow emitting scintillator and a yellow optical filter positioned in front of the camera lens was chosen to further minimize background. Optical filtering also diminishes some spurious signals.

In order to reduce noise, the multiple-frame-capture utility of the image buffer is used to acquire 10 data frames consecutively where each data frame represents integration over a five-second period. A single-beam dosimetry study requires less than one minute. In comparison, the conventional scanning ion chamber approach would take 100 minutes.

During the experiment, the camera was cooled to $3^{o}C$ to reduce dark current. The lens aperture was set at F-number 2.8 to reduce the vignetting effect. Figure 1a shows the central-axis depth intensity profile in comparison to ion chamber measurements for the 18-MV photon beam. Excellent agreement was achieved. Figure 1b shows the iso-intensity contours for the 18-MV photon beam at a high spatial resolution of about 1.5 mm^2. Figure 2 shows similar plots for a 12-MeV electron beam. A discrepancy between ion chamber measurements and scintillation measurements was observed near the surface of the medium.

In summary, good agreement between the scintillation and the ionization data for photon beams are demonstrated.

For next year, we plan to:

a. study the surface discrepancies for electron beams by altering the detector properties and by Monte Carlo simulation;

b. perform uniformity calibration of the system; and

c. extend the system for brachytherapy dosimetry measurements.

1. Wong, J. W., Slessinger, E. D., Hermes, R. E., Harms, W. B., Vannier, M. W., and Roy, T., "Investigation of an Approach to Quantitative Treatment Verification," Proceedings of the Ninth International Conference on the Use of Computers in Radiation Therapy, Tilburg, Netherlands, pp. 461-464, June 22-25, 1987.

2. Wong, J. W., Ge, W. S., and Binns, W. R., "Continuing Development of a Plastic Scintillator Sheet as a Large Area Dosimeter," Medical Physics, 14:483, 1987.

3. Wong, J. W., Binns, W. R., Ge, W. S., Epstein, J. W., Klarmann, J., and Israel, M. H., "Rapid Areal Dosimetry Using a Computer Based Plastic Scintillator - Video Camera System," Proceedings of the Ninth International Conference on the Use of Computers in Radiation Therapy, Tilburg, Netherlands, pp. 417-420, June 22-25, 1987.

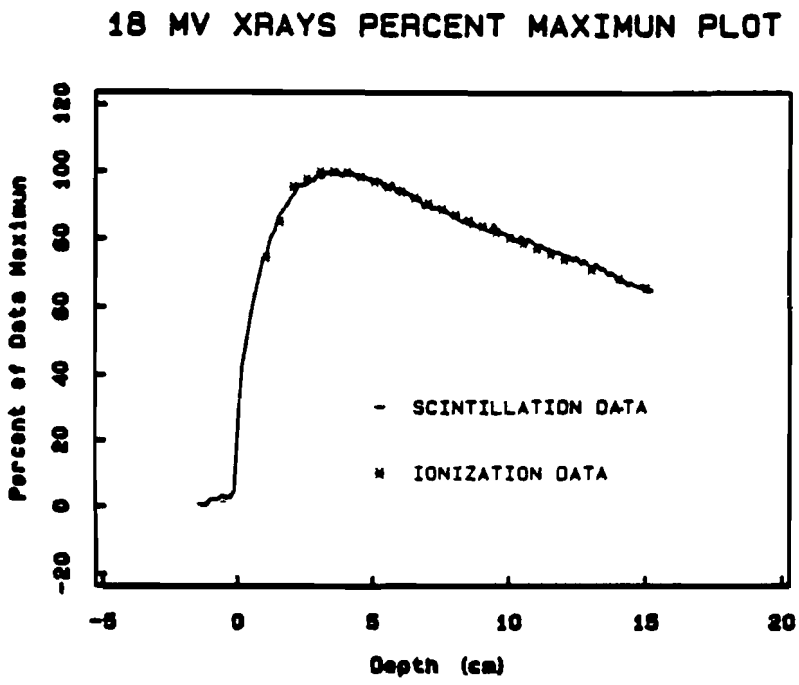

1a

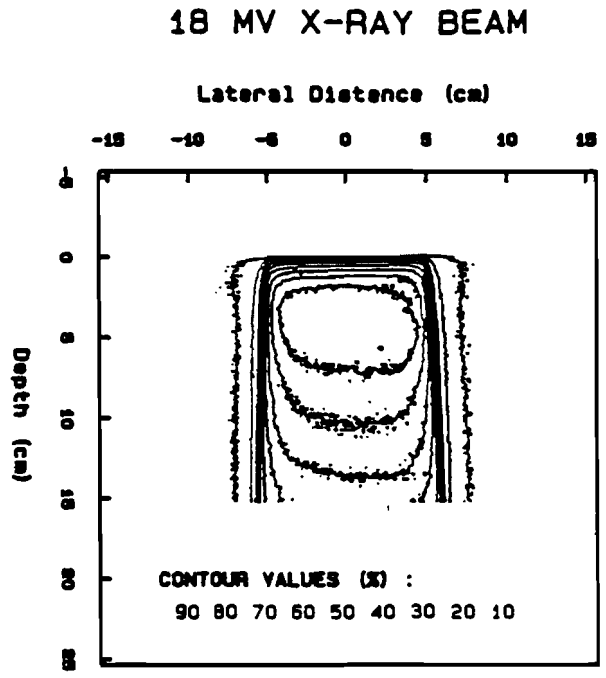

1b

Figure 1. 18-MV Photon Beam; a) Central-Axis Depth Intensity Profile; b) Iso-Intensity Contours.

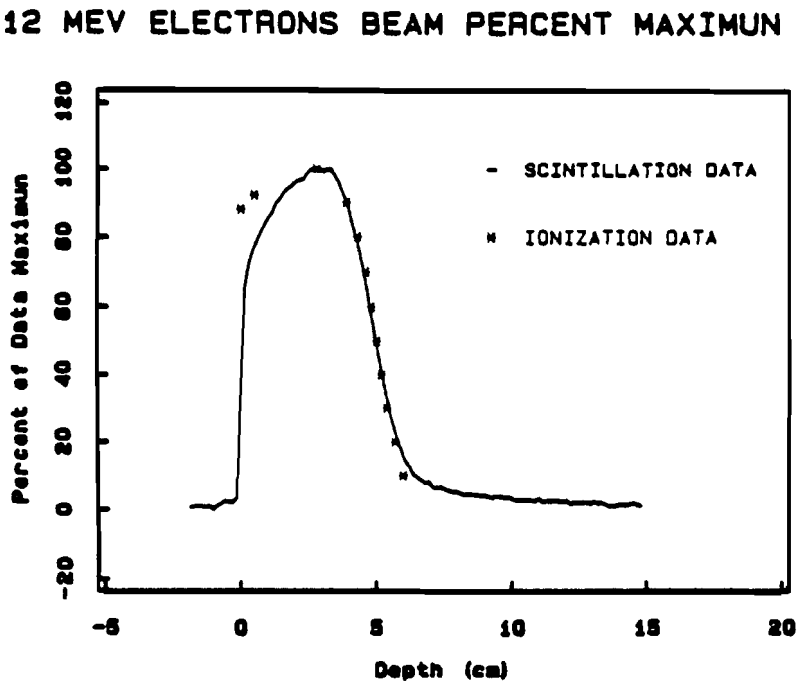

2a

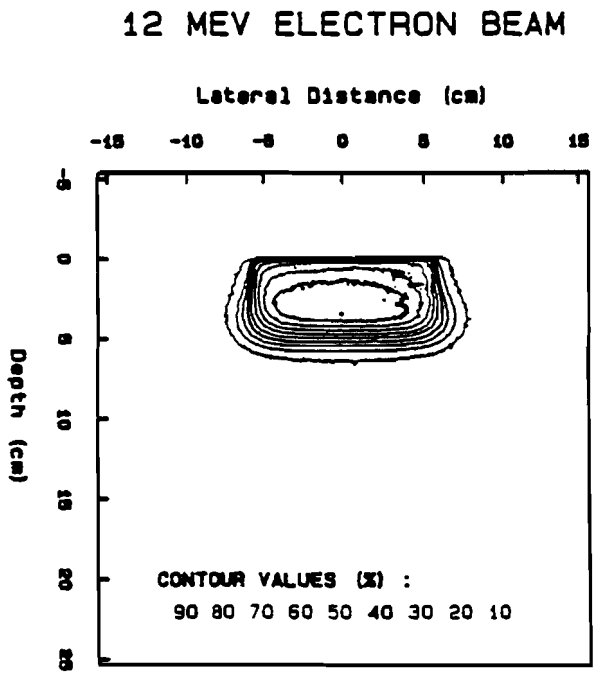

2b

Figure 2. 12-MeV Electron Beam; a) Central-Axis Depth Intensity Profile; b) Iso-Intensity Contours.

D. Ischemic Heart Disease and ECG Analysis

This section reports ongoing collaborations and support activities in cardiology. Collaborations include the assessment of vascular integrity of the myocardium following ischemic injury, the electrophysiological and biochemical factors underlying the genesis of dysrhythmias due to myocardial ischemia and infarction, and the analysis of plasma CK isoforms. Supporting activities include software for cardiologic image processing. Also reported are efforts to construct an annotated clinical-event database of ECG waveforms.

For more than a decade, this section reported activities related to high-speed processing of long-term, tape-recorded electrocardiograms primarily for large multicenter studies sponsored by pharmaceutical corporations or the National Institutes of Health. Those activities have now ceased as have dysrhythmia detection algorithm development efforts. Appropriately, these algorithms have found their way to the commercial sector.

D-1. Assessment of Vascular Integrity of the Myocardium Following Ischemic Injury

Personnel: R. G. Tilton, Ph.D., Pathology
J. Howe, Pathology
C. M. Kilo, M.D., Kilo Foundation
M. P. Land, B.S., Pathology
K. B. Larson, BCL
S. P. Sutera, Ph.D., Mechanical Engineering
D. E. Wexelblat, Pathology
J. R. Williamson, M.D., Pathology

Support: RR 01380
HL 31531
The Kilo Diabetes and Vascular Research Foundation

We have continued our previously reported studies (PR 22, A-4) of the role of the endothelium in the pathogenesis of vascular hemodynamic and permeability changes associated with ischemia and reperfusion. In these studies, we employ external-detection techniques coupled with tracer-kinetic analysis to quantify radiolabeled albumin transport across the coronary vasculature under physiological conditions, and during reperfusion after ischemia in isolated-perfused rabbit hearts. The resulting residue-detection data, analyzed on the basis of a two-compartment model of tracer transport [1], are used to estimate parameters indicative of microvascular integrity, such as permeability and ultrafiltration conductance of endothelium.

During the period covered by this report, we have assessed the separate and combined effects of diabetes and increased dietary fat consumption on coronary vascular hemodynamics, endothelial cell transport

function, and myocyte contractility in isolated Dutch Belted rabbit hearts during 3 hours of constant-pressure reperfusion after 40 minutes of global, no-flow ischemia. Residue-detection data, analyzed with a 2-compartment model, were used to estimate indices of microvascular function. Vascular resistance increased approximately 3x baseline and left ventricular end diastolic pressure increased 8-10x above baseline during reflow after ischemia in control hearts from rabbits fed normal chow. Maximum +dP/dt recovered approximately 45% of baseline values. Intravascular washout of radiolabeled albumin was prolonged 55% and albumin permeation and the mean-transit time of ^{125}I-BSA (bovine serum albumin) were increased 3x and 7x baseline, respectively. In diabetic rabbits and in rabbits fed a high-fat diet, vascular resistance was similar to controls prior to ischemia and increased only half as much during reflow after ischemia. Increases in vascular resistance during reflow were completely blocked in diabetic rabbits fed a high-fat diet. Left-ventricular end-diastolic pressure (LVEDP) did not differ prior to ischemia, but during no flow and reflow, was 50-60% lower in hearts from diabetic rabbits and rabbits fed the high-fat diet. Diabetes plus a high-fat diet completely blocked increases in LVEDP during 40 minutes of no flow and during reflow. Albumin permeation was similar during the pre-ischemic phase for all groups and, during reflow, increased approximately 9-10-fold in the diabetic and high-fat diet groups versus the 3-fold increase in controls. Thus, ischemia-reperfusion injury to myocytes and vascular smooth-muscle cells was ameliorated, but endothelial-cell damage was increased in diabetic rabbits and in rabbits fed a high-fat diet. The metabolic milieu created by diabetes and increased fat consumption completely blocked effects of 40 minutes of global ischemia on myocytes and vascular smooth muscle.

We have also completed studies assessing the stability of isolated hearts perfused with erythrocyte-enriched perfusates. The rationale for these experiments was based on observations that vascular hemodynamics slowly deteriorated in isolated hearts perfused with erythrocyte-enriched buffers. Isovolumically beating isolated hearts from male New Zealand rabbits were perfused retrograde via the aorta at a constant arterior pressure of 75 mm Hg. Perfusates (Krebs-Henseleit buffer with 1% BSA plus either 40% sheep RBC (red blood cells) or 40% bovine RBC) contained either no free fatty acids or 0.25 mM palmitate and 0.25 mM oleic acid. Normalized flow resistance (pressure drop/flow) increased from 5.6 to 10.5 torr(ml/min)$^{-1}$ gm^{-1} during two hours of perfusion in hearts perfused with buffer containing 40% bovine RBC but no free fatty acids and from 8.6 to 11.8 torr(ml/min^{-1} gm^{-1} in hearts perfused with the same buffer + 40% sheep RBC. Flow resistance was higher initially in hearts perfused with 40% bovine RBC + palmitate and oleic acids but remained unchanged after two hours. Addition of palmitate and oleic acid to the perfusate containing 40% sheep RBC was without effect.

1. R. G. Tilton, K. B. Larson, J. R. Udell, B. E. Sobel, and J. R. Williamson, "External Detection of Early Microvascular Dysfunction After No-Flow Ischemia Followed by Reperfusion in Isolated Rabbit Hearts," Circulation Research, 52:210-225, 1983.

D-2. Electrophysiological and Biochemical Factors Underlying the Genesis of Arrhythmias Due to Myocardial Ischemia and Infarction

Personnel: P. B. Corr, Ph.D., Medicine and Pharmacology
M. L. Cohen, M.D., Medicine
S. M. Moore, BCL
S. M. Pogwizd, M.D., Medicine
B. E. Sobel, M.D., Medicine
K. A. Yamada, Ph.D., Medicine

Support: HL 07275
HL 17646
HL 28995
HL 36773

The overall concept of the research is that potential arrhythmogenic metabolites, including lysophosphoglycerides and long-chain acylcarnitines, accumulate in ischemic tissue and contribute to the electrophysiologic derangements and associated arrhythmias. Over the past several years, studies have also been completed demonstrating a major electrophysiologic role of α_1-adrenergic stimulation during myocardial ischemia as well as reperfusion. In addition, we have demonstrated, using radioligand binding procedures, a 2-fold reversible increase in α_1-adrenergic binding sites in ischemic and reperfused myocardium.

Previous results from our laboratory and others indicate that long-chain acylcarnitines (LCA) accumulate in the ischemic heart in vivo and that exogenous LCA induce electrophysiologic alterations in vitro which are likely to be arrhythmogenic. We have demonstrated that local concentrations of endogenous LCA in the sarcolemma (SL) increase 70-fold with hypoxia in isolated myocytes from 2 to 140 $\times$ 10^5 molecules/μm^3 but not when POCA, an inhibitor of carnitine acyltransferase I, is present. Increased endogenous LCA in hypoxic cells was associated with a decreased resting membrane potential (RP) to -25 mV and abolition of depolarizations in contrast to the case in hypoxic but POCA-treated cells (RP = -64 $\pm$ 14 vs 76 $\pm$ 10 mV in controls; action potential amplitude = 77 $\pm$ 17 vs 97 $\pm$ 9 mV). These results strongly implicate endogenous LCA as a mediator of electrophysiologic impairment secondary to hypoxia. Likewise, we have demonstrated the marked antiarrhythmic effect of POCA (7.3 mg/kg) in vivo during myocardial ischemia associated with prevention of the increase in LCA. Since the catabolism of lysophosphatidylcholine (LPC), another arrhythmogenic amphiphile, has been shown to be markedly inhibited by LCA, we recently sought to determine whether inhibition of carnitine acyltransferase I with POCA in vivo would prevent the concomitant accumulation of LPC. LPC and LCA were measured in fast-frozen transmural biopsies obtained simultaneously from normal and ischemic zones 5 minutes after occlusion of the LAD coronary artery in 20 chloralose-anesthetized cats. Ischemia in untreated animals elicited a 3-fold increase in LCA (89 $\pm$ 8, normal zone, versus 311 $\pm$ 64, ischemic zone, pmol/mg protein) and a 2-fold increase in protein. POCA prevented the increase of LCA in the ischemic zone (128 $\pm$ 49 pmol/mg protein), inhibited LPC accumulation (4.0 $\pm$ 0.5 nmol/mg protein), and precluded the development of ventricular fibrillation. Thus, the potent antiarrhythmic efficacy of inhibition of CAT I is dependent on inhibition of accumulation of both LPC and LCA.

Several years ago we demonstrated that ischemia is associated with a 2-fold reversible increase in myocardial α_1-adrenergic receptors. Since hypoxia in isolated myocytes results in increased sarcolemmal (SL) accumulation of LCA, studies were performed to determine whether accumulation of LCA by SL with hypoxia exposes α_1-adrenergic receptors measured with ^{3}H-prazosin in isolated adult canine myocytes separated with collagenase and a BSA-percoll gradient. Hypoxia (100% N_2) for 30 minutes at 25°C or for 10 minutes at 37°C resulted in more than a 2-fold reversible increase in α_1-adrenergic receptor number with no loss of cell viability (1.9 ± 0.2 to 5.4 ± 0.7 fmol/mg protein, n=15, $p < .01$) and no change in receptor affinity (K_D = 0.30 to 0.57 nM). Pretreatment with POCA (10 μM) to inhibit SL accumulation of LCA prevented the increase in receptor number (2.7 ± 0.5 fmol/mg protein, n=9). In contrast, prolonged hypoxia (80 minutes, which decreased cell viability) or lysis of cells with hypotonic HEPES buffer decreased receptor number (1.1 ± 0.4 fmol/mg protein). Addition of exogenous LCA (1 μM) in normoxic myocytes resulted in a 2-fold increase in α_1-adrenergic receptor number. Thus, increased α_1-receptor density induced by hypoxia results, at least in part, from accumulation of LCA in the SL.

Previous measurements of inositol phosphates (IP) in cardiac tissue in response to α_1-adrenergic stimulation have utilized labeled precursors and assessed the accumulation of radioactivity in the IP_1 fraction in the presence of LiCl without actual measurement of IP_3. To quantitatively access α_1-adrenergic synthesis of IP_3 in isolated adult canine myocytes, cells were incubated with norepinephrine (10^{-5}M) for 5-120 sec and the reaction was terminated by acidification with TCA (5%). Extracts were neutralized and applied to anion exchange columns. IP_1, IP_2, IP_3 and IP_4 were eluted sequentially with 0.04, 0.07, 0.19 and 0.30M Na_2SO_4 in TRIS buffer at pH=8.5. Individual fractions were dephosphorylated with alkaline phosphatase and desalted. Recovery of IP_3 to this point was > 95%. Trimethylsilyl derivatives were prepared from lyophilized samples and quantified by capillary gas chromatography at 205°C (sensitivity of 50 fmoles) using chiroinositol as an internal standard. Initial studies demonstrated a 4-fold increase in IP_3 production in cardiac tissue in response to α_1-adrenergic stimulation and indicate that the α_1-adrenergic receptors which increase during hypoxia are coupled to breakdown of phosphatidylinositol bisphosphate.

We have demonstrated that the transition from ventricular tachycardia (VT) to fibrillation (VF) after reperfusion is dependent on acceleration of a nonreentrant mechanism. Accordingly, a study was performed recently to determine whether the same mechanism contributes to the evolution of VF during early ischemia with a three-dimensional mapping system capable of 8 levels of transmural recording from 232 simultaneous sites in the chloralose-anesthetized cat. VT leading to VF, which developed within 2 to 5 minutes after ischemia, initiated in the endocardium with a coupling interval comparable to that of nonsustained VT (214 ± 8 vs 218 ± 9 ms). Both a nonreentrant mechanism and intramural reentry maintained VT. However, VF was due to acceleration to a coupling interval of 95 ± 6 ms by intramural reentry due to nontransmural conduction block with breakthrough to multiple endocardial and epicardial sits. Reentrant pathlengths were as short as 1.4 cm with a radius of 0.22 cm. At the transition from VT to VF, total activation time for each beat exceeded the coupling interval, resulting in multiple simultaneous activations

characteristic of VF. Thus, in contrast to VF with reperfusion, VF with ischemia was not due to acceleration of a nonreentrant focus but was the result of inhomogeneous conduction leading to multiple reentrant circuits.

Recently, we have begun an extensive series of studies to access the cellular mechanisms responsible for the presence of late potentials, as well as the increased frequency content, in the surface electrogram which correlated with an increased propensity to arrhythmogenesis after myocardial infarction. Current systems used for analyzing late potentials from the surface electrocardiogram average up to hundreds of beats to increase signal/noise but consequently lose information about individual complexes which are likely to be critical in arrhythmogenesis after infarction. In addition to signal averaging, filtering performed with some systems does not permit the analysis of the original signal. Accordingly, to analyze the original signal and individual complexes from the surface electrocardiogram, two MicroVAX II computer systems with 140 Mbyte of disk storage have recently been purchased. One system collects three leads of electrocardiogram data, stores the data on disk, and analyzes the data. The second system controls the three-dimensional cardiac mapping system developed previously. The two systems are connected via a network and can correlate the mapping data and electrocardiogram data through timing markers inserted in the data stream. Custom data acquisition equipment for the X, Y and Z leads of the surface electrocardiogram were required for several reasons. The data acquisition equipment consists of a low-noise amplifier and a sensitive (16-bit), high-speed analog to digital (A/D) converter. The amplifier system minimizes the number of beats needed for signal averaging, and the A/D converter has a wide dynamic range. Because the equipment interfaces to the computer system through a parallel port, we are able to use the data acquisition system remotely from the computer system and minimize interference from the MicroVAX. Hardware and software changes needed to convert the mapping system from the PDP-11/34A to the MicroVAX II have been completed. Design and testing of the low-noise amplifier were carried out, and the remote data acquisition has been fabricated. Data can be collected through a parallel port on the MicroVAX and displayed on the computer system. During the next year, the data acquisition system will be evaluated and utilized in the laboratory in animals with previous infarction.

During the next year, major efforts will be directed toward elucidating the electrophysiologic effects in vivo during ischemia of inhibition of carnitine acyltransferase I with the use of the three-dimensional cardiac mapping system. Although initial results with POCA are promising, the irreversible nature of the enzyme inhibition precludes its therapeutic application. Three recently synthesized novel agents to specifically and reversibly inhibit carnitine acyltransferase I are now being evaluated. Adult myocytes in vitro and cat hearts in vivo will be used to determine whether inhibition of carnitine acyltransferase I with these newer agents is equally effective as a therapeutic approach to prevent sudden cardiac death. Additional studies are underway, based on the findings related to the influence of stimulation of the exposed α_1-adrenergic receptors during hypoxia on phosphatidylinositol metabolism, to determine whether the increase in IP_3 results in increases in cytosolic calcium in adult cultured myocytes assessed by spectrofluorimetric analysis of fura-2.

D-3. Software Support for Cardiologic Image Processing

Personnel: T. O. Videen, Ph.D., Neurology
D. G. Politte, BCL

Support: RR 01380
NS 06833

An interactive computer program for displaying and analyzing Super PETT I images, called AP1, was written previously [1]. AP1 allows the user to define several types of regions in a flexible manner and to perform calculations on the image values within the regions.

During the past year AP1 has been modified to accept both Super PETT I and PETT VI data. This allows the investigator to quantitatively compare images produced by either scanner.

1. Videen, T. O., "AP1: Analysis Programs for Super PET I, User's Manual," Biomedical Computer Laboratory Working Note #69.

D-4. Analysis of Plasma CK Isoforms

Personnel: D. R. Abendschein, Ph.D., Medicine
J. J. Billadello, M.D., Medicine
S. R. Devries, M.D., Medicine
H. L. Fontanet, M.D., Medicine
A. S. Jaffe, M.D., Medicine
J. Markham, BCL
R. Nohara, M.D., Medicine
H. Serota, M.D., Medicine
B. E. Sobel, M.D., Medicine
A. W. Strauss, M.D., Pediatrics

Support: HL 17646

We have shown previously that analysis of isoforms of the MM isoenzyme of creatine kinase in plasma provides an early and reliable index of acute myocardial infarction in experimental animals and patients. During the past year, isoform analysis was shown to detect the onset of coronary artery recanalization within 30 minutes after release of a coronary occlusion in conscious dogs [1]. Moreover, in a follow-up experimental study, the rate of increase of the tissue isoform in plasma, identified as the earliest available and most reliable index of reperfusion, was not affected by a high-grade coronary stenosis in the recanalized vessel similar to conditions of reperfusion in patients. A clinical study is in progress to evaluate isoform changes after recanalization by thrombolytic agents and angioplasty.

During the past year, we have developed a rapid, quantitative method to separate isoforms in plasma samples suitable for prompt clinical diagnosis of myocardial infarction and reperfusion. We have also identified the isoform conversion factor in plasma from dogs, normal human subjects and patients after myocardial infarction as carboxypeptidase N. Intravenous injection of individual isoforms in conscious dogs during infusion of an inhibitor of plasma carboxypeptidase N has permitted estimation of the isoform clearance rates in the absence of conversion and provided validation of a linear compartmental model of isoform kinetics in vivo. Experiments are in progress to characterize the mechanism of induction and kinetics of isoforms of the heart-specific MB isoenzyme of creatine kinase.

1. Devries, S. R., Sobel, B. E., and Abendschein, D. R., "Early Detection of Myocardial Reperfusion by Assay of Plasma MM Creatine Kinase Isoforms in Dogs," Circulation, 74:567-572, 1986.

D-5. Annotated Clinical Event Database for Evaluating Ambulatory ECG Analysis Systems

Personnel: K. W. Clark, BCL
C. N. Mead, M.D., Biosensor Corporation
D. A. Schwab, BCL
L. J. Thomas, Jr., BCL

Support: RR 01380
Biosensor Corporation
Washington University

Last year (PR 22, A-1), we had begun construction of an "annotated clinical event" database (ACED). Now assembled, the database consists of 60 six-hour recordings. There are ten recordings in each of six categories: (1) ventricular runs, (2) ventricular pairs, (3) ventricular bigeminy, (4) pauses > 1.5 seconds (or heart rate < 40), (5) paroxysmal supraventricular tachycardia, and (6) paroxysmal atrial fibrillation. Each six-hour recording is dual channel and digitized at 250 samples/second/channel. Each is saved in unfiltered and filtered (1-30 Hz digital convolution) form. Annotations are incomplete.

The need for the ACED surfaced from within and outside our ECG analysis algorithm development efforts. While evaluating our Argus algorithms using the publicly available American Heart Association (AHA) and Massachusetts Institute of Technology/Beth Israel Hospital (MIT/BIH) databases, we found the databases quite helpful in general algorithm development but discovered that the records used for these databases were too short for testing the long-term effects of our algorithm. Meanwhile, vendors of systems using the AHA and MIT/BIH databases were beginning to report performance characteristics in terms of the beat-by-beat annotations available with these databases. Unfortunately, reports from end-user physicians indicated they were not so much interested in beat-by-beat performance but in clinical-event detection performance. The market seemed right for something like the ACED.

The details of our ACED and the concept of the need for such a database were presented at the 1986 IEEE Conference on Computers in Cardiology [1]. Supporting discussions at the conference and during the following weeks prompted us to apply for funds to complete annotations of the ACED and to add a seventh category of ST-segment changes.

1. Mead, C. N., Clark, K. W., and Thomas, Jr., L. J., "An Annotated Clinical Event Database as a Tool for Evaluating Dysrhythmia Detector Performance," IEEE Conference on Computers in Cardiology, IEEE Catalog No. 87CH2476-0, pp. 327-330, Boston, MA, October 7-10, 1986.

E. Systems for Specialized Biomedical Studies

This section describes a number of applications which have arisen as a result of the basic work done in the various major sections of BCL. Because they are so diverse, it is hard to edit them in any very stringent manner. Work continues on DNA restriction mapping and it is likely that this will continue and expand in the coming year. In the previous Progress Report, reference was made to a specialized data acquisition system for use with scintillation probes. This is now in routine use and a statistical analysis package is being written to optimize its utility.

The previously reported new algorithm for electron-microscopic autoradiography has been evaluated in several respects and found to consistently outperform the conventional mask-analysis method. Related work on automated segmentation of biomedical images has the objective of substantially reducing the tedium associated with the analysis of electron-microscopic autoradiographs. As an adjunct to electronmicroscopic techniques, work is progressing on a computerized analog of human stereopsis.

A radically new method of analysis of nerve auditory fibers is being tested and explored; preliminary results suggest that it will considerably sharpen our knowledge of auditory nerve and auditory cortex function. A previously developed color-video perimetry system has been modified to test specifically the blue-yellow discrimination function most commonly damaged in glaucoma.

E-1. DNA Restriction Mapping

Personnel: M. V. Olson, Ph.D., Genetics
J. R. Cox, BCL and Computer Science

Support: RR 01380
GM 28232

This continuing project is aimed at developing general methods of DNA physical mapping. The sites at which site-specific restriction endonucleases cleave DNA are used as landmarks for the development of one-dimensional physical maps of complex DNA sources. Although the emphasis is on generic mapping methods that could be applied to any DNA source, experimental effort has focused to date on the 15-Mb (1 Mb = one million base pairs) genome of the yeast Saccharomyces cerevisiae.

Experimental work during the past year has emphasized continuations of the analysis described in [1]. This publication reports a set of data on the restriction fragments generated by cleavage of 5000 lambda clones of random 15-kb (1 kb = 1000 base pairs) segments of yeast DNA. This clone collection samples the yeast genome with >5-fold redundancy. The mapping is being carried out by using similarities in the sets of fragment sizes generated from different clones to recognize overlap relationships amongst the clones. In [1], the collection of 5000 clones had been reduced to 680 "contigs," where a contig is defined as a set of clones in which each clone is related to at least one other clone in the set by a statistically significant overlap. These 680 contigs appear to include >95% coverage of the genome; the large number of contigs compared to the number of chromosomes (16) is due to such problems as inadequate sampling, systematic absences of some DNA segments from even very large clone collections, and the inability to recognize short overlaps. During the past year, further analysis of the clone collection has reduced the number of contigs to 400. More importantly, a tree-searching algorithm described in [1] has been exhaustively applied to the development of precise overlap maps of all 400 of these contigs.

The achievement of higher connectivity amongst these contigs will require supplementary data, and considerable effort has been devoted to developing the needed experimental techniques. Specifically, a completely connected low-resolution map (100-kb resolution) has been determined for the yeast genome by analyzing the cleavage patterns of restriction enzymes that cleave very infrequently. This analysis was done on uncloned DNA using recently developed techniques for separating and detecting very large DNA molecules. The main strategy for connecting the high-resolution maps (2-kb resolution) that have been determined for the 400 contigs involves superimposing these map segments on the low-resolution map by DNA-DNA hybridization techniques.

The main theoretical effort during the past year has involved simulations of various algorithms for analyzing the overlap relationships amongst the random clones, given data on the sizes of the restriction fragments that can be generated by cleavage of each clone. Previous work has shown that this problem is closely related to the shortest common superstring problem and is NP-complete [2]. In general, computationally

practical approaches to this problem must rely on local searching, in which larger maps are built up from local maps that are constructed from small subsets of the data. Some amount of backtracking can be used to increase the robustness of these procedures, but the algorithms are inherently greedy, proceeding to larger and larger maps by concatenating local maps, each of which is only optimized with respect to a small number of clones. Simulations have shown that performance is much more sensitive to the statistical tests used for choosing these small sets clones and resolving ambiguities in their overlap relationships than to such factors as the amount of backtracking allowed. Further work, therefore, will focus on these steps. We plan both to develop a formal theoretical treatment of the problem and to carry out extensive tests on real data from the yeast project.

1. Olson, M. V., Dutchik, J. E., Graham, M. Y., Brodeur, G. M., Helms, C., Frank, M., MacCollin, M., Scheinman, R., and Frank, T., "A Random-Clone Strategy for Genomic Restriction Mapping in Yeast," Proceedings of the National Academy of Science, 83:7826-7830, 1986.

2. Turner, J. S., "The Complexity of the Shortest Common Matching String Problem," Washington University Computer Science Department, WUCS-86-9, April 1986.

E-2. Isolated Scintillation Probe Data Acquisition System

Personnel: D. E. Beecher, BCL
H. D. Ambos, Medicine
S. R. Bergmann, M.D., Ph.D., Medicine
M. A. Brown, M.B.B.S., Medicine
W. H. Hellberg, BCL

Support: RR 01380
HL 17646

The probe system as described in PR 21, E-4, has been in routine use during the past year with a variety of experimental protocols. No serious problems have been reported.

During the past year, a new statistical analysis package has been developed on the LSI 11/23 host system. This menu-driven system contains sophisticated modules for the generation and manipulation of up to 100 independent data sets. The main calculation modules consist of linear regression and variance analysis.

E-3. Maximum-Likelihood Estimation Applied to Electron-Microscopic Autoradiography

Personnel: M. I. Miller, BCL and Electrical Engineering
D. Fuhrmann, BCL and Electrical Engineering
D. R. Maffitt, BCL
B. Roysam, BCL
J. E. Saffitz, M.D., Ph.D., Pathology and Medicine
L. J. Thomas, Jr., BCL

Support: RR 01380
HL 17646

A new method for analysis of electron-microscopic autoradiographs has been described [1] (PR 21, E-6 [5]) which is based on the maximum-likelihood method of statistics for estimating the intensities of radioactivity in organelle structures. A Poisson statistical model describing the autoradiographic grain distributions is adopted, which we prove results from the underlying Poisson nature of the radioactive decays as well as the additive errors introduced during the formation of grains. Within the model, an iterative procedure derived from the expectation-maximization algorithm of mathematical statistics is used to generate the maximum-likelihood estimates. The algorithm has the properties that at every stage of the iteration process the likelihood of the data increases; and for all initial non-zero starting points the algorithm converges to the maximum-likelihood estimates of the organelle intensities.

The maximum-likelihood (ML) method, and preliminary evaluations of the quantitative accuracy of the ML and crossfire-analysis algorithms have been reported previously [1-3]. More recently [4,5], (PR 22) simulations were systematically extended in scope to cover more realistic situations. First of all, the single-geometry simulations using a Gaussian point-spread function were extended to low-count experiments wherein the performance measures were gathered by performing multiple-realizations on a single phantom. These experiments confirmed our prediction that even when the geometry of micrographs does not vary, i.e., when transition probabilities can be computed perfectly, the maximum-likelihood algorithm out performs the mask-analysis algorithm. We attribute this to the exploitation of actual grain coordinates and to the Poisson model.

We next implemented the $\cos^3\theta$ point-spread function developed in Miller et al., 1985 [1]. We then extended the simulations to cover the multiple independent micrograph case. These simulations demonstrated that while the maximum-likelihood algorithm remained consistently unbiased and showed very little performance degradation with respect to the single-geometry situation, the mask-analysis algorithm degraded substantially in performance.

Due to physical limitations associated with the fact that the tissue samples have extremely small dimensions, it is not possible to precisely maintain the constant thickness of the specimen and emulsion layers throughout an autoradiographic experiment. Furthermore, it is not possible to actually measure these parameters for each tissue section. Consequently, the half-distance number, on which the entire experiment

depends is rarely known accurately. We were thus motivated to investigate the effect of using an inaccurate half-distance value in the analysis. We concluded that the ML algorithm is extremely robust with respect to error in the half-distance value. Its performance, even at extreme errors in the half-distance value (50 to 60%) is superior to that of an ideally implemented crossfire-analysis algorithm.

An important new contribution towards the realization of a portable software package to perform EM autoradiographic experiments on small computers, such as the IBM PC/AT was made by reformulating the problem of computing grain-organelle and transition probabilities in terms of line-integrals taken around the boundaries of structures rather than as area integrals over the regions defining the organelles. This allows us to store only the coordinate sequences defining object-boundaries, instead of the entire raster image. We thus have a method whose memory and CPU requirements can both be met by currently available personal computers. The algorithms for performing the line-integrals have been tested and found to yield the same numbers as the previously derived closed-form integral expressions.

1. Miller, M. I., Larson, K. B., Saffitz, J. E., Snyder, D. L., and Thomas, Jr., L. J., "Maximum-Likelihood Estimation Applied to Electron-Microscopic Autoradiography," Journal of Electron Microscopy Technique, 2:611-636, 1985.

2. Miller, M. I., Larson, K. B., Saffitz, J. E., Snyder, D. L., Thomas, Jr., L. J., and Roysam, B., "A New Method for Analysis of Electron Microscopic Autoradiographs," Cell Biology, 101(5):85a, part 2, 1985 abstract.

3. Miller, M. I., Roysam, B., Saffitz, J. E., Larson, K. B., and Thomas, Jr., L. J., "Validation of Maximum-Likelihood Analysis of Electron Microscopic Autoradiographs," Proceedings of the 70th Annual FASAB Meeting, St. Louis, MO, 45(3):470, 1986 abstract.

4. Roysam, B., "A New Method for EM Autoradiography: Validation and Comparison to Crossfire-Analysis," Master of Science Thesis, Department of Electrical Engineering, Washington University, May 1987.

5. Miller, M. I., Roysam, B., Saffitz, J. E., Larson, K. B., and Thomas, Jr., L. J., "A New Method for the Analysis of Electron Microscopic Autoradiographs," Biotechniques, 5(4):322-328, 1987.

E-4. Automated Segmentation of Biomedical Images

Personnel: D. R. Fuhrmann, BCL and Electrical Engineering
M. A. Brown, BCL
J. E. Saffitz, M.D., Ph.D., Pathology and Medicine
L. J. Thomas, Jr., BCL

Support: RR 01380
HL 17646

Work has continued on the automated segmentation of electron microscope cell images, as described in PR-22, E-5. Several major changes were incorporated into the EMAMAP software package to improve the user interface. The system was used to acquire data from an actual biological experiment, and when the data were analyzed via the maximum likelihood (ML) method (PR-22, E-4) significant biological results were obtained.

In the present system, a trained operator places an electron micrograph on a graphics tablet and hand-digitizes the edges of the desired structures. In contrast to earlier version, the edges are now labelled as a biological type at the time they are drawn. Those edges which form closed contours in the interior of the image can then be filled automatically with the correct region label, using a contour-filling algorithm. It was found that this facility was essential for avoiding operator fatigue and classification errors.

Progress was made in coding the segmented image for efficient storage. We have developed a coding algorithm which represents the image as a quadtree, then encodes a pre-order traversal of this tree using Huffman coding [1].

EMAMAP was used to acquire data from an actual biological experiment in December 1986. In this experiment, there were 41 images containing a total of 506 silver grains. The total acquisition time was about 17 hours, spread out over 8 sessions in a period of two weeks. The total storage required by the digitized data, in uncompressed form, was 10.8 Mbytes. In contrast, the coded data required 442 Kbytes; thus, a compression ratio of over 25:1 was achieved by our coding algorithm. When the data were analyzed using the ML method, significant results, not known from previous methods, were obtained.

Changes in use of the ML method for EM autoradiography have been discussed; such changes will affect the requirements of the data acquisition system. One such change involves grouping of structures of different labeling intensities into single compartments when the grouped structures are not of great interest. Thus, only structures of biological interest will need to be digitized in detail. The effects of combining heterogeneously labeled structures on the accuracy of intensity estimates of adjacent structures will need to be determined.

A report of results to date and a more detailed description of the EMAMAP system are in press [2].

1. Fuhrmann, D. R., and Brown, M. A., "Encoding Biomedical Images with Quadtrees," Proceedings of the 24th Annual Allerton Conference on Communication, Control, and Computing, University of Illinois, pp. 703-704, 1986.

2. Fuhrmann, D. R., Brown, M. A., Miller, M. I., Roysam, B., Saffitz, J. E., and Thomas, Jr., L. J., "A Data Acquisition System for Maximum-Likelihood Analysis of Electron Microscopic Autoradiographs," Journal of Electron Microscopy Technique, in press.

E-5. Computation of Disparity Information From Electron-Microscopic Image Pairs

Personnel: R. L. Winslow, BCL
Q. Wu, BCL
B. D. Skinner, BCL

Support: RR 01380

Given a pair of pictures of a scene taken from different angles, it is possible to reconstruct information about the relative depth of different features in the scene. This reconstruction is possible because features that are located at different depths will have different relative positions (disparity) in the two images. The goal of the stereo vision process is to determine the disparity of corresponding features in the two images. If the camera positions are known, disparity information may then be used to compute the depth of surfaces in the scene. Our objective is to develop and implement computer algorithms for computing disparity and hence depth information from image pairs. We are especially interested in the formulation of algorithms for the quantitative reconstruction of the three-dimensional shape of biological materials using electron-microscopic image pairs.

The most successful approach to computational stereopsis has been based on a theory of human stereo vision first proposed by Marr and Poggio [1], and later implemented by Grimson [2]. The fundamental assumption of this theory is that the physical properties of a surface give rise to changes in the reflectance properties of that surface, and hence to variation in image intensity. Thus, there is a one-to-one correspondence between symbols marking points of intensity change in each image and physical locations on the surface being imaged. The problem of computing disparity information from image pairs can therefore be solved is each symbol marking a point of intensity change in image 1 can be matched with the corresponding symbol in image 2. The difficulty in stereopsis lies in the task of performing this matching correctly when the density of symbols to be matched is high, in which case the probability of a false match and an incorrect disparity estimate is also high.

The Marr-Poggio theory of stereo vision addresses this problem in the following manner. First, image pairs are convolved with a set of N

Gaussian filters, each having a low-pass frequency response with successively higher cutoff frequency. Second, points of intensity change are located in each of the N pairs of filtered images by applying the Laplacian operator to each image pair and storing the location of the resulting zero-crossings. Zero-crossings correspond to extrema in the rate of change of image intensity. Thus, zero-crossings are considered to be the primitive symbols which are in one-to-one correspondence with points on the surface being imaged. The density of zero-crossings in each filtered image decreases with decreasing bandwidth of the Gaussian filter used to generate the image. Marr and Poggio have shown that there is a high probability that there is only 1 zero-crossing in any region of width d, where d is a distance determined by the bandwidth of the Gaussian filter. A zero-crossing at point (x,y) in image 1 is therefore matched to a zero-crossing in image 2 by searching the region (x-d/2,y) to (x+d/2,y) in image 2 for a zero-crossing (only horizontal disparities are considered). If a zero-crossing exists within this region, and if the disparity between point (x,y) and the corresponding point in image 2 has an absolute value less than or equal to d/2, then the correct zero-crossing match has been established with high probability. Unfortunately, the resulting disparity estimate is inaccurate because of the poor spatial localization of the narrowband Gaussian filter used to smooth the images. Disparity estimates generated from image pairs filtered with narrowband Gaussian filters are therefore used to guide the matching process for image pairs filtered using more broadband Gaussian filters with greater spatial resolution, making it possible to solve the false-matching problem without sacrificing disparity resolution.

During the past year we have successfully implemented FORTRAN 77 versions of the Marr-Poggio stereo algorithm which operate on either one- or two-dimensional images [3]. Algorithm performance has been evaluated by processing a large variety of synthetic images (random-dot stereograms) containing known disparity information [3]. Studying the performance of the algorithm using these synthetic images has enabled us to identify several ways in which the implementation described by Grimson [2] may be improved:

(1) The present version of the algorithm dynamically determines the number of times the original image pair must be filtered in order to compute a disparity for every region in the image. The procedures for doing this are ad hoc and error prone. If the maximum height of features in the image can be bounded, the number of filtering operations can be predetermined leading to a much simpler and less time consuming version of the algorithm;

(2) In the present version of the algorithm, zero-crossings in the "left" image are matched to zero-crossings in the "right" image. A simple improvement to the algorithm is to drive the matching process from both images. The resulting matchings will be in agreement only for regions of the surface which are not occluded in either image. Thus, occluded regions may be identified by a comparison of the two matchings.

Objectives for the upcoming year include modification of the two-dimensional algorithm to include the improvements described above. The algorithm will also be modified to compute small vertical disparities in

order to compensate for misalignment which may be present in natural images. In addition, we intend to implement an interpolation algorithm which fits a smooth surface to points in the image where disparity estimates exist (disparity cannot be computed at each point in the image since estimates can only exist where there are zero-crossings). Finally, once algorithm performance on simple synthetic images has been optimized, we will begin to process electron-microscopic image pairs.

1. Marr, D., and Poggio, T., "A Theory of Human Stereo Vision," Proceedings of the Royal Society of London, B., 204:301-328, 1979.

2. Grimson, W. E. L., "A Computer Implementation of a Theory of Human Stereo Vision," Philosophical Transactions Royal Society of London, B, 292:217-253, 1981.

3. Skinner, B., and Winslow, R. L., "Computing Depth Information from Stereo Image Pairs Using the Marr-Poggio Stereo Algorithm," IBC Technical Memorandum No. 322, Washington University, St. Louis, MO 1987.

E-6. EM Algorithms Incorporating Monotonicity Constraints for Removing Recovery-Related Distortion From Auditory-Nerve Discharge Patterns

Personnel: M. I. Miller, BCL and Electrical Engineering
N. Karamanos, BCL

Support: NS 23007

A new method for the analysis of auditory-nerve discharge patterns has been developed. This method models neural discharge as a self-exciting point process in which the intensity is given by the product of two functions $s(t)$ and $r(\tau)$. The function $s(t)$ depends on the acoustic stimulus whereas the function $r(\tau)$ depends on the history of the process. Our method is different from all existing attempts to remove refractory effects in that we do not assume that the function $r(\tau)$ is known. Rather, we estimate $r(\tau)$ jointly with $s(t)$ using maximum-likelihood estimation techniques. We have also embedded in the estimation problem the fact that $r(\tau)$ is assumed to be a monotonic function of time.

The joint likelihood equations which must be maximized with respect to both the s and r functions do not yield an analytic closed form solution. To derive these maximizers we have adopted the expectation maximization (EM) algorithm, and have shown that under very mild conditions unique maximum-likelihood estimates exist and that the EM algorithm globally converges to them.

We have applied this new method to the analysis of populations of auditory-nerve fibers in response to both tones and complex speech stimuli. Preliminary results show:

(1) Neurons have widely varying refractory functions $r(\tau)$.

(2) For sharp onset stimuli such as speech, the effects of refractory are to sharply reduce the onset of discharge.

(3) The statistical effect of the recovery function is to reduce the variability of the large synchronized components in the temporal discharges of response, well below that predicted by a Poisson model, while having little effect on the variability of small synchrony coefficients.

E-7. Color-Perimetry Studies

Personnel: W. M. Hart, Jr., M.D., Ph.D., Ophthalmology
K. W. Clark, BCL
S. R. Phillips, BCL

Support: RR 01380
EY 06582
Washington University

Over the past year the color-video perimetry device has been modified to allow examination of patients using an adapting background light of a yellow color, instead of the white or neutral gray appearance used in prior studies. The yellow background is a diffusely illuminated, featureless screen in which approximately equal contributions are made by the red and green phosphors. Test objects are now modulated in color space from an equiluminant yellow that is indistinguishable from the background towards complete replacement of the red and green phosphors by output from the blue phosphor. This produces a graded series of test objects that vary from yellow through white into a purely blue appearance. Blue versus yellow is the predominant color contrast function being tested, as this is the color discrimination function most commonly damaged in glaucoma. Approximately 130 patients have been enrolled in an on-going prospective study of ocular hypertension to test the sensitivity and specificity of color contrast perimetry for the detection of glaucomatous visual field defects.

1. Hart, W. M., "Color Contrast Testing of the Extrafoveal Macula," presented at the 9th Conference of the International Research Group on Color Vision Deficiencies (IRGCVD), Annapolis, MD, July 3, 1987. Proceedings to be published in the Proceedings Series of Documenta Ophthalmologica, Dr. W. Junk, Publishers, Dordrecht, The Netherlands.

F. Resource Development Activities

Resource development activities are those which contribute to the goals of more than one major program of the laboratory, address the needs of individual users who can benefit from the expertise of the BCL staff and the inventory of computing and specialized test equipment, or identify new technologies which may become appropriate foundations for new experimental tools. Service to users does not follow the usual computation-center pattern with an established fee schedule and a highly centralized facility. Rather, senior laboratory staff members consider requests for assistance from investigators who must address a particular biomedical computing problem. If an appropriate technology exists, investigators may be referred to commercial vendors or fee-for-service organizations when these are available. In other cases, problems may be approached by the laboratory provided that the effort complements other activities of the laboratory. Many times the project can be assigned to a staff member with appropriate experience and completed in a short time. The investigator then has his or her results, and a short note describing the work will appear in the annual report and perhaps the open literature. A few projects, however, may develop into major initiatives within the laboratory. Most of the major projects began in this fashion and the opportunities that supporting activities provide are valued.

The IPAQ project (F-1 thru F-6) has focused laboratory efforts on providing a computational environment which can be utilized in addressing the demanding needs of algorithm development. A distributed approach, multiple computing systems integrated with communication networks, is being developed. Equipment acquisition and system integration continue to be major activities, with more effort now directed to improving the image display and manipulation environment (F-4, F-9).

Network related activities at the University have accelerated during the past year, with the Resource serving as a major participant in these developments (F-7, F-5). The installation of the Biomedical Research Network has already influenced Resource activities and access to supercomputers may have an even greater impact.

Evaluation of a reflectance camera (F-8) for acquisition of biomedical images is an important first step to providing better methods for improving image quality and acquisition techniques. Likewise, exploration of various hardware systems such as the Mercury Array processor and several supercomputers (F-6) will stimulate new ideas for better implementations of complex, computationally demanding algorithms.

F-1. A Distributed Facility for Image Presentation, Analysis and Quantification (IPAQ)

Personnel: G. J. Blaine, BCL
D. E. Beecher, BCL
M. A. Brown, BCL
K. W. Clark, BCL
J. R. Cox, Jr., BCL
R. E. Hermes, BCL
S. M. Moore, BCL
S. R. Phillips,BCL
F. U. Rosenberger, BCL and Computer Systems Laboratory

Support: RR 01380
RR 01379
Digital Equipment Corporation
Washington University

Decentralized computing organized along departmental and research laboratory lines characterizes the environment which continues to evolve at most major medical research institutions. This is particularly true in quantitative imaging where many projects have diverse image-data sources (modalities), different data-acquisition requirements, and dissimilar methods for the extraction of quantitative information. Rather naturally, diverse computing styles and equipment choices have evolved. For example, our major collaborative research groups support installations tailored to their specific measurement and picture transformation needs, for which display peripherals from a variety of manufacturers (DeAnza, Ramtek, and Lexidata) are tightly coupled to different computers (DEC 750, 780, MicroVAX II, PE 3230, 3242). Commonality is limited to little more than the popularity of Vax-class computers and a FORTRAN programming environment. Furthermore, the lack of common program-development tools and display-support software has minimized the opportunities for sharing developments across research programs and has necessitated large host-specific investments by those Resource researchers and collaborators who participate in modeling and algorithm development.

Algorithm development is often characterized by computationally demanding and memory-intensive tasks which must compete with concurrent usage of the existing computing resources for data acquisition and analysis activities. The limited computational capacity available for algorithm development and pressures for expediting the research process biases the investigator's attention toward ad hoc approaches to improvements in execution performance, often at the expense of fundamental algorithm studies which are more likely to yield long term benefits.

The broad goal of this core research and development activity is to create an environment for biomedical image presentation, analysis and quantification (IPAQ) which:

1) is focused on fundamental algorithm developments that individual biological scientists may not have the time, patience or resources to pursue;

2) provides an integrated approach to expedite the development and export to the local and national communities of new algorithms for improved quantification of biological information;

3) improves access for purposes of algorithm development to data from the diverse imaging modalities to encourage modality integration; and,

4) protects existing investments in decentralized and specialized biomedical research systems.

A series of study efforts led to the definition of an architecture and specification of system components capable of addressing the needs of quantitative imaging. The components of the distributed IPAQ facility are to include: 1) acquisition nodes consisting of the specialized imaging resources at the sites of the collaborations; 2) computation-oriented nodes to support development and initial evaluation of algorithms within the Resource; 3) high-performance computation/display nodes which are tailored to export specialized computation and/or picture presentation; and 4) a high-bandwidth network to interconnect our development activities with the collaborative research.

Computer systems integration and software development activities have dominated the current reporting period. Specifics of these activities are described in later sections (F-2 thru F-6). Illustrated in Figure 1, is the current system-resource configuration which is integrated via three levels of interconnection:

a) terminal service at 9600 bps via TERRANET (PR 22, F-10),

b) UNIX to UNIX service via TCP/IP over a baseband Ethernet, and

c) DECNET to UNIX service utilizing DECNET-Ultrix software and an Ethernet on the MIR broadband cable system (F-5).

Users of this distributed network of computers, associated hardware, communication pathways, and diverse collection of software are familiarized with the resources by a series of locally-generated references: the IPAQ User's Notebook, Document Preparation Binder, and Revision Control System Reference (RCS). These references are not intended for use as computer recipe books, but rather, are intended as guides to assist the resource users in getting started by identifying available software and hardware, supplying pointers to detailed documentation, and providing helpful hints for effective resource utilization.

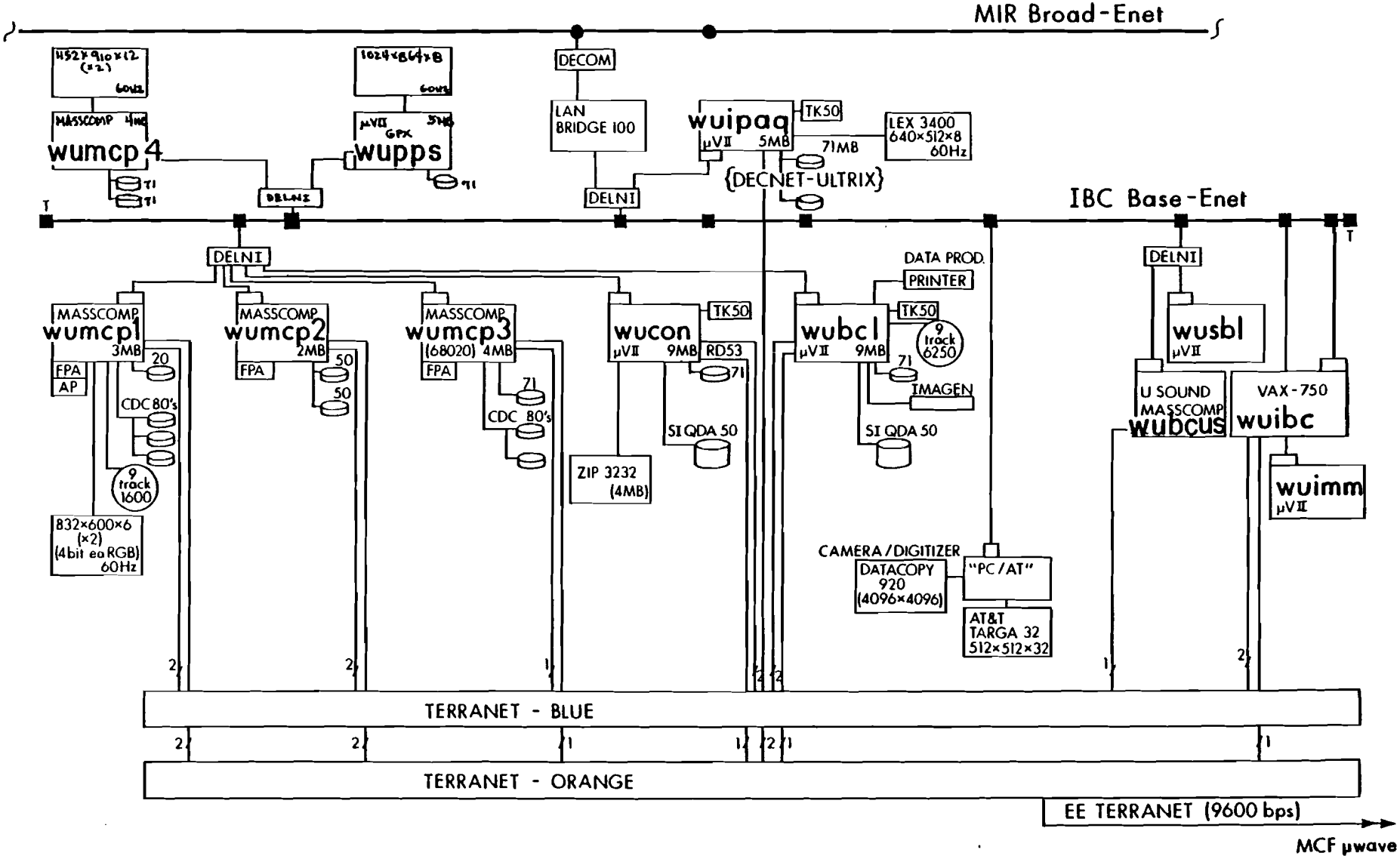

Figure 1. IPAQ Resource Configuration

F-2. IPAQ: System Integration

Personnel: R. E. Hermes, BCL
M. A. Brown, BCL
K. W. Clark, BCL
S. R. Phillips, BCL

Support: RR 01380
Digital Equipment Corporation

Computer system acquisition and integration continues to be a major activity of the IPAQ working group. Dependence upon dated equipment such as PDP 11/34s has been all but eliminated during the past year, with the acquisition of two more computing systems, a VAXstation II/GPX and a MASSCOMP 55020. The table on the following page summarizes the computing resources available within the resource.

The VAXstation II/GPX is a DEC MicroVAX II with a graphics display having 1024x832x8 bits of image memory. The MASSCOMP 55020 includes an Aurora graphics display device with two image buffers of 1152x910x12 bits. Both systems use vendor specific versions of UNIX as the operating system and support FORTRAN and C as the principal programming languages. The machines are connected to the local Ethernet as are all other systems.

The laboratory's image-acquisition system (PR 22, F-11) which includes a Datacopy reflectance camera and an AT&T Targa 32 display, was upgraded from an IBM PC/XT compatible to an IBM PC/AT with a 20 MByte hard disk. An ethernet interface enables efficient image transfer to other systems for processing.

The table also indicates the particular research effort addressed by each system. Common operating systems, programming languages, and ethernet connections found on all machines provides the flexibility needed to devote as many resources as necessary to an activity. In some instances, a machine is dedicated to an activity which requires significant computing capability. This distributed approach to computing perpetuates a style established within the resource.

Computer Systems and Applications

Nodename	WUIPAQ	WUBCL	WUCON	WUPPS	WUMCP1	WUMCP2	WUMCP3	WUMCP4
Machine Type	MicroVAX II	MicroVAX II	MicroVAX II	MicroVAX II	Masscomp 5500	Masscomp 5500	Masscomp 5400	Masscomp 55020
Terminal Ports	9	17	9	1	11	11	4	4
Memory Size	9 MB	9 MB	9 MB	9 MB	3 MB	2 MB	4 MB	4 MB
Disk Configuration	2-71 MB (DEC RD53)	RX50 Floppy 1-71 MB (DEC RD53) 520 MB (Fujitsu 2361)	RX50 Floppy 1-71 MB (DEC RD53) 520 MB (Fujitsu 2361)	1-71 MB (DEC RD53)	Floppy 52 MB Winchester 3-67 MB (CDC 9762)	Floppy 71 MB Winchester 52 MB Winchester	Floppy 71 MB Winchester 2-67 MB (CDC 9762)	Floppy 2-71 MB Winchesters
Other Devices	Floating Point Ethernet TK50 Lexidata	Floating Point Ethernet TK50 9-track tape Imagen Laser Printer Dataproducts Printer	Floating Point Ethernet TK50 Mercury Array Processor	Floating Point Ethernet GPX Graphics	Floating Point Ethernet Masscomp Array Processor Masscomp Independant Graphics Processor	Floating Point Ethernet	Floating Point Ethernet	Lightening Floating Point Ethernet Aurora Graphics Processor
Application Areas	Networking & Communications Computation Display	Program Dev. Text Processing Computation	Program Dev. Computation	Networking & Communications Program Dev. Display	Program Dev. Computation Display	Text Processing	Program Dev. Computation	Computation Display

F-3. IPAQ: System Support

Personnel: R. E. Hermes, BCL
M. A. Brown, BCL
K. W. Clark, BCL
S. M. Moore, BCL
S. R. Phillips, BCL

Support: RR 01380

As the number of machines and demands upon machine resources has increased, so has the need to further develop and support the research computing environment. The coherent computing environment across many distributed computer systems established during the past few years greatly simplifies the many tasks of system support.

During the past year, new operating system releases have been installed on all machines. New software acquisitions include Ultrix-32w and VAX/FORTRAN-Ultrix. Ultrix-32w supports the VAXstation GPX and includes the X-windows system (F-4). VAX/FORTRAN is an optimized FORTRAN compiler for Ultrix which is fully compatible with the Digital VMS FORTRAN compiler.

Additional software for typesetting and document preparation was acquired from AT&T and installed on a MicroVAX to serve an Imagen Printstation laser printer. The software includes: "ditroff" (device-independent troff) for general-purpose text formatting, "eqn" for formatting mathematical symbols and equations, "tbl" for creating tables, "pic" for drawing simple figures, and "grap" for printing graphs. Existing Imagen software was upgraded to support the AT&T software package. The software is extensively used on a day-to-day basis for documentation, slide presentation, report and paper preparation.

We continue to support a Lexidata display system on a MicroVAX. The Lexidata is used for quick display of images and plotting graphs. All software for display was locally developed. The display device is considered adequate for low resolution image viewing, the MASSCOMP Aurora and the MicroVAX GPX are relied upon for more demanding display needs.

F-4. IPAQ: Image Presentation

Personnel: K. W. Clark, BCL
D. E. Beecher, BCL
M. A. Brown, BCL
G. E. Christensen, BCL
G. K. Garg, BCL
J. G. Gutenschwager, BCL
R. E. Hermes, BCL

Support: RR 01380
Washington University

Image Manipulation and Display

A year ago, the IPAQ group considered several alternatives among available image processing software packages. The package to be selected would include an image file structure and image manipulation software offering the greatest flexibility for the IPAQ research activities and for meeting the anticipated needs of the collaborating Washington University community. That chosen was the Washington University Computer Science image processing system which is an amalgamation of VSH (V-shell from the University of North Carolina), PPS/PDS (Picture Processing System/Picture Data Structure from Cornell University), and local software. The software was installed on a MicroVAX at BCL. For MASSCOMP systems, the input/output routines were modified to accomodate the differences between the MASSCOMPs and the MicroVAXes in the way data are read/written; thus, image files are easily transferred among machines, and any differences between the two types are transparent to the user. Since installation and modification of the software, most work has focused upon gaining experience with the utilities offered with the package (filters, image intensity rescaling, FFTs, image data extraction, header creation and removal, etc.). An additional program was written to display and zoom a gray-scale image of any size which would fit on the screen.

Current efforts focus on a routine that simultaneously displays multiple images. Options appear in pop-up menus and selections are made with a hand-held mouse. Window size and placement are arbitrary and set with the mouse. Portions of images larger than the screen can be displayed and panned to the area of interest. Panning is supported in rotate, zoom, and shrink modes. Windows can be re-sized, moved, and deleted. While image-processing users interact with the available utilities and gain experience, overlapping images and presentation optimization are under consideration. Other efforts underway include graybar (or inverted graybar) display, a display of gray values for any horizontal or vertical line of an image, a gray-value histogram of an image, and utility for converting a PPS/PDS image file to a VSH image file.

X - windows

The MIT (Massachusetts Institute of Technology) X-windows network transparent hardware independent graphics system is available on the MicroVAX GPX system. The system, adopted as a standard by most major vendors in the graphics market place including Digital Equipment, MicroVAX

and MASSCOMP, gives BCL a uniform interface to our different graphics devices in a similar manner that the UNIX operating system provides a uniform interface to the different computers. This graphics system is unique because it allows remote network access to image displays and graphics devices. Additionally, the data transport protocol of the network is transparent to the graphics system. Many utilities are available for this software system including image display/manipulation and previewers for various text-processing and graphics software systems such as POSTSCRIPT (Adobe Corporation) and imPRESS (Imagen Corporation).

Datacopy Reflectance Camera

The Datacopy model 920 reflectance camera captures offline images of opaque photographs/objects. The camera is interfaced to an IBM PC/AT with 1 Mbyte of memory and 20 Mbytes of hard disk. An 8 1/2 x 11 inch page (photograph) can be captured in high-resolution mode (3456 x 4472 pixels) or low-resolution mode (1728 x 2240 pixels) @ 8 bits/pixel. The PC is configured with an AT&T Targa-32 board which allows display and manipulation of true-color images (8 bits each - RGB). Images captured with the camera can be previewed with the Targa System and then transferred transferred PC to other image-processing stations for further manipulation. Characteristics of this camera image-acquisition system are described in F-8.

Hardcopy Gray-Scale Images

Utilities are available for producing rectangular gray-scale images in 8.5 x 11 in. hard-copy on the Imagen Printstation. Several gray-scaling (half-tone and dithering methods), reverse-imaging, and contrasting techniques are available; additional techniques are under investigation. A particular reproduction technique may work well for one kind of image but not so well for another. Thus, a user may compare several of the available techniques and choose the one most appropriate.

Photographic Equipment

A Polaroid DS-34 direct-screen camera and a matching CRT hood were purchased in order to capture instant prints of displayed images. A Nikon 2000 35mm camera was purchase in order to make slides of displayed images. One may use Polaroid 35mm instant slide film to obtain slides on-site or use conventional 35mm film to be processed elsewhere. Camera exposure settings and speeds for various film types under assorted conditions (kinds of images, screen size & brightness, etc.) are recorded in the IPAQ Notebook (F-1) as guidelines for future use.

F-5. IPAQ: Networking

Personnel: G. J. Blaine, BCL
R. E. Hermes, BCL
R. L. Hill, BCL and Radiology
A. Kumar, BCL and Radiology
S. R. Phillips, BCL
A. P. Rueter, B.S., Radiology
D. A. Schwab, BCL
E. Senol, BCL

Support: RR 01380
Washington University

Close coupling of algorithm research, development and evaluation to the collaborative research areas is facilitated by a communication network which serves to federate distributed resources. Access to data from specialized imaging instruments located in collaborator's laboratories is important to evaluating algorithm performance. Additionally, the communication network is to support presentation of images to collaborating biomedical scientists. Quick-look capability should stimulate increased participation and reduce the time constant in the necessarily interactive evaluation of algorithm performance.

Information interchange between the distributed image acquisition resources within the medical center, the computation-oriented nodes at the BCL and the presentation nodes (currently located within BCL) can be functionally partitioned into "message" and "service" classes. Two-way query-based conversations are addressed by the "message network." The transport of large data sets for access to measurement and image information is to be supported by bulk-transfer at high rate in a "service network."

Local message network connectivity is supported by TERRANET (PR 22, F-10). Approximately twenty-five terminal ports, twenty-five computer ports and two telephone-line modems are provided 9600-bps switched-circuit access. Dedicated point-to-point 9600-bps channels on the MIR CATV network provide TERRANET access to remote resources such as the MIR PACS VAX 11/750, the CCU-PET computer as well as terminal support to collaborators in Radiation Oncology.

Our current "service network" uses a baseband-Ethernet LAN which spans the Institute's medical campus facilities, and the backbone broadband-Ethernet LAN which is supported on the MIR cable network in the 54-72 MHz channel space. A DEC LAN 100 Bridge supports inter-LAN traffic while minimizing backbone loading. The Ethernet channel supports packet transmission for both DECNET and TCP/IP communication protocols. Digital Equipment's DECNET-Ultrix product installed on a MicroVAX II (nodename: wuipaq) facilitates file transfer from the radiology image database to our UNIX-based computational and display resources.

Connectivity to UNIX-based resources located at the Engineering School campus is supported by a point-to-point 9600-bps channel available on the Medical Computing Facility's 23-GHz microwave system. As a result

of early difficulties with channel robustness, a test set has been developed to assist in the evaluation of 9600-bps channel failure/recovery modes. The bit-error generator (BEG) test set receives a serial asynchronous data stream at 9600 bps, modifies it by introducing random errors at a specified bit-error rate and retransmits a modified serial data stream while remaining transparent to the RS-232 communication line. The errors can be injected as either framing or data errors. The BEG can be connected to communication lines at speeds up to 960 kbps by substituting an appropriate 32X crystal.

The BEG is being tested using a serial port on a MicroVAX II. A software program is used to send and receive data on the serial port with the BEG connected in a loop-back configuration to determine the bit-error rate. The preliminary results suggest that bit-error rates in the range of 0.01 to 0.99999 are generated to a reasonable accuracy. Smaller bit-error rates produced questionable results which require further testing and evaluation.

Development was completed on a locally designed frame buffer (PR 22, F-8). The buffer, capable of storing and displaying an image of 512 x 512 x 8 bits, was an experiment to demonstrate the delivery of images via high-speed data communication to a low-cost display buffer. A total of four buffers were fabricated and used to evaluate data transfer over a 1-MHz serial channel on the MIR CATV cable system. Issues of image distribution to addressable buffers and system robustness were examined.

F-6. IPAQ: Computation

Personnel: S. M. Moore, BCL
D. E. Beecher, BCL
K. W. Clark, BCL
D. G. Politte, BCL
B. D. Skinner, BCL
K. R. Smith, BCL
E. E. Witte, BCL

Support: RR 01380
Boeing Computer Services

Algorithm development and computing for quantitative imaging is the central activity of the Resource. Satisfying the computing needs of these project areas is a significant part of the IPAQ activity. Attention has been focused on two major goals:

1. the reduction of computation time needed for current studies employing computationally intensive algorithms and

2. understanding the relative performance of different processors to allow prediction of computation times for future studies and implementations of algorithms.

Pursuant to the first goal, much time was devoted in the last year to implementing the EM algorithm for Maximum-Likelihood Image Reconstruction (A-7) on the Mercury Computer Systems ZIP 3232 array processor. Initial efforts were devoted to understanding the architecture of the array processor and developing a set of programs to test software and hardware provided by the vendor. After system testing, we implemented the EM algorithm using one-dimensional data and compared the results to those gained on a MicroVAX II computer. The numerical results were comparable to within the accuracy of the machines, and the array processor implementation was four times faster than the implementation on the MicroVAX.

After the one-dimensional studies, the EM algorithm was implemented on the array processor using PET data simulated and processed in the (X,Y) space. Computation time on the array processor for this implementation was a function of the number of counts in the data, but was on the order of 15 minutes. Studies by Liu suggested that the computation time could be reduced by performing some of the calculations in the original data space (TOF, Distance) (A-7). This version was implemented on the array processor, and computation times for one iteration are presented in the table below for a phantom containing 100,000 counts.

Computation Times for One Iteration of the EM Algorithm (minutes)

Implementation Space	System	
	ZIP Array Processor	MASSCOMP 55020
(X,Y)	14:39	14:23
(T,D)	5:24	3:02

In the two-dimensional implementation of the EM algorithm on the Mercury array processor, it became obvious that certain architectural characteristics would limit the algorithm execution speed. Since PET data within a field of view are rather sparse, it is algorithmically more efficient to examine individual pixels rather than data vectors. Random access of individual pixels is a simple operation for conventional computers but poses a particular problem for the array processor with only a 16-bit address register. This single limitation imposes a significant performance penalty on the two-dimensional array processor implementation. Alternate array processor implementations are being explored to overcome the architectural limitations.

To assess the relative performance differences of computers within the resource, a set of tests was performed on each machine. Though these tests are not meant to provide an index which could be used in all cases to compare machines, they do provide a good set of data which can be used to estimate machine performance on similar algorithms. The tests computed the area under a zero-mean, unit-variance Gaussian probability density over the limits from -5 to +5 using a polynomial approximation to the Gaussian pdf. The table below gives the execution time of 1000 iterations of a single precision calculation using FORTRAN on several machines. In all cases, optimizing compiler optimizers were used.

Times for Single-Precision Calculation
of the Area under a Gaussian (sec)

MASSCOMP 500	40
MASSCOMP 5400	48
MASSCOMP 55020	8.4
MicroVAX II	87
PE3230	38

The EM algorithm in the (X,Y) space and the voxel method for generating 3-Dimensional images (F-9) were implemented on a Cray XMP vector processor during a 2-week session at Boeing Computer Services, via a grant supported by The Division of Research Resources, NIH. The Cray performed the EM algorithm 50 times faster and the voxel algorithm 44 times faster than a MicroVAX even though the compiler was not able to vectorize all of the code. It is believed that greater speedups could have been achieved had there been more time available for manipulating the algorithm on the Cray machine.

F-7. Campus-Wide Network Program

Personnel: G. J. Blaine, BCL and Radiology
J. R. Cox, Jr., BCL and Computer Science
R. E. Hermes, BCL
R. L. Hill, BCL and Radiology
D. G. Hirsh, B.A., Office of the Network Coordinator
R. G. Jost, M.D., Radiology
A. Kumar, BCL and Radiology
S. R. Phillips, BCL
A. P. Rueter, B.S., Radiology
D. E. Schwab, BCL
E. Senol, BCL
G. M. Tormo, BCL

Support RR 01380
RR 03522
AT & T Corporation
Digital Equipment Corporation
Washington University

Networking at Washington University

Distributed computing, the decentralized deployment of inexpensive personal workstations and laboratory computers and the sharing of more expensive processing, storage and printing resources has long been the defacto style of computing for researchers at Washington University. At the Biomedical Computer Laboratory (BCL) in 1967 several computers (that would now be called workstations) were connected to the central University computer by twisted wire-pairs and leased telephone lines. This style of

networking grew on the campus so that today electronic switches connect more than 1300 terminals and personal computers to computing resources. At the School of Medicine alone, the Medical Computing Facilities serves over 500 users via twisted wire-pairs and a central electronic switch.

Computer networking that allowed direct high-speed transmission of data between computers became popular about 1980. Washington University's Mallinckrodt Institute of Radiology (MIR) began installing DECnet (Digital Equipment Corporation's proprietary computer network) in that year and has developed a large network of computers over the years since then. When Ethernet became available commercially in 1983 several laboratories at Washington University installed this LAN to serve nearby users. In the years that followed, almost two dozen such installations appeared on the two campuses. Baseband signaling is the most common method for Ethernet communication since it provides for inexpensive network taps. Two limitations exist, however: the distance between network nodes cannot exceed 2800 meters and the physical medium can support only one channel.

Work toward a picture archiving and communication system (PACS) was begun in 1982 through a collaborative program between the Mallinckrodt Institute of Radiology and the Biomedical Computer Laboratory. A broadband CATV cable was installed to study the problems associated with picture transmission. This system for PACS development now carries radiological images in both digital and video form to several sites in the School of Medicine.

Several universities, notable among them Carnegie-Mellon, MIT, Stanford, Brown, Johns Hopkins and Dartmouth, have engaged in substantial centrally-funded programs to implement large-scale networks on their campuses. Our approach has recognized the decentralized nature of our research community and provides a focus for establishing connectivity between computing resources both at the individual researcher and departmental levels. Network activities have been funded through a mixture of equipment grants (Digital Equipment Corporation 3 years/$15 million; Division of Research Resources, Shared-Instrument Grant $300,000, AT & T University Equipment Program $250,000) and personnel support from related research activities, the Medical school and the central administration.

Program Organization

To address the issues of a campus-wide network the Office of the Network Coordinator (ONC) was formed in May 1985. The ONC (directed by J. R. Cox, Jr.) is a small organization whose principal role is planning and coordination. A meeting of system managers and interested individuals within the university is hosted monthly. Additionally, the "Midwest Workshop on Communications Systems," was organized and hosted at Washington University consisting of a two-day program of invited speakers representing a wide spectrum of communications activities, from local area networks to national networks. The goal of 100 participants was achieved.

Project Activities

- Supercomputer Access

A three-year, 1.2 million dollar grant from the National Science Foundation has been awarded to fund MIDnet, a regional network that will connect eight midwestern universities to the National Center for Supercomputer Applications (NCSA) at the University of Illinois, Champaign-Urbana and to NSFnet a national network that connects all five of the NSF sponsored supercomputer centers. Researchers at Washington University will be able to have interactive access to any of these five centers. Both the NCSA and the Pittsburg Supercomputer Center have solicited researchers at Washington University. This service will be available in late 1987.

- Network for Biomedical Research

A Shared-Instrument Grant from the Division of Research Resources has funded the installation of a network to provide high-speed communications within the broad community of biomedical investigators at Washington University. The shared facility, to be completed in late 1987, will enable investigators to exchange scientific data and ideas throughout both university campuses. Principal components of the ethernet based portion of network are: a CATV-based backbone, an intercampus ethernet via microwave, and distributed departmental baseband ethernets. Plans also exist for supporting video transmission of images.

A CATV-based backbone has been designed and is being installed on the hilltop campus. Site surveys, FCC license application, and equipment orders have been completed for the intercampus 10-Mbps Ethernet channel and a full-duplex broadcast-quality video channel. The channels will span a 2.5-mile line-of-sight distance and utilize 23-GHz microwave equipment. The medical-school-campus portion of the network will utilize a channel of the existing MIR CATV-based backbone.

Five Ethermodems were purchased from the Chipcom Corporation to activate a second channel on the MIR CATV backbone. These modems operate in the 252-270 Mhz range, performing the same function as the Digital Equipment Corporation modems (DECOMs) which operate in the 52-70 Mhz range and are used to support the MIR PACS channel. By using both DECOMs and Ethermodems on the same CATV backbone, greater utilization of the network bandwidth is achieved, thereby maintaining good network performance as traffic increases.

Ethermodems were evaluated via two methods. First, standalone tests were performed using the self-test features for both RF and Digital loopback. No problems were identified. Secondly, online data-transfer tests were conducted to contrast broadband performance to that of the IBC baseband ethernet. The baseband tests were conducted twice: once during a period of low network utilization and once during average utilization. The results did not differ significantly and were then used as metrics to compare transfer statistics gathered during Ethermodem tests. Ethermodem transfer tests were conducted using two MicroVAXes connected via a point-to-point link of two Ethermodems to simulate a broadband network. Identical data transfers tests to those used in the baseband experiment were conducted. Each Ethermodem was tested in this manner, yielding nearly

identical results in each case. The Ethermodems have been connected to the CATV system and further testing continues.

- A Campus-Wide Software Library

While there are a great many benefits to networks of autonomous mini and microcomputers, decentralized computing as it is practiced by most organizations suffers from a lack of software. Organizations typically have enough money to purchase machines but do not a budget for a rich collection of software. Consequently programmers and users are continually "reinventing the wheel" building programs that emulate the functions of commercially available software or writing programs that have been previously written by other programmers within and without the university community. If the average price of commercial software could be significantly reduced and if public-domain and quasi-commercial software could be more efficiently distributed, people would be encouraged to build their applications with more sophisticated tools. This is the motivation behind the Washington University Campus-Wide Software Library.

The library begins operation in July, 1987. Our first significant action is a contract that ONC has negotiated with Digital Equipment Corporation that will allow users of VAX computers to pay a fixed annual fee, based on processor-size. In exchange for this annual fee the machine is granted a one-year license for a collection of twenty-five software products, including operating systems, network software, compilers, application development tools, databases and a smattering of office automation products. We expect that over sixty systems will participate in the first year of this program.

The library will also distribute the MT-XINU release of the UNIX operating system and network software from Meridian Technology, Incorporated. Over time we expect that the library will also catalog and distribute: 1) commercial software for personal computers such as the PC and Macintosh; 2) public-domain software for all classes of machines, and 3) special-purpose scientific software.

F-8. Evaluation and Characterization of the DATACOPY Reflectance Camera

Personnel: G. K. Garg, BCL
D. E. Beecher, BCL
M. A. Brown, BCL

Support: RR 01380

The Datacopy model 920 reflectance camera is intended to be used for offline image capture of opaque photographs/objects. The model 920 offers two resolution modes. In high-resolution mode, an 8 1/2 x 11 inch page can be captured as a 3456 x 4472 pixel (8 bits/pixel) image, while in low-resolution mode this is decreased to 1728 x 2240. The camera is interfaced to an IBM PC/AT with 1 Megabyte of memory and a 20-Megabyte hard disk for

image storage. The PC is also configured with an AT&T Targa 32 board which allows display and manipulation of true-color images (8 bits each - RGB).

Images captured by the camera can be transferred via Ethernet to other image processing stations using Excelan network utilities. It takes about 6-7 minutes for the camera to capture a gray scale image in low resolution mode and another 2 minutes (at least) to run startup tests on the camera, adjust the target on the field of view, and focus the camera. Thus a typical image capture session may require 15-20 minutes. To print an image on an Imagen laser printer typically takes about 8-10 minutes under normal system load.

The camera has a gray-capture capability for 256 levels of gray. The goal is to create a dedicated image-capture facility to allow researchers a convenient mechanism for digitizing images into machine readable form. Unfortunately the camera has limitations which do not allow it to produce images which are perfect reproductions of the respective targets. An attempt is being made to characterize the camera and correct (if possible), for limitations discovered during characterization.

The field of view of the camera is currently illuminated by four incandescent lamps. Each of these lamps has its point of maximum illumination, i.e. a "hot spot" in a fairly small area compared to the field of view. Therefore the field of view is unevenly illuminated. One way to eliminate this would be to have only one lamp situated a modest distance from the camera but this would reduce illumination to an unacceptable level. Instead, the lighting arrangement is being adjusted to achieve the most uniformly illuminated field possible. Since it is difficult to guarantee a stable environment, the arrangement will have to be tested periodically and readjusted. A hood was also constructed to eliminate ambient light.

The elements of the CCD array in the camera do not provide a linear response to light intensities. The array is linear within a limited range of "Gray Scale Values," but underestimates the level of gray outside this range. The array also saturates at a gray scale value below the maximum of 255.

Tests indicate that the camera can resolve black and white patterns at 1 line per pixel. However, at this resolution, the camera does not provide full contrast. The camera requires a minimum of seven pixels to provide full contrast when making the transition from black to white.

Work in progress includes identifying the linear range of the CCD array, characterizing the degree of non-linearity and determining the modulation transfer function for the system and a characterization of the degree of aliasing observed.

F-9. Three-Dimensional View Generation Utilizing Voxel Models

Personnel: D. E. Beecher, BCL
J. R. Cox, Jr., Computer Science and BCL

Support: RR 01380

Since the last report on this topic (PR 22, F-9), significant progress has been made on improving the execution speed of these algorithms. Modifications of the algorithms responsible for the speedup include an extremely fast method for determining the "shading coefficient" at any given point in the final rendering. This can be performed on-the-fly as the image is being formed from the voxel volume. This technique yields an order-of-magnitude speed increase in the overall rendering time, which is now on the order of 10 seconds per view (on a 68020-based MASSSCOMP system). This time is for a 64x64x64 volume where the final image is 128x128 pixels.

Preliminary studies have shown that this speed could be reduced to approximately 1-2 seconds by porting the algorithms to a PIXAR Image Computer or other equally fast host. We believe that real-time 3-dimensional image manipulation could be achieved with an implementation in special-purpose hardware.

VII. TRAINING ACTIVITIES AND SEMINARS

Training activities of the Biomedical Computer Laboratory are directed toward the goals of informing the local and national scientific communities about resource projects and facilities and of instructing a broad spectrum of people in the application of advanced computer-techniques to problems in clinical medicine and biological research. Training activities include the teaching of formal courses at the School of Medicine and the School of Engineering as well as supervision of graduate students by Laboratory staff. Both individual and small-group training about resource facilities are made available to the biomedical scientist. National workshops and symposia on topics of interest and importance to the resource and community are supported.

The bringing together of biomedical scientists, engineers, and computer scientists provides important cross-fertilization between disciplines. In these settings, students and staff find the need and opportunity to test the relevance of theory and the usefulness of technology in applications to real problems. Also, the biomedical scientists are aided in learning new techniques for acquiring useful information. To this end, some of the courses offered are addressed to biologists without strong technical backgrounds who want and need a below-the-surface appreciation of biomedical computing. Laboratory personnel also participate in regularly scheduled conferences in the clinical departments where both the biological and technological issues are examined.

Seminars and presentations relating to resource projects and applications are conducted by Laboratory staff as well as scientists and engineers from the national community. During the year the following activities were supported:

Seminars

"Algorithms for Estimating Parameters in Dynamic Tracer Studies Using Positron-Emission Tomography"	Mr. John M. Ollinger Department of Electrical Engineering Washington University St. Louis, MO
August 11, 1986	
"PET REVIEW: 'Sampling' 'Eigenvalues' 'Searching'"	Dr. Michael I. Miller Dr. Donald L. Snyder Dr. Daniel R. Fuhrmann Mr. Kurt Smith Mr. Dave Politte Biomedical Computer Laboratory Washington University St. Louis, MO
August 15, 1986	

"log(x) or adventures in precision" August 18, 1986	Dr. Lewis J. Thomas, Jr. Biomedical Computer Laboratory Washington University St. Louis, MO
"The Design of a 512 × 512 × 8 Frame Buffer" August 21, 1986	Mr. Arun Kumar Computer Science Department Washington University St. Louis, MO
"Evaluation of Apollo Workstation Environment and Newest High and Low Performance Workstations" August 26, 1986	Mr. Tom Cummings Apollo Computer Inc. St. Louis, MO
"Review of ACM SIGGRAPH '86" August 27, 1986	Mr. Russ E. Hermes Mr. David E. Beecher Biomedical Computer Laboratory Washington University St. Louis, MO
"ZIP 3232 Array Processor Tests and Comments" September 12, 1986	Ms. Ellen Witte Mr. Brian Skinner Biomedical Computer Laboratory Washington University St. Louis, MO
"Photometric System Demonstration/Discussion September 19, 1986	Mr. Richard Akiens Photometrics, LTD. Tucson, AR
"Hyperchannel - B" September 22, 1986	Mr. Tim Halvorson Network Systems Corporation
"Modeling Ion Channel Blockade: A Tool for Understanding Anti-arrhythmic Drugs" October 2, 1986	Mr. C. F. Starmer Duke University

"Programming on the Masscomp" November 19, 1986	Dr. R. Martin Arthur Department of Electrical Engineering Washington University St. Louis, MO
"Stripes and Spots: The Geometry of Patterning in Polysphondylium Pallidum" April 6, 1987	Dr. James McNally Princeton University
"Validation and Comparison to Crossfire-Analysis of A New Method for EM Autoradiography April 20, 1987	Mr. Badrinath Roysam Department of Electrical Engineering Washington University St. Louis, MO
"Mapping the EM Algorithm for Time-of-Flight Positron Emission Tomography onto Parallel Architectures" May 4, 1987	Mr. Kurt R. Smith Department of Electrical Engineering and Institute for Biomedical Computing Washington University St. Louis, MO
"Efficient Computation of the EM Algorithm in Time-of-Flight Positron-Emission Tomography" June 29, 1987	Mr. Stephen K. Liu Department of Electrical Engineering Washington University St. Louis, MO

- - - - - - - - - - - -

Other Activities

A Lecture Series in support of Biomedical Engineering 3/2 Intensive Course
Sponsored by the Program in Biomedical Engineering
Sever Institute of Technology
Washington University

"Scope of Biomedical Engineering" December 29, 1986	Harold W. Shipton Biomedical Computer Laboratory Washington University St. Louis, MO
"Physical Principles of Tracer Kinetics" December 30, 1986	Kenneth B. Larson Biomedical Computer Laboratory Washington University St. Louis, MO

a film - "The Brain" January 1, 1987	Harold W. Shipton Biomedical Computer Laboratory Washington University St. Louis, MO
"An Engineer Looks at the Brain" January 2, 1987	Harold W. Shipton Biomedical Computer Laboratory Washington University St. Louis, MO
"Biomedical Instrumentation and Transducers" January 7, 1987	R. Martin Arthur Department of Electrical Engineering Biomedical Computer Laboratory Washington University S.t Louis, MO
"Computers: Communication and Storage" January 8, 1987	G. James Blaine Biomedical Computer Laboratory Washington University St. Louis, MO
"Computers, Cardiologists and Cardiograms" January 9, 1987	Lewis J. Thomas, Jr. Biomedical Computer Laboratory Washington University St. Louis, MO

VII. PUBLICATIONS AND ORAL PRESENTATIONS

Abendschein, D. R., Fox, K. A. A., Ambos, H., D., Sobel, B. E., and Bergmann, S. R., "Metabolism of Beta-Methyl [1-^{11}C] Heptadecanoic Acid in Canine Myocardium," International Journal of Nuclear Medicine and Biology, in press.

Akita, H., Creer, M. H., Yamada, K. A., Sobel, B. E., and Corr, P. B., "Electrophysiologic Effects of Intracellular Lysophosphoglycerides and Their Accumulation in Cardiac Lymph with Myocardial Ischemia in Dogs," Journal of Clinical Investigation, 78:271-280, 1986.

Ambos, H. D., Markham, J., Lindsay, B. D., and Cain, M. E., "Spectral Analysis of Signal-Averaged Electrocardiograms from Patients with and without Ventricular Tachycardia, "Proceedings of the IEEE Conference on Computers in Cardiology, IEEE Catalog No. 87CH2476-0, Boston, MA, pp. 529-532, October 7-10, 1986.

Barrett, R. C., McCarthy, A. W., Miller, M. I., and Morley, R. E., "Gaussian Convolutions on a Massively Parallel Processor," Proceedings of the Twenty-First Annual Conference on Information Sciences and Systems, The Johns Hopkins University, Baltimore, MD, pp. 373-374, March 1987.

Beecher, D. E., "Maximum Likelihood Image Reconstruction for PET," presented at the Boeing Supercomputer Institute, Seattle, WA, July 1986.

Beecher, D. E., "Three Dimensional View Generation Using Voxel Models," presented at the Boeing Supercomputer Institute, Seattle, WA, July 1986.

Bergmann, S. R., Fox, K. A. A., and Ludbrook, P. A., "Determinants of Salvage of Jeopardized Myocardium After Coronary Thrombolysis," Cardiology Clinics, 5:67-77, 1987.

Bergmann, S. R., Ludbrook, P. A., and Sobel, B. E., "Coronary Thrombolysis with Tissue-Type Plasminogen Activator," Cardiology Clinics, 5:101-111, 1987.

Blaine, G. J., and Cox, Jr., J. R., "Campus-wide Network for Picture Transmission," invited presentation at the First Midwest Workshop on Communication Systems, Washington University, St. Louis, MO, November 1986.

Broadstone, S. R., and Arthur, R. M., "An Approach to Real-Time Reflection Tomography Using the Complete Dataset," IEEE 1986 Ultrasonics Symposium Proceedings, IEEE Catalog No. 86CH2375-4, B. R. McAvoy, ed., New York, 2:829-831, 1986.

Broadstone, S. R., and Arthur, R. M., "Time-of-Flight Approximation for Medical Ultrasonic Imaging," Acoustical Imaging, in press.

Brown, M. A., Marshall, D. R., Sobel, B. E., and Bergmann, S. R., "Delineation of Myocardial Oxygen Utilization with Carbon-11 Labeled Acetate," Circulation, in press.

Brown, M. A., Myears, D. W., Marshall, D. R., Sobel, B. E., and Bergmann, S. R., "Assessment of Regional Myocardial Oxygen Utilization by Positron Tomography with ^{11}C-Acetate," Journal of the American College of Cardiology, 9:73A, 1987 (abstract).

Corr, P. B., and Cain, M. E., "Electrophysiology," in Cardiovascular Pathophysiology, G. G. Ahumada, ed., Oxford University Press, New York, pp. 34-73, 1986.

Corr, P. B., Saffitz, J. E., and Sobel, B. E., "Contributions of Altered Lipid Metabolism to Arrhythmogenesis in the Ischemic Heart," in Life Threatening Arrhythmias During Ischemia and Infarction, D. J. Hearse, A. S. Manning, and M. J. Janse, eds., Raven Press, New York, p. 91-114, 1987.

Corr, P. B., Saffitz, J. E., and Sobel, B. E., "Lysophyspholipids, Long Chain Acylcarnitines and Membrane Dysfunction in the Ischemic Heart," in Lipid Alterations in the Normoxic and Ischemic Heart, Basic Research in Cardiology, Springer-Verlag, Vol. 82, pp. 199-208, 1987.

Corr, P. B., Yamada, K. A., Creer, M., Sharma, A. D., and Sobel, B. E., "Lysophosphoglycerides and Ventricular Fibrillation Early after Onset of Ischemia," Journal of Molecular and Cellular Cardiology, in press.

Corr, P. B., Yamada, K. A., and Witkowski, F. X., "Mechanisms Controlling Cardiac Autonomic Function and Their Relation to Arrhythmogenesis," in The Heart and Cardiovascular System: Scientific Foundations, H. A. Fozzard, E. Haber, R. B. Jennings, A. M. Katz, and H. E. Morgan, eds., Raven Press, New York, pp. 1343-1403, 1986.

Cox, Jr., J. R., and Zeelenberg, C., "Computer Technology: State-of-the-Art and Future Trends," Journal of the American College of Cardiology, 9(1):204-214, January 1987.

Creer, M. H., Knabb, M. T., Pogwizd, S. M., Saffitz, J. E., Sobel, B. E., and Corr, P. B., "Antiarrhythmic Effect of Inhibition of Accumulation of Long Chain Acylcarnitines with Ischemia," Circulation, 74(II):II-66, 1986 (abstract).

Eisen, H. J., Eisenberg, S. B., Bakke, J. E., Saffitz, J. E., Bolman, R. M., Sobel, B. E., and Bergmann, S. R., "Non-Invasive Detection of Cardiac Allograft Rejection with ^{111}Indium Labeled Lymphoctytes," Circulation 74:II-219, 1986 (abstract).

Eisenberg, J. D., Sobel, B. E., and Geltman, E. M., "Differentiation of Ischemic from Nonischemic Cardiomyopathy and Positron Emission Tomography," American Journal of Cardiology, 59:1410, 1987.

Eisenberg, P. R., Sherman, L., Rich, M., Schwartz, D., Schechtman, K. B., Geltman, E. M., Sobel, B. E., and Jaffe, A. S., "Importance of Continued Activation of Thrombin Reflected by Fibrinopeptide A to the Efficacy of Thrombolysis," Journal of the American College of Cardiology, 7:1255, 1986.

Fields, L. E., Daugherty, A., and Bergmann, S. R., "Effect of Exogenous Fatty Acid Levels on Mechanical Performance and Lipid Content of Hearts Isolated from Alloxan-Diabetic Rabbits," American Journal of Physiology: Heart and Circulatory Physiology, in press.

Fox, K. A. A., Knabb, R. M., Bergmann, S. R., and Sobel, B. E., "Progress in Cardiac Positron Emission Tomography with Emphasis on Carbon-11 Labeled Palmitate and Oxygen-15 Labeled Water," in Noninvasive Imaging of Cardiac Metabolism, E. E. Van der Wall, ed., Martinus Nijoff Publishers, Boston, pp. 203-240, 1987.

Fox, K. A. A., Saffitz, J. E., and Corr, P. B., "Pathophysiology of Myocardial Reperfusion," in Thrombolysis and the Heart, B. E. Sobel, ed., Cardiology Clinics, W. B. Saunders, Co., Philadelphia, pp. 31-48, 1987.

Fuhrmann, D. R., "An Algorithm for Subspace Computation, with Applications in Signal Processing," SIAM Proceedings on Linear Algebra in Signals, Systems, and Control, Boston, MA, in press.

Fuhrmann, D. R., and Brown, M. A., "Encoding Biomedical Images with Quadtrees," Proceedings of the 24th Allerton Conference on Communications, Control and Computing, University of Illinois at Urbana, Urbana, IL, pp. 703-704, October 1986.

Fuhrmann, D. R., Brown, M. A., Miller, M. I., Roysam, B., Saffitz, J. E., and Thomas, Jr., L. J., "A Data Acquisition System for Maximum Likelihood Analysis of Electron Microscopic Autoradiographs," Journal of Electron Microscopy Technique, in press.

Fuhrmann, D. R., and Liu, B., "Rotational Search Methods for Adaptive Pisarenko Harmonic Retrieval," IEEE Transactions on Acoustics, Speech and Signal Processing, ASSP-34:1550-1565, December 1986.

Fuhrmann, D. R., and Miller, M. I., "On the Singularity of Maximum Likelihood Estimates of Structured Covariance Matrices," Proceedings of the Twenty-First Annual Conference on Information Sciences and Systems, The Johns Hopkins University, Baltimore, MD, pp. 549-552, March 1987.

Geltman, E. M., Serota, H., Schaab, C., Baird, T., Ambos, H. D., and Jaffe, A. S., "Assessment of Myocardial Perfusion with $H_2{}^{15}O$ and Dynamic Positron Emission Tomography," Circulation 74(II):II-41, 1986.

Gross, R. W., Corr, P. B., and Sobel, B. E., "Alterations in Phospholipid Metabolism During Myocardial Ischemia and Their Electrophysiologic and Biophysical Sequelae," in Cardiac Function under Ischemia and Hypoxia, K. Yamada, A. M. Katz, and J. Toyama, eds., University of Nagoya, Japan, 1987.

Harms, W. B., Slessinger, E. D., Wong, J. W., and Purdy, J. A., "Experimental Tests for Three-Dimensional Dose Calculations," Medical Physics, 13:590, 1986.

Hart, Jr., W. M., "Color Contrast Perimetry: Hue Discrimination Defects in Acquired Dyschromatopsias," Documente Ophthalmologica Proceedings Series 46, pp 267-273, 1987.

Heathers, G. P., Yamada, K. A., Kanter, E. M., and Corr, P. B., "Hypoxia Induced Exposure of α_1-Adrenergic Receptors in Adult Myocytes: Dependence on Endogenous Long Chain Acylcarnitines," Circulation, 74(II):II-321, 1986 (abstract).

Heathers, G. P., Yamada, K. A., Kanter, E. M., and Corr, P. B., "Long-Chain Acylcarnitines Mediate the Hypoxia Induced Increase in Alpha$_1$-Adrenergic Receptors on Adult Canine Myocytes," Circulation Research, in press.

Herrero, P., Markham, J., Myears, D. W., Weinheimer, C. J., and Bergmann, S. R., "Measurement of Myocardial Blood Flow with Positron Emission Tomography: Correction for Count Spillover and Partial Volume Effects," Sixth International Conference on Mathematical Modeling, in press (abstract).

Hughes, B., Bergmann, S. R., Corr, P. B., and Sobel, B. E., "External Detection of β-Adrenoceptors with ^{125}I-Hydroxybenzylpindolol in Isolated Perfused Hearts," International Journal of Nuclear Medicine and Biology, 13:565-571, 1986.

Jaffe, A. S., Biello, D. R., Sobel, B. E., and Geltman, E.M., "Enhancement of Metabolism of Jeopardized Myocardium by Nifedipine," International Journal of Cardiology, in press.

Jaffe, A. S., Serota, H., Grace, A., and Sobel, B. E., "Diagnostic Changes in Plasma Creatine Kinase Isoforms Early After the Onset of Acute Myocardial Infarction," Circulation, 74:105, 1986.

Johnston, P. H., and Miller, J. G., "A Comparison of Backscatter Measured by Phase Sensitive and Phase Insensitive Detection," IEEE Transactions on Ultrasonics, Ferroelectrics, and Frequency Control, UFFC-33:78, 1986 (abstract).

Johnston, P. H., and Miller, J. G., "Phase-Insensitive Detection as an Approach to the Estimation of Attenuation from Backscattered Ultrasound," Ultrasonic Imaging, 8:48-49, 1986 (abstract).

Johnston, P. H., and Miller, J. G., "Phase-Insensitive Detection for Measurement of Backscattered Ultrasound," IEEE Transactions on Ultrasonics, Ferroelectrics, and Frequency Control, UFFC-33:713-721, 1986.

Karamanos, N., "EM Algorithms Incorporating Monotonicity Constraints for Removing Recovery-Related Distortion from Auditory-Nerve Discharge Patterns," informal presentation at Johns Hopkins University, Baltimore, MD, March 27, 1987.

Knabb, R. M., Bergmann, S. R., Fox, K. A. A., and Sobel, B. E., "The Temporal Pattern of Recovery of Myocardial Perfusion and Metabolism Delineated by Positron Emission Tomography after Coronary Thrombolysis," Journal of Nuclear Medicine, in press.

Knabb, R. M., Rosamond, T. L., Fox, K. A. A., Sobel, B. E., and Bergmann, S. R., "Enhancement of Salvage of Reperfused Ischemic Myocardium by Diltiazem," Journal of the American College of Cardiology, 8:861-871, 1986.

Kramer, J. B., Saffitz, J. E., and Corr, P. B., "Mechanisms of Arrhythmogenesis During Chronic Myocardial Infarction," European Heart Journal, 7(A):149-156, 1986.

Krippner, K., Wong, J. W., Harms, W. B., and Purdy, J., A., "The Use of an Array Processor for the Delta-Volume Dose Computation Algorithm," Proceedings of the 9th International Conference on the Use of Computers in Radiation Therapy, Tilburg, The Netherlands, North Holland, The Netherlands, pp. 533-536, June 22-25, 1987.

Kumar, A., "Design of a Frame Buffer for Radiology Applications," Department of Computer Science, Sever Institute of Technology, Washington University, St. Louis, MO, December 1986 (Master of Science Thesis).

Larson, K. B., "Physical and Mathematical Principles of Tracer Kinetics in Biological Applications," seminar presented to Washington University Three-Two Program students, St. Louis, MO, December 30, 1986.

Larson, K. B., Markham, J., and Raichle, M. E., "Distributed-Parameter Kinetic Models for Estimating Cerebral-Blood Flow," invited paper presented at the 6th Conjoint Winter Meeting of the Society of Nuclear Medicine, San Antonio, TX, February 4, 1987.

Larson, K. B., Markham, J., and Raichle, M. E., "Tracer-Kinetic Models for Measuring Cerebral-Blood Flow Using Externally Detected Radiotracers," Journal of Cerebral Blood Flow and Metabolism, 7:443-463, 1987.

Lerch, R. A., and Bergmann, S. R., "Non-Invasive Assessment of Myocardial Fatty Acid Metabolism with Positron Emission Tomography and Gamma Imaging," in New Concepts in Cardiac Imaging 1988, J. L. Ritchie, ed., Chicago, Year Book Medical Publishers, in press.

Liu, S. K., "Efficient Computation of the EM Algorithm in Time-of-Flight Positron-Emission Tomography," Department of Electrical Engineering, Sever Institute of Technology, Washington University, St. Louis, MO, 1987 (Master of Science Thesis).

Madaras, E. I., Perez, J. E., Sobel, B. E., and Miller, J. G., "Anisotropy of Ultrasonic Backscatter in Canine Myocardium: Results in Vivo," Ultrasonic Imaging, 8:35-36, 1986 (abstract).

Mead, C. N., Clark, K. W., and Thomas, Jr., L. J., "An Annotated Clinical Event Database as a Tool for Evaluation of Ambulatory ECG-Analysis Studies," Proceedings of the IEEE Conference on Computers in Cardiology, IEEE Catalog No. 87CH2476-0, Boston, MA, pp. 327-330, October 7-10, 1986.

Miller, M. I., "Strategies for the Representation of Broadband Stimuli in the Discharge Patterns of Auditory Nerve Fibers," in Auditory Frequency Selectivity, NATO Advanced Research Workshop on Auditory Frequency Selectivity, B. Moore and R. Patterson, eds., Cambridge, England, pp. 265-272, 1986.

Miller, M. I., Barta, P. E., and Sachs, M. B., "Strategies for the Representation of a Tone in Background Noise in the Temporal Aspects of the Discharge Patterns of Auditory-Nerve Fibers," Journal of the Acoustical Society of America, 81(3):665-679, March 1987.

Miller, M. I., and Fuhrmann, D. R., "Maximum Likelihood Estimation of Direction of Arrivals of Multiple Narrowband Signals in Noise," Proceedings of the Twenty-First Annual Conference on Information Sciences and Systems, The Johns Hopkins University, Baltimore, MD, pp. 710-712, March 1987.

Miller, M. I., Roysam, B., Saffitz, J. E., Larson, K. B., Fuhrmann, D., and Thomas, Jr., L. J., "A New Method for the Analysis of Electron Microscopic Autoradiographs," Biotechniques, 5(4):322-328, 1987.

Miller, M. I., and Snyder, D. L., "An Alternating Maximization of the Entropy/Likelihood Function for Image Reconstruction and Spectrum Estimation," Transactions of SPIE in Advanced Architectures and Algorithms, San Diego, CA, 696:163-166, 1986.

Miller, M. I., and Snyder, D. L., "The Application of Maximum-Entropy and Maximum-Likelihood for Spectral Estimation," Proceedings of the IEEE International Information Theory Symposium, IEEE Information Theory Group, Ann Arbor, MI, p. 53, October 1986 (abstract).

Miller, M. I., and Snyder, D. L., "Iterative Algorithms for Maximum-Entropy/Likelihood Estimates: Applications to Tomographic Image Reconstruction," presented at the Sixth Annual Workshop on Maximum Entropy and Methods in Applied Statistics, Seattle University, Seattle, WA, August 5-8, 1986.

Miller, M. I., and Snyder, D. L., "The Role of Likelihood and Entropy in Incomplete-Data Problems: Applications to Estimating Point-Process Intensities and Toeplitz Constrained Covariances," Proceedings of the IEEE, 75(7):892-907, 1987.

Miller, M. I., Snyder, D. L., and Turmon, M. J., "Iterative Maximum-Likelihood Estimation of Toeplitz-Constrained Covariances," Proceedings of the 24th Annual Allerton Conference on Communication, Control, and Computing, University of Illinois, Urbana-Champaign, IL, pp. 111-112, October 1986.

Miller, T. R., Grossman, S. J., Schechtman, K. B., Biello, D. R., Ludbrook, P. A., and Ehsani, A. A., "Left Ventricular Diastolic Filling and Its Association with Age," Journal of the American College of Cardiology, 58:531-535, 1986.

Mottley, J. G., and Miller, J. G., "Anisotropy of Ultrasonic Backscatter in Canine Myocardium: Theory and Results in Vitro," Ultrasonic Imaging, 8:34-35, 1986 (abstract).

Myears, D. W., Sobel, B. E., and Bergmann, S. R., "Substrate Utilization in Ischemic and Reperfused Canine Myocardium: Quantitative Considerations," American Journal of Physiology, Heart and Circulatory Physiology, in press.

Ollinger, J. M., "Algorithms for Parameter Estimation in Dynamic Tracer Studies Using Positron-Emission Tomography," Department of Electrical Engineering, Sever Institute of Technology, Washington University, St. Louis, MO, August 1986 (D.Sc. Dissertation).

Ollinger, J. M., "Estimation Algorithms for Dynamic Tracer Studies Using Positron-Emission Tomography," IEEE Transactions on Medical Imaging, MI-6(2):115-125, June 1987.

Ollinger, J. M., "An Evaluation of a Practical Algorithm for Estimating Histograms in Dynamic Tracer Studies Using Positron-Emission Tomography," IEEE Transactions on Nuclear Science, NS-34(1):349-353, February 1987.

Pogwizd, S. M., and Corr, P. B, "Electrophysiologic Mechanisms Underlying Arrhythmias Due to Reperfusion of Ischemic Myocardium," Circulation, in press.

Pogwizd, S. M., and Corr, P. B., "Mechanisms of Arrhythmogenesis During Myocardial Ischemia and Reperfusion: A Perspective of Our Current Understanding," Journal of Molecular and Cellular Cardiology, 18:43-47, 1986.

Pogwizd, S. M., and Corr, P. B., "Nonreentrant Mechanisms as a Contributor to the Development of Ventricular Fibrillation During Reperfusion," Circulation, 74(II):II-117, 1986 (abstract).

Pogwizd, S. M., and Corr, P. B., "Reentrant and Non-reentrant Mechanisms Contribute to Arrhythmogenesis During Early Myocardial Ischemia: Results Using Three-Dimensional Mapping," Circulation Research, in press.

Pogwizd, S. M., Onufer, J. R., Kramer, J. B., Sobel, B. E., and Corr, P. B., "Induction of Delayed Afterdepolarizations and Triggered Activity in Canine Purkinje Fibers by Lysophosphoglycerides," Circulation Research, 59:416-426, 1986.

Politte, D. G., "Positron Emission Tomography Image Processing," presented to HKN (Eta Kappa Nu, Electrical Engineering Honorary), St. Louis, MO, December 10, 1986.

Purdy, J. A., Harms, W. B., Wong, J. W., Matthews, J. W., and Emami, B. E., "Three Dimensional Radiation Treatment Planning System," Medical Physics, 13:590, 1986 (abstract).

Purdy, J. A., Harms, W. B., Wong, J. W., Matthews, J. W., Slessinger, E. D., and Emami, B. E., "Three Dimensional Radiation Treatment Planning System," International Journal of Radiation Oncology, Biology and Physics, 12(1):125-126, 1986 (abstract).

Purdy, J. A., Wong, J., and Harms, W. B., "New Developments in Three Dimensional Planning," Proceedings of the PC Users Group Symposium, Tokyo, Japan, Radiotherapy System Research, 3:1-25,, 1986.

Purdy, J. A., Wong, J. W., and Harms, W. B., "Treatment Planning Computers (Present and Future)," in Monograph of American Association of Physics in Medicine, 1986 Summer School, in press.

Purdy, J. A., Wong, J. W., Harms, W. B., Drzymala, R. E., Emami, B., Matthews, J. W., Krippner, K., and Ramchander, P. K., "Three Dimensional Radiation Treatment Planning System," in The Use of Computers in Radiation Therapy, I. A. D. Bruinvis, P. H. Van der Giessen, H. J. Van Kleffens, and F. W. Wittkamper, eds., Elsevier Science Publishers, pp. 277-279, 1987.

Purdy, J. A., Wong, J. W., Harms, W. B., Emami, B. E., and Matthews, J. W., "State-of-the-Art High Energy Photon Treatment Planning," in Frontiers of Radiation Therapy and Oncology, Treatment Planning in the Radiation Therapy of Cancer, J. M. Vaeth, ed., S. Karger, Basel, Switzerland, 21:4-24, 1987.

Rosamond, T. L., Abendschein, D. R., Sobel, B. E., Bergmann, S. R., and Fox, K. A. A., "The Metabolic Fate of Radiolabeled Palmitate in Ischemic Canine Myocardium: Implications for Positron Emission Tomography," Journal of Nuclear Medicine, in press.

Rosamond, T. L., Mack, D. L., and Bergmann, S. R., "Time Dependent Conversion of Canine Myocardial Xanthine Dehydrogenase to Oxidase Activity During Ischemia and Reperfusion in vivo," Journal of the American College of Cardiology, 9:186A, 1987 (abstract).

Roysam, B., "A New Method for EM Autoradiography: Validation and Comparison to Crossfire Analysis," Department of Electrical Engineering, Sever Institute of Technology, Washington University, St. Louis, MO, May 1987 (Master of Science Thesis).

Saffitz, J. E., and Corr, P. B., "Autoradiographic Detection of Alterations of Myocardial Adrenergic Receptors Induced by Ischemia," in Neural Mechanisms and Cardiovascular Disease, B. Lown, A. Malliani, and M. Prosdocimi, eds., Liviana Press, Padova, Vol. 5, pp. 363-370, 1986.

Shipton, H. W., "Topography," in Encyclopedia of Neuroscience, G. Adelman, ed., Birkhauser, Boston, Vol. II, p. 1227, 1987.

Skinner, B., and Winslow, R. L., "Computing Depth Information from Stereo Image Pairs Using the Marr-Poggio Stereo Algorithm," IBC Technical Memorandum No. 322, May 1987.

Slessinger, E., Wong, J., Vannier, M., Hermes, R., and Roy, T., "Clinical Application of a New Treatment Verification Approach," Medical Physics, 13:600, 1986 (abstract).

Snyder, D. L., and Miller, M. I., "The Use of Grenander's Sieves in Quantum-Limited Imaging," Proceedings of the Twenty-Fourth Annual Allerton Conference on Communication, Control, and Computing, University of Illinois, Urbana-Champaign, IL, p. 213, October 1986 (summary).

Snyder, D. L., Miller, M. I., Thomas, Jr., L. J., and Politte, D. G., "Noise and Edge Artifacts in Maximum-Likelihood Reconstruction for Emission Tomography," IEEE Transactions on Medical Imaging, MI-6(3):228-238, 1987.

Snyder, D. L., Whitehouse, H. J., Wohlschlaeger, J. T., and Lewis R. C., "A New Approach to Radar/Sonar Imaging," Proceedings of SPIE 30th Annual International Conference on Advanced Algorithms and Architectures, San Diego, CA, 696:134-136, August 1986.

Sutera, S. P., Tilton, R. G., Nowak, M. O., Howe, J., Larson, K. B., and Williamson, J. R., "Vascular Flow Resistance in Isolated Rabbit Hearts: in vivo Viscosity of Red Cell Suspensions," 6th International Congress Biorheology, Biorheology, 23:231, 1986 (abstract).

Sutera, S. P., Tilton, R. G., and Williamson, J. R., "Vascular Flow Resistance in Maximally Dilated Rabbit Hearts: in vivo Viscosity of RBC Suspensions," Federation Proceedings, 46:1542, April 1987 (abstract).

Thomas, III, L. J., Barzilai, B., Wickline, S. A., Gessler, C. J., Sobel, B. E., Perez, J. E., and Miller, J. G., "Real-Time Two-Dimensional Imaging Based on Quantitative Integrated Backscatter," Ultrasonic Imaging, 8:36, 1986 (abstract).

Tilton, R. G., Cole, P. A., Zions, J. D., Daugherty, A., Larson, K. B., Sutera, S. P., Kilo, C., and Williamson, J. R., "Increased Ischemia-Reperfusion Injury to the Heart Associated with Short Term, Diet-Induced Hypercholesterolemia," Circulation Research, in press.

Tilton, R. G., Larson, K. B., Sutera, S. P., and Williamson, J. R., "Albumin Modulates Capillary Permeability in Isolated Buffer-Perfused Rabbit Hearts," Federation Proceedings, 46:1543, April 1987 (abstract).

Toga, A. W., Arnicar, T. L., Samaie, M., Lothman, E. W., and Collins, R. C., "Three Dimensional Study of Functional Anatomy of Experimental Seizures," American Academy of Neurology, 36(4):337, 1986.

Toga, A. W., Santori, M. S., and Samaie, M., "Regional Distribution of Flunitrazepam Binding Constants: Visualizing Kd and Bmax by Digital Image Analysis," Journal of Neuroscience, 6(9):2747-2756, 1986.

Turmon, M. J., and Miller, M. I., "Simulation Results for Maximum-Likelihood Estimation of Toeplitz Constrained Covariances," Proceedings of the Twenty-First Annual Conference on Information Sciences and Systems, The Johns Hopkins University, Baltimore, MD, p. 548, March 1987.

Vered, Z., Barzilai, B., Mohr, G. A., Thomas, III, L. J., Perez, J. E., Sobel, B. E., and Miller, J. G., "Real-Time Two-Dimensional Imaging Based on Radio Frequency Derived Integrated Backscatter in Normal Volunteers and Patients," Ultrasonic Imaging, in press (abstract).

Vered, Z., Barzilai, B., Mohr, G. A., Thomas, III, L. J., Sobel, B. E., Miller, J. G., and Perez, J. E., "Ultrasonic Tissue Characterization in Man with Real-Time Quantitative Integrated Backscatter Imaging and Delineation of Integrated Backscatter Dependence on the Cardiac Cycle," Journal of the American College of Cardiology, 9:212A, 1987 (abstract).

Walsh, M. N., Serota, H., Bergmann, S. R., Sobel, B. E., and Geltman, E. M., "Assessment of Relative Coronary Flow Reserve with Dynamic Positron Emission Tomography and $H_2{}^{15}O$," Journal of the American College of Cardiology, 9:160A, 1987 (abstract).

Wickline, S. A., Thomas III, L. J., Miller, J. G., Sobel, B. E., and Perez, J. E., "Sensitive Detection of the Effects of Reperfusion on Myocardium by Ultrasonic Tissue Characterization with Integrated Backscatter," Circulation, 74:389-400, 1986.

Wong, J., Binns, W. R., Epstein, J. W., Klarmann, J., and Israel, M. H., "Plastic Scintillator Sheet as a Real Dosimeter in Radiotherapy," Medical Physics, 13:609, 1986 (abstract)

Wong, J. W., Binns, W. R., Ge, W. S., Epstein, J. W., Klarmann, J., and Israel, M. H., "Rapid Areal Dosimetry Using a Computer Based Plastic Scintillator-Video Camera System," Proceedings of the 9th International Conference on the Use of Computers in Radiation Therapy, Tilburg, The Netherlands, North Holland, The Netherlands, pp. 417-420, June 22-25, 1987.

Wong, J. W., Ge, W. S., Monthofer, S., and Hancock, S. S., "Spatial Distributions of Charged Particles Emitted by Pair Productions," Medical Physics, 14:474, 1987.

Wong, J. W., and Purdy, J. A., "Basis of Recent Methods of Photon Dose Calculations," Proceedings of the 9th International Conference on the Use of Computers in Radiation Therapy, Tilburg, The Netherlands, North Holland, The Netherlands, pp 319-322, June 22-25, 1987.

Wong, J., and Purdy, J., "An Examination of Recent Methods of Photon Dose Calculations," Medical Physics, 13:592, 1986 (abstract).

Wong, J. W., Slessinger, E. D., Hermes, R. E., Harms, W. B., Vannier, M. W., and Roy, T., "Investigation of an Approach to Quantitative Treatment Verification," Proceedings of the 9th International Conference on the Use of Computers in Radiation Therapy, Tilburg, The Netherlands, North Holland, The Netherlands, pp. 461-464, June 22-25, 1987.

Wong, J. W., Slessinger, E., Hermes, R., and Vannier, M., "Investigation of an Approach to Quantitative Treatment Verification," presented at the 28th Annual Meeting of the American Society of Therapeutic Radiation Oncology, Los Angeles, CA, November 2-7, 1986.

Yamada, K. A., and Corr, P. B., "α_1-Adrenergic Blockade Enhances Salvage of Reperfused, Ischemic Myocardium Independent of Regional Blood Flow," Circulation, 74(II):II-69, 1986 (abstract).

Yamada, K. Y., Saffitz, J. E., and Corr, P. B., "Role of Alpha- and Beta-Adrenergic Receptor Stimulation in the Genesis of Arrhythmias During Myocardial Ischaemia," European Heart Journal, 7(A):87-90, 1986.

Yu, C. X., Wong, J. W., and Purdy, J. A., "Photon Dose Perturbations Due to Small Inhomogeneities," Medical Physics, 14:78-83, 1987.

VIII. MONOGRAPHS AND WORKING NOTES

The Biomedical Computer Laboratory's Monograph Series was established to systematize the many reports, reprints, program descriptions and other documents written at BCL or supported in part by the Laboratory's facilities or staff.

A forum, much less formal than our monograph series, has been instituted to serve as a repository for materials such as: research notes, system and component documentation, technical survey notes and prepublication drafts. Working Note Files are maintained for access by anyone associated with the Institute for Biomedical Computing. Distribution for outside use can be made available with the consent of the contributing author.

Monographs

Following is a list of the monographs published by BCL during the past year. Copies of the complete index to the Monograph Series are available on request.

Monograph Number	Author(s)	Title	Date
476	Ollinger, J. M.	Algorithms for Parameter Estimation in Dynamic Tracer Studies Using Positron-Emission Tomography	9/86
477	Ollinger, J. M.	An Evaluation of a Practical Algorithm for Estimating Histograms in Dynamic Tracer Studies Using Positron-Emission Tomography	10/86
478	Kumar, A.	Design of a Frame Buffer for Radiology Applications	12/86
479	Snyder, D. L. Miller, M. I. Thomas, L. J., Jr. Politte, D. G.	Noise and Edge Artifacts in Maximum-Likelihood Reconstructions for Emission Tomography	1/87
480	Snyder, D. L. Miller, M. I. Thomas, L. J., Jr. Politte, D. G.	Noise and Edge Artifacts in Maximum-Likelihood Reconstructions for Emission Tomography (Revised)	5/87
481	Politte, D. G. Hoffman, G. R. Beecher, D. E. Ficke, D. C. Holmes, T. J. Ter-Pogossian, M. M.	Image-Reconstruction of Data From Super PETT I: A First-Generation Time-of-Flight Positron-Emission Tomograph	5/87

Working Notes

Following is an index of notes submitted during the current reporting period.

Working Note Number	Author(s)	Title	Date
75	Thomas, L. J., Jr.	Misadventures in Precision: Log(x)	8/86
76	Hellberg, W.	Stat-Pack Statistical Analysis Software Package	1/87

IPAQ Working Notes

Working Note Number	Author(s)	Title	Date
8	Witte, E. Skinner, B.	ZIP 3232 Array Processor Tests and Comments	9/86
9	Hermes, R.	Survey of Raster Graphics Systems	10/86
10	Brown, M.	CONCH at BCL	3/87
11	Senol, E.	Bit Error Generator	6/87
12	Politte, D. Hermes, R.	Results of an Experiment to Measure the Speed of Floating Point Operations on Local Computer Resources	6/87